Spring 2024 – Systems Biology of Reproduction
Discussion Outline – Reproductive Endocrinology Systems
Michael K. Skinner – Biol 475/575
CUE 418, 10:35-11:50 am, Tuesday & Thursday
April 4, 2024
Week 13

Reproductive Endocrinology Systems

Primary Papers:

1. Stotzel, et al. (2012) Theriogenology 78:1415-1428
2. Toufaily, et al. (2020) J Endocrinology 244(1):111-122
3. Barban, et al. (2016) Nat Genetics 48:1462

Discussion

Student 9: Reference 1 above

- What endocrine parameters were synchronized and what regulatory agent tested?
- What experimental model was used?
- What model was established and validated?

Student 10: Reference 2 above

- What was the experimental design and technology used?
- Why is the LH surge important?
- What was identified regarding the progesterone regulated phasic LH secretion?

Student 11: Reference 3 above

- What was the experimental design and technology used?
- What reproductive factors were used and what traits were associated?
- What conclusions can be drawn on genomic control of reproduction?

Available online at www.sciencedirect.com

SciVerse ScienceDirect

Theriogenology 78 (2012) 1415–1428

Theriogenology

www.theriojournal.com

Advances in modeling of the bovine estrous cycle: Synchronization with PGF2α

C. Stötzel[a,*], J. Plöntzke[b], W. Heuwieser[b], S. Röblitz[a]

[a] *Computational Systems Biology Group, Numerical Analysis and Modeling, Zuse Institute Berlin, Takustr. 7, 14195 Berlin, Germany*
[b] *Clinic for Animal Reproduction, Faculty of Veterinary Medicine, Freie Universität Berlin, Königsweg 65, 14163 Berlin, Germany*

Received 6 October 2011; received in revised form 25 April 2012; accepted 26 April 2012

Abstract

Our model of the bovine estrous cycle is a set of ordinary differential equations which generates hormone profiles of successive estrous cycles with several follicular waves per cycle. It describes the growth and decay of the follicles and the corpus luteum, as well as the change of the key reproductive hormones, enzymes and processes over time. In this work we describe recent developments of this model towards the administration of prostaglandin F2α. We validate our model by showing that the simulations agree with observations from synchronization studies and with measured progesterone data after single dose administrations of synthetic prostaglandin F2α.

Keywords: Cow; Reproduction; Hormone patterns; Differential equations; Systems biology; Synchronization

1. Introduction

Throughout the last decades, increasing amounts of biological data have become available, and mathematical modeling aims at relating and interpreting these data with the help of powerful computational tools and efficient algorithms. As part of the rapidly expanding research field systems biology, this approach is highly interdisciplinary, and requires a close collaboration between mathematicians and natural scientists. Although a few models are already available [1–4], systems biology modeling in animal sciences is still at an early stage of development [5].

The purpose of this paper is to demonstrate how dynamic mathematical models can enhance the understanding of synchronization in the bovine estrous cycle. The model used in this article is based on a model that was presented in previous studies [4,6]. It describes the key feedback mechanisms within the bovine estrous cycle, and generates hormonal profiles of successive estrous cycles over time. The long-term goal of developing such a model of the endocrine mechanisms in the bovine is to assist with research and application in drug testing, management decision making, or therapeutic strategies. On the one hand, we want to contribute to a better understanding of the complex biological mechanisms that drive the estrous cycle, and on the other hand we aim to exploit the predictive abilities of such a mathematical model, e.g., by simulating external influences. The short-term goal and current aim of this article is to validate and improve the existing model, thus to make a step towards a reliable model, which makes predictions more adequate.

The starting point of our work was the validation of the model used in [6]. For this purpose we investigated

* Corresponding author. Tel: +49 30 84185 335; Fax: +49 30 84185 107
E-mail address: stoetzel@zib.de (C. Stötzel).

0093-691X/$ – see front matter © 2012 Elsevier Inc. All rights reserved.
http://dx.doi.org/10.1016/j.theriogenology.2012.04.017

how adequately the model simulations match available information. Experimental data required for model validation would for example consist of measured hormonal concentrations of healthy, untreated, individual cows at different stages of estrous cycle. Unfortunately, measurements published in literature are rare and do often not meet the requirements for validation; observed time scales are often too small or too coarse, or too few substances are measured. Therefore, we were looking for alternative information that we could monitor with the model. We wanted to check the correctness of the model for a specific scenario where the system answer is known. More precisely, synchronization protocols [7] drew our attention to prostaglandin F2α ($PGF_{2\alpha}$). In veterinary medicine, $PGF_{2\alpha}$ and its analogues are administered to cows mainly to make use of their luteolytic action, e.g., in estrus synchronization protocols. It is known that the sudden rise of this hormone at certain stages of the estrous cycle results in an immediate decay of the responsive corpus luteum (CL), and an immediate fall of progesterone levels in plasma. In a first validation step of our model, we simulated the administration of $PGF_{2\alpha}$ and compared the outcome of our simulation with known responses reported in literature. Furthermore, we used measurements taken after single injections of $PGF_{2\alpha}$ to validate our simulation.

The above described validation is an iterative process. Whenever simulations with the original model were not satisfactory, adjustments to the model were made. In particular, during simulations for the administration of hormones, we figured out that this model still had some shortcomings regarding the growth and decay of the CL. A replacement of mechanisms involved in ovulation and the refinement of luteolysis became necessary.

The objective of this paper is to describe the adjustments to the original model, and to show that the advanced model captures the known effects after $PGF_{2\alpha}$ administration.

2. Materials and methods

Our modeling approach aims to reproduce how the various components involved in the bovine estrous cycle function together. Instead of only investigating individual parts, we describe the biological system on the whole-organism level, in order to capture the most important dynamic feedback mechanisms. We mostly consider regulatory mechanisms (inhibitory and stimulatory effects of hormones), and model them as continuous functions over time. The model in [4] was constructed by first defining a number of key components of the system and their interactions, which were then represented in a flow chart. Subsequently, a set of differential equations was derived to describe the relations within the flow chart mathematically. For every model component, e.g., a hormonal concentration or the follicular capacity to produce hormones, one ordinary differential equation (ODE) was developed. The dependencies between the components are described in the right hand sides of the ODEs. Hill functions are used to model inhibitory and stimulatory relations. A slightly modified version of the model in [4] with improved luteolysis was used in [6], which we will refer to as the original model in the following. The model derived in this paper is the result of several adjustment of the original model, which will be described in detail. An overview of the final model is given in Figure 4. As we aim to validate our model with the help of external manipulations, we will describe the background of this administration first, before going into the details of the model advancements.

2.1. Background of $PGF_{2\alpha}$ administration - estrus synchronization protocols

Protocols of estrus synchronization consist of consecutive administration of different hormones or their analogues following a certain order. They have the goal to synchronize the estrus of individual females in order to facilitate timing of following artificial insemination, indepently of estrous cycle stage at the start of the protocol. They are commonly used in cattle and in other domestic and non-domestic species [8]. Our approach to validate the model of the bovine estrous cycle was to include synchronization protocols as described in [7,9]. Here, we restrict ourselves to single and double administrations of $PGF_{2\alpha}$, which is used in these protocols as single or double injection. We model the administration of $PGF_{2\alpha}$ at different stages of the estrous cycle.

The $PGF_{2\alpha}$ is responsible for the onset of luteolysis in the cow. With luteolysis the luteal phase of the cycle ends and a new estrus can take place. The $PGF_{2\alpha}$ induces functional luteolysis by reducing progesterone production followed by structural luteolysis with tissue degeneration and cell death [10,11]. The $PGF_{2\alpha}$ is synthetized in the endometrium and released in pulses, regulated by estradiol (E_2), progesterone (P_4) and oxytocin (OT) during the estrous cycle [12–14]. In animal production, administration of synthetical analogues of $PGF_{2\alpha}$ (e.g., Cloprostenol, Luprostiol, Tiaprost) or original $PGF_{2\alpha}$ (e.g., Dinoprost) is used for various pur-

poses in the cow, such as induction of estrus or synchronization protocols. The effect of the treatment depends on the stage of estrous cycle which determines the responsiveness of the CL on the luteolytic effect of $PGF_{2\alpha}$ [11]. At midluteal stage of the estrous cycle administration of $PGF_{2\alpha}$ leads to luteolysis within a few hours. This results in a decrease of P_4 concentration, increase of E_2, a peak of the Luteinizing Hormone (LH) and ovulation [15].

Virtual administration of $PGF_{2\alpha}$ to the cow model was conducted on various days of the estrous cycle. With the original model, the simulation outcome of the model after $PGF_{2\alpha}$ application was not as expected, which gave us a starting point to improve the model.

2.2. Advancements in the model

To improve the model with respect to the expected effects of a single $PGF_{2\alpha}$ injection, we introduced some new features which are described in this section. A list of the Hill functions—sigmoidal functions to model inhibitory or stimulatory effects as described in [4]—can be found in Appendix B. Here H^+ and H^- denote scaled positive, respectively negative Hill functions. Parameter values are specified in Appendix C.

In the former model, the equation for the CL described the change of the capacity of the CL to produce P_4. For reasons described later in this section, we now interpret this equation as the development of the size (e.g., diameter) of the CL over the cycle. This is also advantageous as soon as we deal with ultrasound measurements for the corpus luteum. Likewise, the equation for the follicles (Foll) now describes the development of the total size of all follicles.

2.2.1. Drug administration

We add an additional model component for analogues of $PGF_{2\alpha}$, denoted PGF_{syn} in the following. It is reported that $PGF_{2\alpha}$ and its analogues have a very short half-life [16,17], thus we chose to model PGF_{syn} with a rapid decay. Furthermore, it is known that $PGF_{2\alpha}$ analogues have an up to three times higher biological activity than original $PGF_{2\alpha}$ [17]. Even low doses of PGF_{syn} cause a peak in $PGF_{2\alpha}$ that exceeds the natural level [18]. Due to this high potency of PGF_{syn}, we chose to model PGF_{syn} with a three times higher relative level compared to normal $PGF_{2\alpha}$ levels. We model the effect of the synthetical analogue by summing the level of PGF_{syn} to the normal $PGF_{2\alpha}$ level.

To model the rise of PGF_{syn} in the system, we take a function which is zero before dosing time (t_D), and has a sharp left-skewed peak with maximum shortly after t_D. This leads to a slight delay in the effect of the injection. As suggested in [19] and based on techniques described in

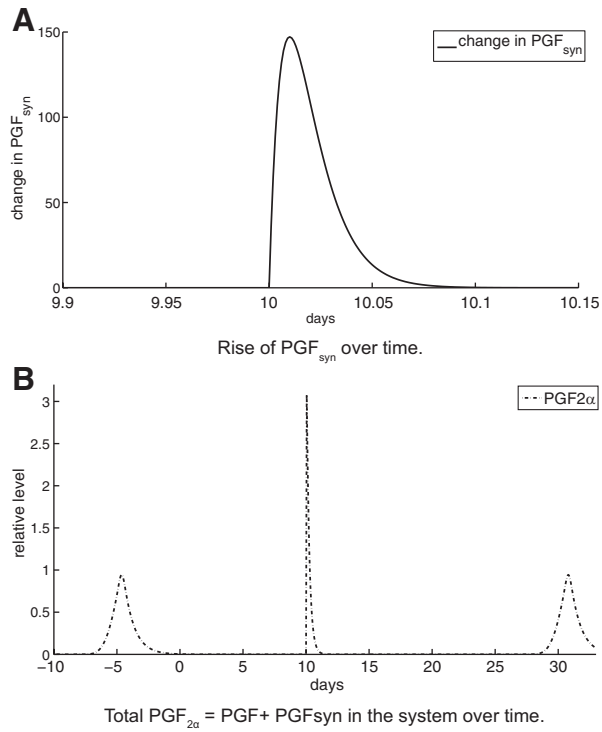

Fig. 1. Change in PGF_{syn} and Administration of PGF_{syn} at time $t_D=10$. Parameters are $D = 4$ and $\beta=100$. Maximum rise of PGF_{syn} is at $t = t_D + 1/\beta=10.01$. The level of $PGF_{2\alpha}$ is the result of summing PGF_{syn} levels to naturally arising $PGF_{2\alpha}$.

[20], we take the probability density function of the Gamma-distribution with fixed shape parameter $\alpha = 2$, and inverse scale parameter β leading to a left-skewed curve which has its maximum at $t = 1/\beta$. The change of concentration of synthetic $PGF_{2\alpha}$ is calculated as

$$\frac{d}{dt}PGF_{syn}(t) = D \cdot \beta^2 \cdot t_{mod}(t) \cdot \exp(-\beta \cdot t_{mod}(t)) - c_{PGF_{syn}} \cdot PGF_{syn}(t).$$

The parameter D represents the amount of administered drug scaled to obtain the designated height of the relative level of PGF_{syn}, see Figure 1. The parameter c_{PGFsyn} denotes the clearance rate constant of PGF_{syn}. The modified time function t_{mod} denotes time after dosing, and is given by

$$t_{mod}(t) = \max(0, t - t_D)$$

The rise of PGF_{syn} is large right after dosing time and approaches zero quickly thereafter, leading to a rapid decay of the function $PGF_{syn}(t)$.

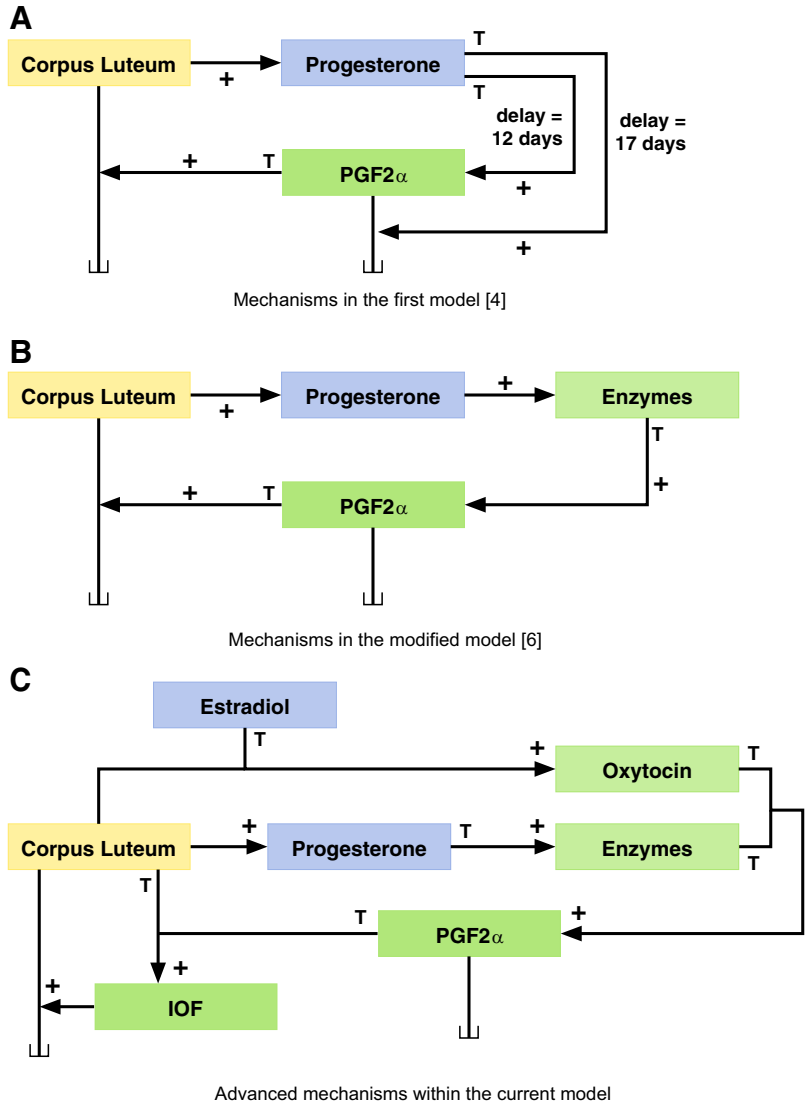

Fig. 2. Changes in the mechanisms involved in luteolysis. "+" marks a stimulatory effect, "T" denotes a threshold within a Hill function. No description means a transition, and "⊔" marks a degraded substance. In (A), P_4 was driving luteolysis with large time delays. In (B), enzymes were responsible for the rise of $PGF_{2\alpha}$. In the advanced model (C), we have added oxytocin and interovarian factors to the drivers of luteolysis.

2.2.2. *Improvement of luteolysis*

In [4], the rise of $PGF_{2\alpha}$ triggering the decay of the CL was modeled as a black box, depending with large delays on P_4 only. In [6], this was improved as enzymes were introduced that stimulate $PGF_{2\alpha}$, and the model became more robust. However, in simulating the administration of $PGF_{2\alpha}$ we detected that the modeling of luteolysis still had some shortcomings. It is known that after the administration of $PGF_{2\alpha}$ the responsive CL decays immediately [21]. In the original model, complete luteolysis took too much time after administration of PGF_{syn}, and also after rise of the regular $PGF_{2\alpha}$. Simply accelerating the CL decay lead to an accelerated fall of P_4 levels, and thus to very low P_4 levels already at the beginning of the second follicular wave, which had undesired consequences on the rest of the model output. Thus, since P_4 levels should stay on a high level for the duration of the first two follicular waves, we required the CL still being active at this time. Therefore, the starting point of its decay must occur later. This means we need the initiator of luteolysis,

$PGF_{2\alpha}$, to appear a couple of days later compared to the original model. To account for this effect, we now model the mechanisms that lead to a rise in $PGF_{2\alpha}$ differently. The development of the model regarding luteolysis is illustrated in Figure 2.

Instead of leaving only the enzymes (Enz) being responsible for $PGF_{2\alpha}$ levels as in [6], we now also include OT as another initiator of $PGF_{2\alpha}$ [22]. The E_2 stimulates OT synthesis in the granulosa cells [23] and the effect of OT on $PGF_{2\alpha}$ [13]. We assume that OT production depends on the surface of the CL and thus quadratically on CL size, and that it is cleared with constant rate c_{OT}. The equation for the rise and fall of OT is now

$$\frac{d}{dt}OT(t) = H_{17}^{+}(E2) \cdot CL(t)^2 - c_{OT} \cdot OT(t).$$

The OT together with Enz are now responsible for the rise of $PGF_{2\alpha}$. With the function $H_{16}^{+}(Enz\ \&\ OT)$, which represents a stimulatory effect if the levels of Enz and OT are both high, and the constant clearance rate c_{PGF}, the equation for $PGF_{2\alpha}$ becomes

$$\frac{d}{dt}PGF(t) = H_{19}^{+}(Enz\&OT) - c_{PGF} \cdot PGF(t).$$

In the former model, $PGF_{2\alpha}$ triggered luteolysis directly, independent of estrous stage. However, it is known that the CL is resistant to the action of $PGF_{2\alpha}$ at early luteal stage. We therefore remodeled the action of $PGF_{2\alpha}$ on the CL. According to [11], the direct action of $PGF_{2\alpha}$ on the CL is mediated by local factors: endothelin-1-system, cytokines, and nitric oxide. The expression of these interovarian substances is upregulated by $PGF_{2\alpha}$, and strictly depends on the stage of the CL. Summarizing these local factors, we introduce a new component to our model and call it interovarian factors (IOF). IOF is stimulated by $PGF_{2\alpha}$ only if the CL has reached a certain size, and is cleared with constant rate c_{IOF},

$$\frac{d}{dt}IOF(t) = H_{18}^{+}(PGF\&CL) - c_{IOF} \cdot IOF(t).$$

The rise of the interovarian factors now induces luteolysis.

2.2.3. Improvement of ovulation

In the original model, LH was the initiator of ovulation, responsible for decay of the dominant follicle, and at the same time the initiator of the rise of the CL 4.5 days after the LH peak. A delay differential equation was needed to model this effect. The atretic follicles disappeared from the system, and the CL emerged independently of the size of the just ovulated dominant follicle.

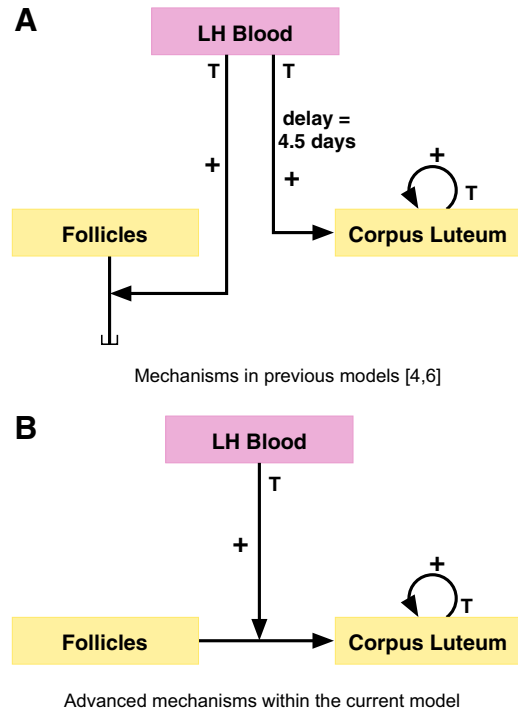

Fig. 3. Changes in the mechanisms involved in ovulation. "+" marks a stimulatory effect, "T" denotes a threshold within a Hill function. Arrows without description mean a transition, and "⊔" marks a degraded substance. In both models, ovulation includes the degradation of the follicles, and the formation of the CL, triggered by LH. In previous models (A), the CL arose independently from the size of the follicles, only regulated by the timepoint of the LH peak. In (B), a new dependency is introduced as the degraded follicles transform to the newly arising CL, making thus the size of the CL directly dependent on the follicles.

However, it is known that thecal and granulosa cells of the ruptured follicle transform to small and large luteal cells which form the rising CL [24]. Therefore, to make the model more realistic and to be able to account for different sizes of the dominant follicle [25], we changed the involved mechanisms. The ovulatory follicle now directly influences the initiation of CL growth, and no further delay differential equation is needed. The old and new mechanisms are illustrated in Figure 3. The equations for the follicular size (denoted Foll) and the CL are modified as follows:

$$\frac{d}{dt}Foll(t) = \widetilde{H}_{11}^{+}(FSH_{Bld}) - (H_{12}^{+}(P4) + H_{13}^{+}(LH_{Bld})) \cdot Foll(t),$$

$$\frac{d}{dt}CL(t) = SF \cdot H_{13}^{+}(LH_{Bld}) \cdot Foll(t) + H_{14}^{+}(CL) - H_{15}^{+}(IOF) \cdot CL(t).$$

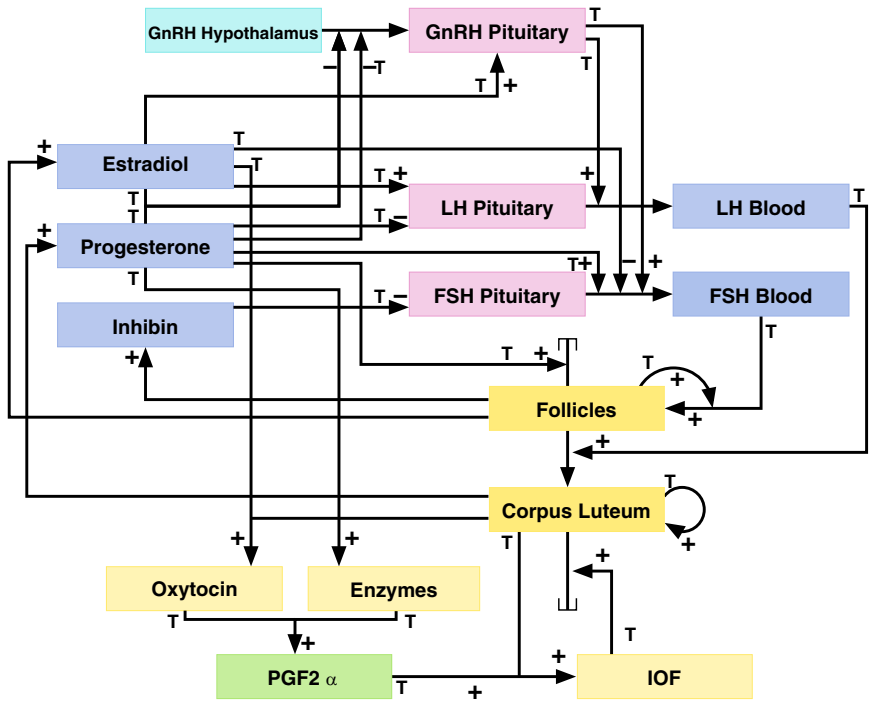

Fig. 4. Schematic representation of the components and relations in the herein presented advanced model of the bovine estrous cycle. Each box represents a substance for which a differential equation is derived, the color resp. grayscale of a box indicates the different physiological compartments where the substance mainly occurs: hypothalamus (GnRH), pituitary (GnRH, LH, FSH), blood (LH, FSH, estradiol, progesterone, inhibin), ovaries (follicles, corpus luteum, oxytocin, enzymes, IOF), uterus ($PGF_{2\alpha}$). The arrows represent the regulations between the substances in the model, where "+" marks a stimulatory effect, "T" denotes a threshold within a Hill function. No description means a transition, and '⊔' marks a degraded substance.

In the model, the part of the follicles decaying due to LH, i.e., the ovulated follicle, is now preserved in the system, forming the rising CL. The scaling factor *SF* is included to keep the relative levels of the substances between 0 and 1. Further growth of the CL is still modeled by a self-growth, i.e., a positive influence of the CL on its own size from a certain size on. Since the CL therefore starts to grow earlier now, the threshold and rate of self-growth have been adjusted.

2.2.4. Further modifications

Because the development of the CL depends on three mechanisms (an initiating impulse from LH, a self-growth and the decay caused by the interovarian factors), the level of the CL changes as follows: Right after ovulation the CL starts to grow, reaches the size needed for self-growth, and then grows with constant rate until the rise of $PGF_{2\alpha}$. In the original model, with the former mechanisms of delayed rise of the CL after ovulation, the course of CL was interpreted as "capacity to produce P_4", and thus the P_4 profile looked similar. Available experimental data for P_4 lead us to modify its production in the model. In particular, data from a study with single dose $PGF_{2\alpha}$ administration showed that the P_4 profile stayed low for about 10 days after the $PGF_{2\alpha}$ administration. Therefore, and since it is known that P_4 production of the CL is not absolutely proportional to the CL size [26], the mechanisms leading to the rise of P_4 were adjusted to obtain a P_4 production which is lower at start of CL growth compared to later luteal stages. We now interpret the equation for CL as development of the "size of the CL", and assume that production of P_4 depends on the surface size and thus quadratically on CL. The equation for P_4 becomes

$$\frac{d}{dt}P4(t) = c_{CL}^{P4} \cdot CL(t)^2 - c_{P4} \cdot P4(t).$$

In the former model, the capacity of the follicles to produce E_2 and inhibin (Inh) was described in one equation, and E_2 and Inh levels were proportional to the relative level of this component. For consistency reasons we now also assume a quadratic relationship between the follicles and E_2, respectively Inh, and the corresponding equations become

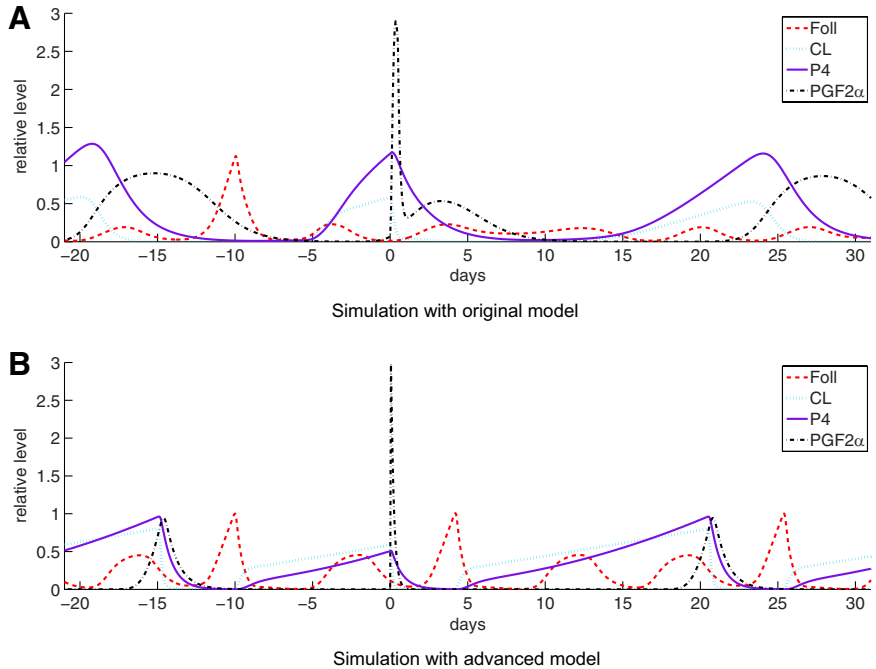

Fig. 5. Comparison of the simulation output of the previous model (shown in A) and the advanced model (shown in B) after a single administration of PGF_{syn} on day zero. Under investigation are Foll, CL, P_4, and total $PGF_{2\alpha}$. A high peak of Foll indicates ovulation. In both plots, the last ovulation has occurred ten days before administration. The original model does not capture the known effects after PGF_{syn} application, but the improved model in particular shows a rapid CL and P_4 decline and ovulation in the next follicular wave.

$$\frac{d}{dt}E2(t) = c_{Foll}^{E2} \cdot Foll(t)^2 - c_{E2} \cdot E2(t),$$

$$\frac{d}{dt}Inh(t) = c_{Foll}^{Inh} \cdot Foll(t)^2 - c_{Inh} \cdot Inh(t).$$

Diminishing the former delay for inhibin on FSH has been possible by augmenting the threshold for inhibin until its negative influence on FSH synthesis arises, at the same time steepening the regulatory effect on FSH. Moreover, the production rate of inhibin as well as its clearance rate have been lowered in order to defer the simulated inhibin curve. The FSH threshold for its influence on the follicles has also been increased. The fact that we were able to dispose of this delay without changing the differential equation at all was only possible because the delay was quite short (1.41 days in [6]).

A flow chart of the complete mechanisms of the model is shown in Figure 4.

3. Results and discussion

The here presented advanced model of the bovine estrous cycle consists of 15 ordinary differential equations and 60 parameters, generating successive estrous cycles of 21 days with three follicular waves per cycle. It does not contain time delays anymore. Therefore, there is no longer a need for a delay differential equation solver. We now use a linear implicit Euler method with extrapolation, implemented in the code LIMEX [27]. Parameters are identified with the software NLSCON developed at the Zuse Institute. This software uses subtle mathematical techniques, such as affine covariant Gauss-Newton methods that take into account sensitivities and linear dependencies of the parameters [28,29].

Our model of the bovine estrous cycle is dimensionless in the sense of [30], i.e., the numerical values of the components are independent of the standard of measurement. Simulated hormone levels and ovarian components have been scaled to be between 0 and 1 by dividing the equation by its maximum output level. Once we have measurement data available we will scale the functions to the corresponding quantities by scaling the involved parameters. This can be done because until now none of the parameters has a fixed value verified by experiments. We refer to the simulated dimensionless output functions as relative levels.

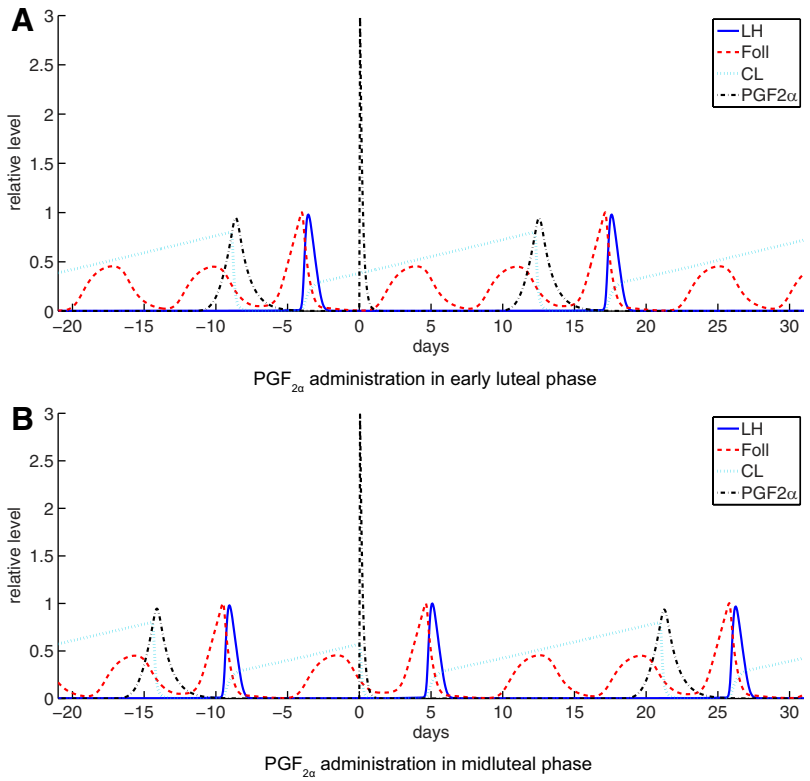

Fig. 6. Simulation results with the advanced model for Foll, CL, and LH, and total $PGF_{2\alpha}$ after administration of PGF_{syn} on different stages of the cycle. A high peak of Foll indicates ovulation. In (A) it is shown that there is no response if ovulation has occurred only four days before administration, in (B) we can observe that giving $PGF_{2\alpha}$ ten days after ovulation leads to a decay in CL, an LH peak and ovulation within five days after administration.

3.1. Simulation of single administration of $PGF_{2\alpha}$ at different stages of the cycle

The changes in the model described in the previous section have led to the following changes in the simulation results (Fig. 5). In contrast to the previous model, after administration of $PGF_{2\alpha}$ on Day 10 after ovulation the CL now decays immediately to zero. P_4 levels follow shortly after. Right after administration, $PGF_{2\alpha}$ does not have high levels right anymore, but stays low for 21 days. The most important difference between the outcome of the former and the advanced model can be observed in the follicles. Before, the administration of $PGF_{2\alpha}$ did not affect regular function, anovulatory waves stayed anovulatory. Now, the next arising follicular wave does not decay but continues to rise, leading to ovulation.

In Figure 6 we can observe that virtual administration of $PGF_{2\alpha}$ in the early luteal stage does not lead to a decay of the CL, while at later time points of the cycle it results in an immediate decay of the responsive CL, an LH peak, and ovulation during the following follicular wave.

3.2. Simulation of repeated administration of $PGF_{2\alpha}$ at different stages of the cycle

As described in Section 2.1, protocols of estrus synchronization often contain two administrations of $PGF_{2\alpha}$. It is known that the success of these protocols depends on the time interval between the two doses [31]. We thus investigated several time intervals with our model. In Figure 7, the effect of this application on the follicles is shown. On day zero, $PGF_{2\alpha}$ is administered to six cows in different phases of their cycles. A high peak in the course of Foll of a cow corresponds to the ovulatory wave of this cow. As can be observed in Figure 7A, a single dose of $PGF_{2\alpha}$ results in an ovulation in the next follicular wave in some cows (cow3, cow4, cow5, cow6), while in other cows (cow1 and cow2) it does not have any effect. In Figure 7B, a second dose of $PGF_{2\alpha}$ is given to the same cows seven days after the first application. Here too, some cows are affected by this administration (cow1 and cow2 are responsive), while others are not affected. This is due to the mechanisms driving luteolysis, where the

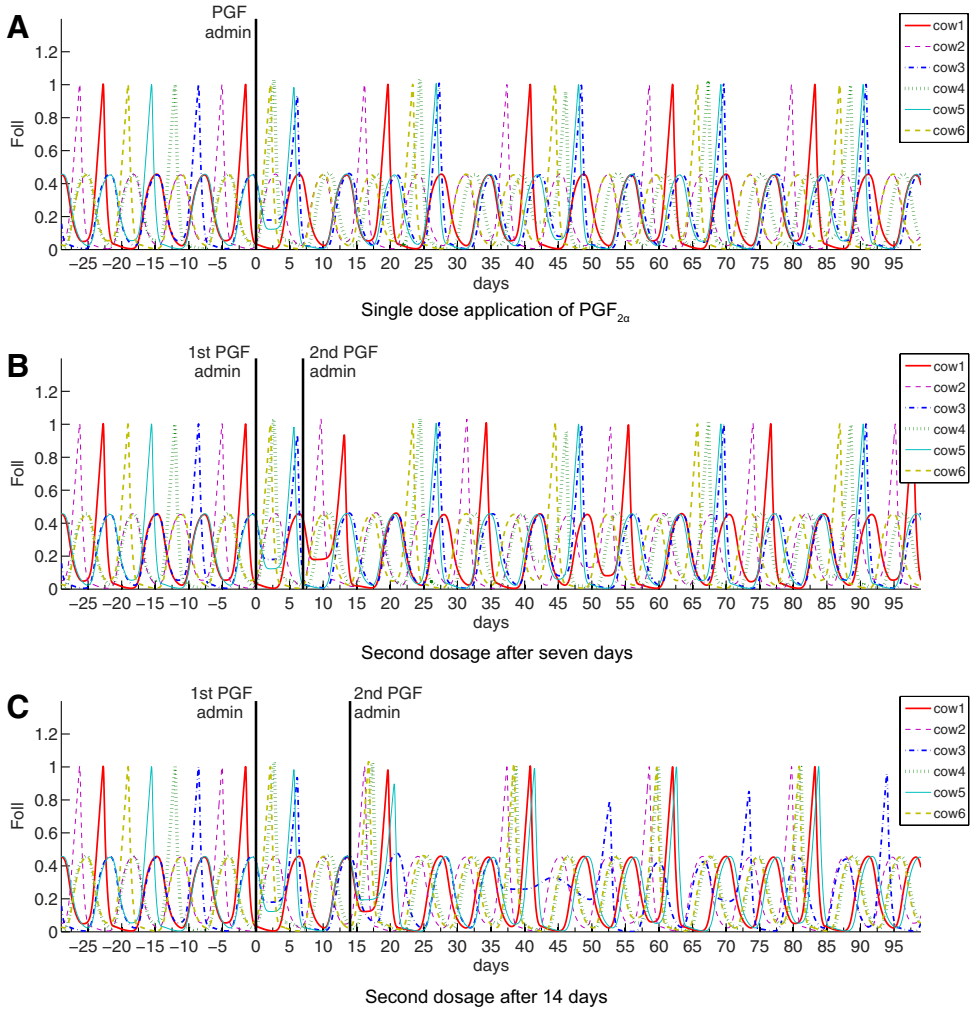

Fig. 7. Simulation results for the follicles of six different cows during virtual administration of $PGF_{2\alpha}$. Day zero denotes the day of first administration, when the cows are each in a different stage of their estrous cycle, the high peaks of the curves denoting the timepoints of ovulation. In (A), a single dose of $PGF_{2\alpha}$ is given, which impacts the cycle of at least two cows (cow3 and cow4). In (B), a second dose is given seven days after the first dosage, now influencing the cycle of two other cows (cow1 and cow2). In (C), the second dose is given 14 days after the first dose, now influencing four cows (cow3, cow4, cow5 and cow6).

CL is not responsive to $PGF_{2\alpha}$ early after its rise. The cows affected by the first dosage are now in the early luteal stage and thus not responsive to the second dosage, while the cows not responsive at the first administration are now in a later luteal stage where they respond to $PGF_{2\alpha}$. This suggests giving the second application when the cows affected by the first dosage are again in the phase of their estrous cycle where they have a responsive CL. In Figure 7C, the second dose is given 14 days after the first dose, leading to a synchronization effect within almost all of the cows under investigation.

Before the first administration to the cows in Figure 7, the ovulation timepoints of the cows were evenly distributed, while after double administration within 14 days they were brought much closer together, such that the cows ovulate within a timespan of 4.5 days. This is consistent with the double injection 11 to 14 days apart in common synchronization protocols as reviewed in [31]. Only for some cows in a certain stage of their cycle (e.g., cow 5 in Fig. 7C), the synchronization effect in our model is not as desired, which is in line with observations after presynch protocols [32]. Nevertheless, this result validates our model in the sense that it captures the known effects after this certain external manipulation of the bovine estrous cycle.

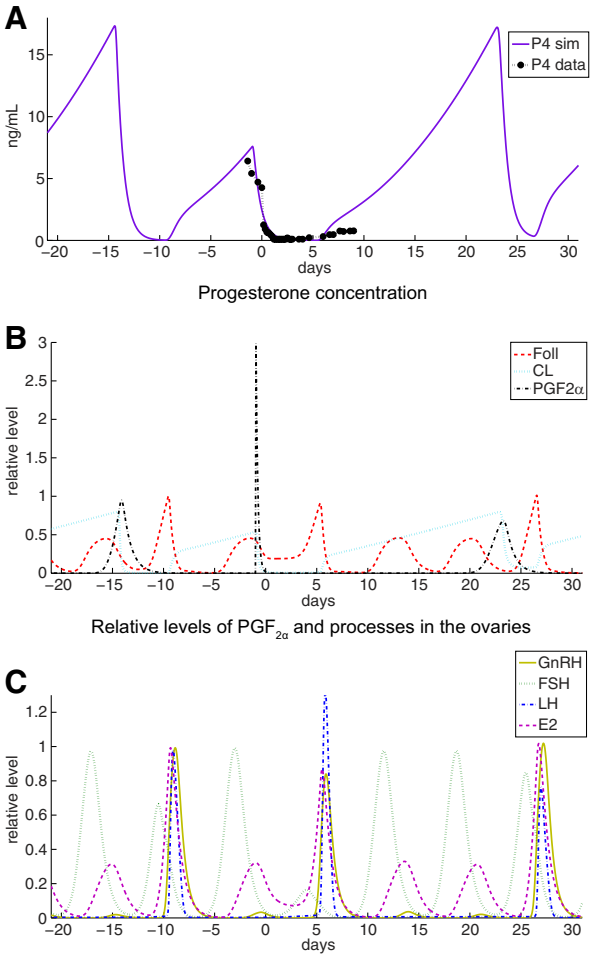

Fig. 8. Simulation of a single dose of PGFα and its impact on other components of the model. Parameters have been fitted such that the simulated P_4 levels match the given experimental P_4 data. With the set of identified parameters, we can investigate the course of the other model components. In particular, we can observe that ovulation occurs six days after injection. (C) Relative levels of selected other hormones.

3.3. Comparison with progesterone measurements after single administration of $PGF_{2\alpha}$

In a recent study performed at the institute of animal reproduction, Department of Veterinary Medicine at Freie Universität Berlin, a single dose of 5 mg $PGF_{2\alpha}$ was injected to seven cows, and plasma progesterone concentrations were measured before and after the administration. In particular, blood was collected every morning (8:00h) and evening (17:00h) before the injection, every four h after the injection, and twice a day after ovulation, detected by ultrasound.

Model parameters have been identified so that the simulated P_4 level matches the given data. Note that we now observe and simulate concentrations instead of relative levels for progesterone. Certain parameter units therefore have to be adapted adequately. In Figure 8A an example of measured P_4 concentrations for one of the examined cows is shown, together with the simulated P_4 concentration. Ovulation has been detected by ultrasound a couple of days after the PG injection. This is well captured in the simulation. Not only does this approve our model, we can also observe substances that are not measured within the experiment, and our simulation gives us insight into the development of these substrates after a single $PGF_{2\alpha}$ injection. For example, in Figure 8C we observe a GnRH peak after administration of $PGF_{2\alpha}$, which can be understood as an increase in pulse frequency and is in the scope of expected observations.

4. Conclusions

In this work we have enhanced the model of the bovine estrous cycle which was introduced in [4,6] towards the simulation of synchronization protocols. We have replaced the mechanisms regarding ovulation and refined the modeling of luteolysis. The new components representing oxytocin and interovarian factors have been introduced, integrated, and connected to the other components of the model. To eliminate time delays, certain growth and decay rates, as well as several thresholds and steepness factors have been adjusted. To account for effects observed in experimental data, the relationship between CL growth and the rise of P_4 levels has been modified, the action of Foll has been adjusted accordingly. We have validated our model by capturing the synchronization effect of double $PGF_{2\alpha}$ administration. In our model, the responsiveness of the corpus luteum is the decisive factor for synchronization effects after $PGF_{2\alpha}$ injection.

We have shown simulation results for cows with three follicular waves per cycle. Different parameterizations can also lead to cycles with different wave numbers or irregular wave patterns, but those simulations would go beyond the scope of this work. The original motivation of developing a model of the bovine estrous cycle [4] was to better understand the underlying biological mechanisms and dynamics, but this motivation is not exclusive.

In the future, the model of the bovine estrous cycle could be used within study planning or evaluation, for educational purposes or to assist management decisions. The model could be integrated into existing models, e.g., metabolic networks [1]. New models could also be developed for other aspects interacting with the cycle, e.g., stress, negative energy balance, or milk

production, and then coupled to the model presented in this work. Further applications could be the modeling of pathologic situations, e.g., cystic ovarian disease, anestrous, or inflammation. The model could be used to deeper investigate their interaction with fertility hormones of the cow. Further, an optimal control problem could be formulated to design synchronization protocols regarding optimal dosing and frequency. A future refinement could require the inclusion of reactions that take place on single-cell level, e.g., receptor binding mechanisms as in [33]. The level of detail will be adjusted according to the applications. The direction of future research will highly depend on future collaborations and input from animal reproduction experts. The prospectives will thus depend crucially on the available experimental data and interest of animal scientists in systems biology methods.

Acknowledgments

The authors would like to thank Marike Boer for discussions about luteolysis, Vishal Suthar for providing the progesterone data from the $PGF_{2\alpha}$ study, and Peter Deuflhard for the provided support. Susanna Röblitz and Claudia Stötzel have been supported by the DFG Research Center MATHEON 'Mathematics for Key Technologies' in Berlin, Germany.

References

[1] Baldwin RL. Modeling Ruminant Digestion and Metabolism. Chapman & Hall 1995.
[2] Hill SR, Knowlton KF, Kebreab E, France J, Hanigan MD. A model of phosphorus digestion and metabolism in the lactating dairy cow. J Dairy Sci 2008;91:2021–32.
[3] Dijkstra J, Neal HD, Beever DE, France J. Simulation of nutrient digestion, absorption and outflow in the rumen: model description. J Nutr 1992;122:2239–56.
[4] Boer HMT, Stötzel C, Röblitz S, Deuflhard P, Veerkamp RF, Woelders H. A simple mathematical model of the bovine estrous cycle: follicle development and endocrine interactions. J Theor Biol 2011;278:20–31.
[5] Woelders H, Te Pas MFW, Bannink A, Veerkamp RF, Smits MA. Systems biology in animal sciences. Animal 2011;5:1036–47.
[6] Boer HMT, Röblitz S, Stötzel C, Veerkamp RF, Kemp B, Woelders H. Mechanisms regulating follicle wave patterns in the bovine estrous cycle investigated with a mathematical model. J Dairy Sci 2011;94:5987–6000.
[7] Stevenson JL, Dalton JC, Santos JE, Sartori R, Ahmadzadeh A, Chebel RC. Effect of synchronization protocols on follicular development and estradiol and progesterone concentrations of dairy heifers. J Dairy Sci 2008;91:3045–56.
[8] Schiewe MC, Bush M, Phillips LG, Citino S, Wildt DE. Comparative aspects of estrus synchronization, ovulation induction, and embryo cryopreservation in the scimitar-horned oryx, bongo, eland, and greater kudu. J Exp Zool 1991;258:75–88.
[9] Lauderdale JW. ASAS centennial paper: contributions in the journal of animal science to the development of protocols for breeding management of cattle through synchronization of estrus and ovulation. J Anim Sci 2009;87:801–12.
[10] McCracken JA, Custer EE, Lamsa JC. Luteolysis: A neuroendocrine-mediated event. Physiol Rev 1999;79:263–323.
[11] Skarzynski DJ, Ferreira-Dias G, Okuda K. Regulation of luteal function and corpus luteum regression in cows: hormonal control, immune mechanisms and intercellular communication. Reprod Domest Anim 2008;43:57–65.
[12] Silvia WJ, Lewis GS, McCracken JA, Thatcher WW, Wilson L Jr. Hormonal regulation of uterine secretion of prostaglandin F2α during luteolysis in ruminants. Biol Reprod 1991;45:655–63.
[13] Asselin E, Goff AK, Bergeron H, Fortier MA. Influence of sex steroids on the production of prostaglandins F2α and E2 and response to oxytocin in cultured ephithelial and stromal cells of the bovine endometrium. Biol Reprod 1996;54:371–99.
[14] Xiao CW, Liu JM, Sirois J, Goff AK. Regulation of cyclooxygenase-2 and prostaglandin F synthase gene expression by steroid hormones and interferon-τ in bovine endometrial cells. Endocrinology 1998;139:2293–9.
[15] Schallenberger E, Schams D., Bullermann B, Walters DL. Pulsatile secretion of gonadotrophins, ovarian steroids and ovarian oxytocin during prostaglandin-induced regression of the corpus luteum in the cow. J Reprod Fertil 1984;71:493–501.
[16] Stellflug JN, Louis TM, Hafs HD, Seguin BE. Luteolysis, estrus and ovulation, and blood prostaglandin F after intramuscular administration of 15, 30 or 60 mg prostaglandin F2α. Prostaglandins 1975;9:609–15.
[17] Kroker R. Beeinflussung der Uterusfunktion KR. In: Löscher W, Ungemach F, Kroker R, editors. Pharmakotherapie bei Haus- und Nutztieren; 6th ed. Buchverlag: Parey; 2003, p. 168–71.
[18] Ginther OJ, Araujo RR, Palhão MP, Rodrigues BL, Beg MA. Necessity of sequential pulses of prostaglandin F2α for complete physiologic luteolysis in cattle. Biol Reprod 2009;80:641–8.
[19] Reinecke I. Mathematical modeling and simulation of the female menstrual cycle. Ph.D. Thesis; Freie Universität Berlin; 2009.
[20] Keenan DM, Veldhuis JD. A biomathematical model of time-delayed feedback in the human male hypothalamic-pituitary-leydig cell axis. Am J Physiol Endocrinol - Endocrinol Metab 1998;275:E157–76.
[21] Hixon JE, Hansel W. Evidence for preferential transfer of prostaglandin F2α to the ovarian artery following intrauterine administration in cattle. Biol Reprod 1974;11:543–52.
[22] Kotwica J, Skarzynski D, Miszkiel G, Melin P, Okuda K. Oxytocin modulates the pulsatile secretion of prostaglandin F2α in initiated luteolysis in cattle. Res Vet Sci 1999;66:1–5.
[23] Voss AK, Fortune JE. Estradiol-17β has a biphasic effect on oxytocin secretion by bovine granulosa cells. Biol Reprod 1993;48:1404–9.
[24] Rathbone MJ, Kinder JE, Fike K, Kojima F, Clopton D, Ogle CR, Bunt C. Recent advances in bovine reproductive endocrinology and physiology and their impact on drug delivery system design for the control of the estrous cycle in cattle. Adv Drug Deliv Rev 2001;50(**3**);50:277–320.

[25] Rodgers RJ, Irving-Rodgers HF. Morphological classification of bovine ovarian follicles. Reproduction 2010;139:309–18.
[26] Kastelic JP, Bergfelt DR, Ginther OJ. Relationship between ultrasonic assessment of the corpus luteum and plasma progesterone concentration in heifers. Theriogenology 1990;33: 1269–78.
[27] Deuflhard P, Nowak U. Extrapolation integrators for quasilinear implicit ODEs. Progr Sci Comp 1987;7:37–50.
[28] Nowak U, Deuflhard P. Numerical identification of selected rate constants in large chemical reaction systems. Appl Numer Math 1985;1:59–75.
[29] Deuflhard P, Nowak U. Efficient numerical simulation and identification of large chemical reaction systems. Berichte der Bunsenges Bunsengesellschaft für Phys Chem 1986;90:940–6.
[30] Lin CC, Segel LA. Mathematics Applied to Deterministic Problems in the Natural Sciences; vol. 11. Society for Industrial Mathematics; 1988.
[31] Murugavel K, Yániz JL, Santolaria P, López-Béjar M, López-Gatius F. Prostaglandin based estrus synchronization in postpartum dairy cows: an update. J Appl Res Vet Med 2003;1:51–65.
[32] Stevenson JS, Phatak AP. Rates of luteolysis and pregnancy in dairy cows after treatment with cloprostenol or dinoprost. Theriogenology 2010;73:1127–38.
[33] Röblitz S, Stötzel C, Deuflhard P, Jones H, Azulay DO, van der Graaf P, Martin S. A Mathematical Model of the Human Menstrual Cycle for the Administration of GnRH Analogues. ZIB-Report 11-16. Berlin: Zuse Institute Berlin; 2011, p. 11–6. Available at: http://vs24.kobv.de/opus4-zib/frontdoor/index/index/docId/1273.

Appendix A. Equations

The model describing the bovine estrous cycle without external manipulation consists of 15 ordinary differential equations with 60 parameters. For virtual administration of $PGF_{2\alpha}$ we use one additional ordinary differential equation (ODE) containing three extra parameters.

GnRH:

$$\frac{d}{dt}GnRH_{Hypo}(t) = Syn_{GnRH}(t) - Rel_{GnRH}(t) \quad (1)$$

$$Syn_{GnRH}(t) = c_{GnRH,1} \cdot \left(1 - \frac{GnRH_{Hypo}(t)}{GnRH_{Hypo}^{\max}}\right)$$

$$Rel_{GnRH}(t) = (H_1^-(P4\,\&\,E2) + H_2^-(P4)) \cdot GnRH_{Hypo}(t)$$

$$\frac{d}{dt}GnRH_{Pit}(t) = Rel_{GnRH}(t) \cdot H_3^+(E2) - c_{GnRH,2} \cdot GnRH_{Pit}(t) \quad (2)$$

FSH:

$$\frac{d}{dt}FSH_{Pit}(t) = Syn_{FSH}(t) - Rel_{FSH}(t) \quad (3)$$

$$Syn_{FSH}(t) = H_4^-(Inh)$$

$$Rel_{FSH}(t) = (b_{FSH} + H_5^+(P4) + H_6^-(E2) + H_7^+(GnRH_{Pit})) \cdot FSH_{Pit}(t)$$

$$\frac{d}{dt}FSH_{Bld}(t) = Rel_{FSH}(t) - c_{FSH} \cdot FSH_{Bld}(t) \quad (4)$$

LH:

$$\frac{d}{dt}LH_{Pit}(t) = Syn_{LH}(t) - Rel_{LH}(t) \quad (5)$$

$$Syn_{LH}(t) = H_8^+(E2) + H_9^-(P4)$$

$$Rel_{LH}(t) = (b_{LH} + H_{10}^+(GnRH_{Pit})) \cdot LH_{Pit}(t)$$

$$\frac{d}{dt}LH_{Bld}(t) = Rel_{LH}(t) - c_{LH} \cdot LH_{Bld}(t) \quad (6)$$

Follicles and corpus luteum:

$$\frac{d}{dt}Foll(t) = \widetilde{H}_{11}^+(FSH_{Bld}) - (H_{12}^+(P4) + H_{13}^+(LH_{Bld})) \cdot Foll(t) \quad (7)$$

$$\frac{d}{dt}CL(t) = SF \cdot H_{13}^+(LH_{Bld}) \cdot Foll(t) + H_{14}^+(CL) - H_{15}^+(IOF) \cdot CL(t) \quad (8)$$

Hormones produced in the ovaries:

$$\frac{d}{dt}P4(t) = c_{CL}^{P4} \cdot CL(t)^2 - c_{P4} \cdot P4(t) \quad (9)$$

$$\frac{d}{dt}E2(t) = c_{Foll}^{E2} \cdot Foll(t)^2 - c_{E2} \cdot E2(t) \quad (10)$$

$$\frac{d}{dt}Inh(t) = c_{Foll}^{Inh} \cdot Foll(t)^2 - c_{Inh} \cdot Inh(t) \quad (11)$$

Enzymes, oxytocin and inter-ovarian factors:

$$\frac{d}{dt}Enz(t) = H_{16}^+(P4) - c_{Enz} \cdot Enz(t) \quad (12)$$

$$\frac{d}{dt}OT(t) = H_{17}^+(E2) \cdot CL(t)^2 - c_{OT} \cdot OT(t) \quad (13)$$

$$\frac{d}{dt}IOF(t) = H_{18}^+(PGF\,\&\,CL) - c_{IOF} \cdot IOF(t) \quad (14)$$

$PGF_{2\alpha}$ and synthetic prostaglandin

$$\frac{d}{dt}PGF(t) = H_{19}^{+}(Enz\,\&\,OT) \; - \; c_{PGF} \; \cdot \; PGF(t) \qquad (15)$$

$$\frac{d}{dt}PGF_{syn}(t) = \; D \; \cdot \; \beta^2 \; \cdot \; t_{mod}(t) \; \cdot \; \exp(-\beta \; \cdot \; t_{mod}(t) \;) \; - \; c_{PGF_{syn}} \; \cdot \; PGF_{syn}(t)$$

$$t_{mod}(t) : \; = \; \max(0, t - t_D)$$

Appendix B. List of hill functions

Positive resp. negative Hill functions are defined as

$$h^{+}(S(t);T,n) : = \frac{S(t)^n}{T^n + S(t)^n}, \qquad h^{-}(S(t);T,n) : = \frac{T^n}{T^n + S(t)^n}.$$

The Hill functions listed below are the full notations of the Hill functions mentioned in Section 2.2, in Appendix A. They represent a majority of the mechanisms shown in Fig. 4.

$$H_1^{-}(P4\,\&\,E2) = m_{P4\&E2}^{GnRH} \; \cdot \; (h^{-}(P4(t);\, T_{P4}^{GnRH,1}, 2) \; + \; h^{-}(E2(t),\; T_{E2}^{GnRH,1},\; 2) \; - h^{-}(P4(t);\, T_{P4}^{GnRH,1}, 2) \; \cdot \; h^{-}(E2(t),\; T_{E2}^{GnRH,1}, 2))$$

$$H_2^{-}(P4) = m_{P4}^{GnRH,2} \; \cdot \; h^{-}(P4(t),\; T_{P4}^{GnRH,2}, 2)$$

$$H_3^{+}(E2) = m_{E2}^{GnRH,2} \; \cdot \; h^{+}(E2(t),\; T_{E2}^{GnRH,2}, 5)$$

$$H_4^{-}(Inh) = m_{Inh}^{FSH} \; \cdot \; h^{-}(Inh(t),\; T_{Inh}^{FSH}, 5)$$

$$H_5^{+}(P4) = m_{P4}^{FSH} \; \cdot \; h^{+}(P4(t);\, T_{P4}^{FSH}, 2)$$

$$H_6^{-}(E2) = m_{E2}^{FSH} \; \cdot \; h^{-}(E2(t);\, T_{E2}^{FSH}, 2)$$

$$H_7^{+}(GnRH_{Pit}) = m_{GnRH}^{FSH} \; \cdot \; h^{+}\,(GnRH_{Pit}(t);\, T_{GnRH}^{FSH}, 1)$$

$$H_8^{+}(E2) = m_{E2}^{LH} \; \cdot \; h^{+}(E2(t);\, T_{E2}^{LH}, 2)$$

$$H_9^{-}(P4) = m_{P4}^{LH} \; \cdot \; h^{-}(P4(t);\, T_{P4}^{LH}, 2)$$

$$H_{10}^{+}(GnRH_{Pit}) = \; m_{GnRH}^{LH} \; \cdot \; h^{+}(GnRH_{Pit}(t);\, T_{GnRH}^{LH}, 5)$$

$$\widetilde{H}_{11}^{+}(FSH_{Bld}) = \; m_{FSH}^{Foll} \; \cdot \; h^{+}(FSH_{Bld}(t);\, \widetilde{T}_{FSH}^{Foll}(t), 2), \;\; \widetilde{T}_{FSH}^{Foll}(t) = T_{FSH}^{Foll} \; \cdot \; h^{-}(Foll(t);\, T_{Foll}^{FSH},\; 2)$$

$$H_{12}^{+}(P4) = m_{P4}^{Foll} \; \cdot \; h^{+}(P4(t);\, T_{P4}^{Foll}, 5)$$

$$H_{13}^{+}(LH_{Bld}) = m_{LH}^{Ovul} \; \cdot \; h^{+}(LH_{Bld}(t);\, T_{LH}^{Ovul},\; 2)$$

$$H_{14}^{+}(CL) = \; m_{CL}^{CL} \; \cdot \; h^{+}(CL(t),\; T_{CL}^{CL},\; 2)$$

$$H_{15}^{+}(IOF) = \; m_{IOF}^{CL} \; \cdot \; h^{+}(IOF(t);\, T_{IOF}^{CL},\; 5)$$

$$H_{16}^{+}(P4) = m_{P4}^{Enz} \; \cdot \; h^{+}(P4(t);\, T_{P4}^{Enz},\; 5)$$

$$H_{17}^{+}(E2) = m_{E2}^{OT} \; \cdot \; h^{+}(E2(t);\, T_{E2}^{OT},\; 2)$$

$$H_{18}^{+}(PGF\,\&\,CL) = m_{PGF\&CL}^{IOF} \cdot \; h^{+}(PGF(t) \; + \; PGF_{syn}(t);\, T_{PGF}^{IOF},\; 5) \; \cdot \; h^{+}(CL(t);\, T_{CL}^{IOF}, n_{CL}^{IOF},\; 10)$$

$$H_{19}^{+}(Enz\,\&\,OT) = m_{Enz\&OT}^{PGF} \cdot \; h^{+}(Enz(t);\, T_{Enz}^{PGF},\; 5) \; \cdot \; h^{+}(OT(t);\, T_{OT}^{PGF},\; 2)$$

Appendix C. Parameter values

[·] stands for the unit of the substance, usually a concentration, and can be specified from measurements. Typical units are [FSH] = [LH] = IU/l, [P4] = ng/mL, and [E2] = pg/ml. If units of FSH and luteinizing hormone (LH) differ in pituitary and blood, release-terms have to be scaled adequately. t denotes "'time'"; in our model [·] stands for "'days'"

Par. No.	Symbol	Value	Unit
1	$GnRH_{Hypo}^{\max}$	16	$[GnRH_{Hypo}]$
2	$c_{GnRH,1}$	2.75	$\frac{[GnRH_{Hypo}]}{[t]}$
3	$m_{P4\&E2}^{GnRH}$	2.05	1/[t]
4	$T_{E_2}^{GnRH,1}$	0.0972	[E2]
5	$T_{P_4}^{GnRH,1}$	0.35	[P4]
6	$m_{P_4}^{GnRH,2}$	1.91	1/[t]
7	$T_{P_4}^{GnRH,2}$	0.252	[P4]
8	$m_{E_2}^{GnRH,2}$	0.99	$\frac{[GnRH_{Pit}]}{[GnRH_{Hypo}]}$
9	$T_{E_2}^{GnRH,2}$	0.648	[E2]
10	$c_{GnRH,2}$	1.63	1/[t]
11	m_{Inh}^{FSH}	4.21	[FSH]/[t]
12	T_{Inh}^{FSH}	0.118	[Inh]
13	b_{FSH}	0.948	1/[t]
14	$m_{P_4}^{FSH}$	0.293	1/[t]
15	$T_{P_4}^{FSH}$	0.152	[P4]
16	$m_{E_2}^{FSH}$	0.396	1/[t]
17	$T_{E_2}^{FSH}$	0.312	[E2]
18	m_{GnRH}^{FSH}	1.23	1/[t]
19	T_{GnRH}^{FSH}	0.0708	$[GnRH_{Pit}]$
20	c_{FSH}	2.73	1/[t]
21	$m_{E_2}^{LH}$	0.376	[LH]/[t]
22	$T_{E_2}^{LH}$	0.243	[E2]

Par. No.	Symbol	Value	Unit
23	$m_{P_4}^{LH}$	2.71	[LH]/[t]
24	$T_{P_4}^{LH}$	0.0269	[P4]
25	b_{LH}	0.0141	1/[t]
26	m_{GnRH}^{LH}	2.22	1/[t]
27	T_{GnRH}^{LH}	0.69	[$GnRH_{Pit}$]
28	c_{LH}	12.0	1/[t]
29	m_{FSH}^{Foll}	0.562	[Foll]/[t]
30	T_{FSH}^{Foll}	0.57	[FSH]
31	T_{Foll}^{FSH}	0.22	[Foll]
32	$m_{P_4}^{Foll}$	1.1	1/[t]
33	$T_{P_4}^{Foll}$	0.126	[P4]
34	m_{LH}^{Ovul}	3.49	1/[t]
35	T_{LH}^{Ovul}	0.171	[LH]
36	SF	0.2	[CL]/[t]
37	m_{CL}^{CL}	0.0353	[CL]/[t]
38	T_{CL}^{CL}	0.1	[CL]
39	m_{IOF}^{CL}	41.39	1/[t]
40	T_{IOF}^{CL}	1.32	[IOF]
41	$c_{CL}^{P_4}$	2.25	$\frac{[P_4]/[CL]^2}{[t]}$
42	cP_4	1.41	1/[t]
43	$c_{Foll}^{E_2}$	2.19	$\frac{[E2]/[Foll]^2}{[t]}$
44	c_{E2}	1.23	1/[t]
45	c_{Foll}^{Inh}	1.41	$\frac{[Inh]/[Foll]^2}{[t]}$
46	c_{Inh}	0.475	1/[t]
47	m_{P4}^{Enz}	3.58	[Enz]/[t]
48	T_{P4}^{Enz}	0.77	[P4]
49	c_{Enz}	2.98	1/[t]
50	m_{E2}^{OT}	1.59	$\frac{[OT]/[CL]^2}{[t]}$
51	T_{E2}^{OT}	0.143	[E2]
52	c_{OT}	0.644	1/[t]
53	$m_{PGF\&CL}^{IOF}$	39.68	[IOF]/[t]
54	T_{PGF}^{IOF}	1.22	[PGF]
55	T_{CL}^{IOF}	0.6	[CL]
56	c_{IOF}	0.298	1/[t]
57	$m_{Enz\&OT}^{PGF}$	53.91	[PGF]/[t]
58	T_{Enz}^{PGF}	1.43	[Enz]
59	T_{OT}^{PGF}	1.087	[OT]
60	c_{PGF}	1.23	1/[t]
	D	3.7	[PGF]
	β	100	1/[t]
	$c_{PGF_{syn}}$	5.5	1/[t]

RESEARCH

Impaired LH surge amplitude in gonadotrope-specific progesterone receptor knockout mice

Chirine Toufaily[1,*], Gauthier Schang[1,*], Xiang Zhou[1], Philipp Wartenberg[2], Ulrich Boehm[2], John P Lydon[3], Ferdinand Roelfsema[4] and **Daniel J Bernard[1]**

[1]Department of Pharmacology and Therapeutics, McGill University, Montréal, Québec, Canada
[2]Department of Experimental Pharmacology, Center for Molecular Signaling, Saarland University School of Medicine, Homburg, Germany
[3]Department of Molecular and Cellular Biology, Baylor College of Medicine, Houston, Texas, USA
[4]Department of Internal Medicine, Section Endocrinology and Metabolic Diseases, Leiden University Medical Center, Leiden, The Netherlands

Correspondence should be addressed to D J Bernard: daniel.bernard@mcgill.ca

*(C Toufaily and G Schang contributed equally to this work)

Abstract

The progesterone receptor (PR, encoded by *Pgr*) plays essential roles in reproduction. Female mice lacking the PR are infertile, due to the loss of the protein's functions in the brain, ovary, and uterus. PR is also expressed in pituitary gonadotrope cells, but its specific role therein has not been assessed *in vivo*. We therefore generated gonadotrope-specific *Pgr* conditional knockout mice (cKO) using the Cre-LoxP system. Overall, both female and male cKO mice appeared phenotypically normal. cKO females displayed regular estrous cycles (vaginal cytology) and normal fertility (litter size and frequency). Reproductive organ weights were comparable between wild-type and cKO mice of both sexes, as were production and secretion of the gonadotropins, LH and FSH, with one exception. On the afternoon of proestrus, the amplitude of the LH surge was blunted in cKO females relative to controls. Contrary to predictions of earlier models, this did not appear to derive from impaired GnRH self-priming. Collectively, these data indicate that PR function in gonadotropes may be limited to regulation of LH surge amplitude in female mice via a currently unknown mechanism.

Key Words

- progesterone receptor
- LH
- FSH
- gonadotropes

Journal of Endocrinology (2020) **244**, 111–122

Introduction

The progesterone receptor (PR, product of the *Pgr* gene) plays fundamental and pleiotropic roles in the control of reproduction. This is perhaps most clearly demonstrated in female *Pgr*-knockout mice, which are infertile because of impairments in LH surges from the pituitary, LH-induced meiotic maturation and ovarian follicle rupture, uterine decidualization, and sexual behavior (Lydon *et al.* 1995, Chappell *et al.* 1999). The LH surge is driven by ovarian estrogens, which have positive feedback effects at both the hypothalamic and pituitary levels. In the hypothalamus, estrogens stimulate expression of kisspeptin (*Kiss1*) in neurons of the anteroventral periventricular nucleus (AVPV); kisspeptin, in turn, stimulates GnRH release (Messager *et al.* 2005, d'Anglemont de Tassigny *et al.* 2008). In the pituitary, high levels of estrogens increase the sensitivity of gonadotrope cells to GnRH, amplifying LH release (Lasley *et al.* 1975, Dafopoulos *et al.* 2004). Estrogens stimulate PR expression in multiple cell types, and PRs in kisspeptin neurons play essential roles in estrogen-positive feedback. Indeed, estradiol-induced LH surges, ovulation (as reflected by corpora lutea numbers), and fertility (e.g., litter size) are impaired in female mice with conditional

https://joe.bioscientifica.com
https://doi.org/10.1530/JOE-19-0013

deletion of *Pgr* in kisspeptin neurons (Stephens *et al*. 2015, Gal *et al*. 2016). Though kisspeptin expression appears to be normal in the AVPV of these animals, the data indicate that LH surges in mice depend, at least in part, on intact PR function in kisspeptin neurons.

These results do not, however, rule out an additional role for the PR in estrogen-positive feedback and LH surge generation at the pituitary level. Estrogens induce PR expression in gonadotropes and PR has been suggested to modulate GnRH action (i.e., self-priming) therein (Turgeon & Waring 1994, Aguilar *et al*. 2003). GnRH self-priming is a phenomenon in which prior GnRH pulses potentiate the actions of subsequent GnRH pulses on LH release (Waring & Turgeon 1980, Higuchi & Kawakami 1982). Self-priming, which is more pronounced in rats than mice, is estrogen and protein-synthesis dependent, but does not require increases in GnRH receptor numbers (Pickering & Fink 1976, Colin *et al*. 1996). Rather, GnRH actions appear to be enhanced in a cAMP- and PR-dependent manner (Turgeon & Waring 1994, Abdilnour & Bourne 1995). For example, GnRH self-priming is reduced, though not completely eliminated, in estradiol-treated pituitary cultures of *Pgr*-knockout mice (Turgeon & Waring 2001). Similarly, GnRH self-priming is blocked in ovariectomized, estradiol-treated *Pgr*-knockout mice *in vivo* (Chappell *et al*. 1999). Nevertheless, the necessity for PR function in gonadotropes for gonadotropin production, LH surge dynamics, and fertility have not been assessed. To address these gaps in knowledge, we generated gonadotrope-specific *Pgr*-knockout mice.

Materials and methods

Animals

The $Pgr^{fx/fx}$ and $Gnrhr^{IRES\text{-}Cre/IRES\text{-}Cre}$ (GRIC) mice were described previously (Wen *et al*. 2008, Fernandez-Valdivia *et al*. 2010). $Pgr^{fx/fx}$ males were crossed with GRIC females to generate $Pgr^{fx/+}$;$Gnrhr^{GRIC/+}$ progeny. $Pgr^{fx/+}$;$Gnrhr^{GRIC/+}$ females were then crossed to $Pgr^{fx/fx}$ males to generate $Pgr^{fx/fx}$;$Gnrhr^{+/+}$ controls and $Pgr^{fx/fx}$;$Gnrhr^{GRIC/+}$ conditional knockouts (cKOs). In order to purify gonadotropes by fluorescence-activated cell sorting (FACS), we crossed $Pgr^{fx/fx}$ animals with $Gt(ROSA26)^{ACTB\text{-}tdTomato\text{-}EGFP}$ mice (mTmG/mTmG, stock 007676 from Jackson Laboratories) to generate $Pgr^{fx/fx}$;$Rosa26^{mTmG/mTmG}$ males, which were then crossed to $Pgr^{fx/+}$;$Gnrhr^{GRIC/+}$ females to generate $Pgr^{fx/fx}$;$Gnrhr^{GRIC/+}$;$Rosa26^{mTmG/+}$ males and females. Controls for FACS were generated by crossing $Rosa26^{mTmG/mTmG}$ and GRIC mice to generate $Pgr^{+/+}$;$Gnrhr^{GRIC/+}$;$Rosa26^{mTmG/+}$ progeny. Genotyping and assessment of genomic recombination were conducted as previously described (Zhou *et al*. 2016) (primers listed in Table 1). All animal experiments were performed in accordance with institutional and federal guidelines and were approved by the McGill University and Goodman Cancer Centre Facility Animal Care Committee (Protocol 5204).

Fluorescence-activated cell sorting of gonadotropes

FACS was performed at the Cell Vision Core Facility for Flow Cytometry and Single Cell Analysis of the Life Science Complex at the Rosalind and Morris Goodman Cancer Research Centre at McGill University. Pituitary cell dispersion and cell sorting were performed as previously described (Ho *et al*. 2011, Li *et al*. 2017). Here, EGFP-positive (gonadotropes) and tdTomato-positive (non-gonadotropes) cells were sorted from control and cKO animals. On average, 1.2×10^4 EGFP-positive and 2.5×10^5 tdTomato-positive cells were obtained from each group (ten mice per group).

Assessment of female puberty onset, estrous cyclicity, and fertility

Females were monitored daily after weaning (postnatal day 21) to determine the onset of vaginal opening. At 6 weeks of age, estrous cyclicity was assessed by daily vaginal swabs for 3 weeks. Vaginal cells were smeared on glass slides and stained with 0.1% methylene blue to identify cycle stages (Caligioni 2009). The number of days spent in each stage (proestrus, estrus, or diestrus/metestrus) was then counted and divided by the total number of days to determine the relative proportion of time spent in each stage. At 9 weeks of age, a group of females ($n=6$ per genotype) were mated with wild-type age-matched C57BL/6 males (Charles River) for 6 months. Breeding cages were monitored daily, and the date of birth and number of pups were recorded.

Reproductive organ collection

Testes, seminal vesicles, ovaries, and uteri were dissected from 10-week-old control and cKO males and females. Females were killed at 07:00 h on the morning of estrus. All organs were weighed on a precision balance.

Blood collection

Blood was collected from 10-week-old control and cKO males and females (07:00 h on estrus morning) by cardiac

https://joe.bioscientifica.com
https://doi.org/10.1530/JOE-19-0013

Table 1 Primer sequences.

Genotyping primers	
Pgr primer 1 (forward)	GTATGTTTATGGTCCTAGGAGCTGGG
Pgr primer 2 (reverse)	TGCTAAAGGTCTCCTCATGTAATTGGG
Pgr primer 3 (recombination; reverse)	CTGGAAGTAGGATAGAATAATTGGCCTT
GRIC primer 1 (forward)	GGACATGTTCAGGGATCGCCAGGC
GRIC primer 2 (reverse)	GCATAACCAGTGAAACAGCATTGCTG
mTmG primer 1 (WT forward)	AGGGAGCTGCAGTGGAGTAG
mTmG primer 2 (mutant forward)	TAGAGCTTGCGGAACCCTTC
mTmG primer 3 (common reverse)	CTTTAAGCCTGCCCAGAAGA
qPCR primers	
Rpl19 (forward)	CGGGAATCCAAGAAGATTGA
Rpl19 (reverse)	TTCAGCTTGTGGATGTGCTC
Fshb (forward)	GTGCGGGCTACTGCTACACT
Fshb (reverse)	CAGGCAATCTTACGGTCTCG
Lhb (forward)	ACTGTGCCGGCCTGTCAACG
Lhb (reverse)	AGCAGCCGGCAGTACTCGGA
Cga (forward)	TCCCTCAAAAAGTCCAQGAGC
Cga (reverse)	GAAGAGAATGAAGAATATGCAG
Gnrhr (forward)	TTCGCTACCTCCTTTGTCGT
Gnrhr (reverse)	CACGGGTTTAGGAAAGCAAA
Pgr (forward)	GTCACTATGGCGTGCTTACCT
Pgr (reverse)	TCAGACGACATGCTGGGCA

puncture, allowed to clot for 30 min at room temperature, and spun down at 850***g*** for 10 min to collect serum. Sera were stored at −20°C until assayed for LH and FSH. To assess LH pulsatility in males, four microliters of blood were collected from the tail tip, every 10 min over 4 h, starting 2 h before lights off. To assess LH surge amplitude in females, four blood samples (four microliters each) were collected from the tail tip over 10 consecutive days: at 10:00 h and at 18:00, 19:00 and 20:00 h (light cycle on/off at 07:00 h/19:00 h). For all tail tip blood collections, the animals were acclimatized to the procedure by massaging the tail for 2 weeks prior to the start of the blood collection. All tail tip blood samples were immediately diluted (1:30) in 1× PBS containing 0.05% of Tween, gently vortexed, and placed on dry ice. Blood dilutions were stored at −80°C until LH ELISAs were performed.

In the LH surge experiment, we compared the maximal LH level obtained from each animal on proestrus afternoon (peak). In females surging more than once over the 10-day sampling period, an average of the maximal value was calculated and used in the analysis. With the sampling method used, we may have missed the true peak of the LH surge. Nevertheless, it enabled us to observe one or more surges in all animals, which would not have been the case if we relied exclusively on vaginal smears for staging proestrus. Moreover, the same approach was used for all animals, and the pattern of results was comparable between the two genotypes.

Hormone analyses

Serum FSH levels were assessed by a Milliplex kit (Millipore, MPTMAG-49K, custom-made for FSH only) following the manufacturer's instructions (minimal detection limit: 9.5 pg/mL; intra-assay CV <15%). Serum and whole blood LH levels were measured using an in-house sandwich ELISA as previously described in Steyn *et al*. (2013), Czieselsky *et al*. (2016), Li *et al*. (2017) (detection limit: 0.117 to 30 ng/mL; an intra-assay CV <10%). As we reported previously (and as seen here), LH levels are higher in serum than whole blood samples (Li *et al*. 2018*b*).

Reverse transcription and quantitative-PCR

Pituitary glands were dissected from control and cKO animals (10 weeks old; females were killed at 07:00 h on estrous morning), snap-frozen in liquid nitrogen, and stored at −80°C. Pituitaries were homogenized in TRIzol reagent (15596018, ThermoFisher Scientific), and total RNA was extracted following the manufacturer's guidelines. For cells from the FACS experiments, total RNA was extracted using a Total RNA Mini Kit (Geneaid, RB300, New Taipei City, Taiwan). Reverse transcription was performed as previously described (Turgeon *et al*. 2017) using Moloney murine leukemia virus reverse transcriptase (0000172807, Promega) and random hexamers (0000184865, Promega). qPCR was run on a Corbett Rotorgene 600 instrument (Corbett Life Science) using EvaGreen qPCR Mastermix

https://joe.bioscientifica.com
https://doi.org/10.1530/JOE-19-0013

(ABMMmix-S-XL; Diamed, Mississauga, ON, Canada) and the primers are listed in Table 1. Expression levels of genes of interest were determined using the $2^{-\Delta\Delta Ct}$ method (Livak & Schmittgen 2001) and ribosomal protein L19 (*Rpl19*) for normalization. All primers were validated for efficiency and specificity.

GnRH self-priming

The protocol to examine GnRH self-priming was adapted from Chappell *et al.* (1999), with some modifications based on Higuchi & Kawakami (1982). Indeed, changes were required because we were unsuccessful in reliably and consistently observing GnRH self-priming in wild-type mice using the protocol described in Chappell *et al.* (1999). We developed a reliable and reproducible self-priming method after several rounds of optimization. Females (7 to 9 weeks of age) were ovariectomized in accordance with standard operating procedure 206 of the McGill University and Goodman Cancer Centre Facility Animal Care Committee. Briefly, an incision was made at the midline of the mid-dorsum of the animal. On each side of the animal, a small incision was made in the muscle above the ovary, and the ovary pulled out of the body cavity with forceps. The tissue was then cauterized at the level of the oviduct and the ovary was removed. All incisions were closed by sutures. One week following ovariectomy, each female was given a s.c. injection of 2 µg estradiol benzoate (EB, E8515, Sigma-Aldrich) dissolved in sesame oil (100 µL of a 0.02 µg/µL solution) between 09:30 and 10:00 h. At 07:00 h on the next day, blood from the tail tip was collected as described above. Each female was then given six consecutive s.c. injections of 50 ng GnRH (L8008, Sigma-Aldrich) (100 µL of a 0.5 ng/µL solution) at 1-h intervals. Blood from the tail tip was collected 10 min after each GnRH administration. To minimize stress associated with frequent sampling and injections, mice were handled daily for 2 weeks prior to the onset of injections. Blood samples were diluted and frozen as described above. Samples were then stored at −80°C until LH ELISAs were performed.

Immunofluorescence

GRIC mice were crossed to eR26-τGFP mice (Wen *et al.* 2011) to produce animals in which Cre-expressing cells are tagged with τGFP (GRIC/eR26-τGFP). Eight week-old animals were transcardially perfused with 4% paraformaldehyde (158127 Sigma-Aldrich) in 0.1 M PBS (P3813, Sigma-Aldrich) under ketamine/xylazine (7005294 and 10124950, Serumwerk Bernburg, Bernburg, Germany) anesthesia. Brains were removed, soaked in fixative for 2 h and 18% sucrose overnight, and then frozen in optimal cutting temperature (OCT) (14020108926, Leica). Serial 14-µm coronal cryosections were thaw mounted onto SuperFrost Plus slides (10149870 Thermo Fisher). Brain sections were blocked in 0.1 M PBS, 0.3% Triton X-100, 10% donkey serum (017-000-121, Jackson ImmunoResearch) and 3% BSA (A2153, Sigma-Aldrich) and incubated with chicken anti-GFP (1:1000, A10262, Thermo Fisher) and rabbit anti-kisspeptin (1:500, AB9754, Millipore) overnight at 4°C, followed by goat anti-chicken 488 (1:500, A11039, Thermo Fischer, Waltham, Massachusetts, USA) and biotinylated donkey anti-rabbit (1:500, BA-1000, Vector Laboratory, Burlingame, CA, USA) and streptavidin CY5 (1:500, 016-170-084, Jackson ImmunoResearch Inc). For nuclear staining, sections were incubated with 5 µg/mL Hoechst 33258 dye (14530, Sigma-Aldrich) in 0.1 M PBS for 5 min and mounted with Fluoromount-G (0100-01, Southern Biotech, Birmingham, Alabama, USA). Sections were analyzed on an Imager.M2 microscope equipped with AxioVision software (Zeiss).

Statistical analysis

All data were analyzed on GraphPad Prism 6 using Student *t*-tests. Results were considered statistically significant when $P<0.05$. For LH pulses, data were deconvoluted using MatLab (Veldhuis *et al.* 2016) and number of pulses were compared between genotypes using Student *t*-test. Comparisons between the two groups of mice challenged with GnRH were done with the GLM procedure for repeated measurements. Calculations were performed with Systat 13 (Systat Software, Inc, San Jose, CA, USA).

Results

Generation of progesterone receptor conditional knockout mice

To address the role of the PR in gonadotropes, we generated gonadotrope-specific *Pgr*-knockout (cKO) mice by crossing floxed *Pgr* ($Pgr^{fx/fx}$) and GRIC mice ($Gnrhr^{GRIC/GRIC}$). First, we verified *Pgr* recombination in different tissues from controls and cKOs of both sexes. As expected, recombination was restricted to the pituitary of both females and males, and to the testes and epididymides of males (Fig. 1A). Next, we quantified the efficiency and specificity of *Pgr* recombination by assessing the level of *Pgr* mRNA expression in purified gonadotropes (Cre-recombinase expressing cells, EGFP-positive) compared to other cell

https://joe.bioscientifica.com
https://doi.org/10.1530/JOE-19-0013

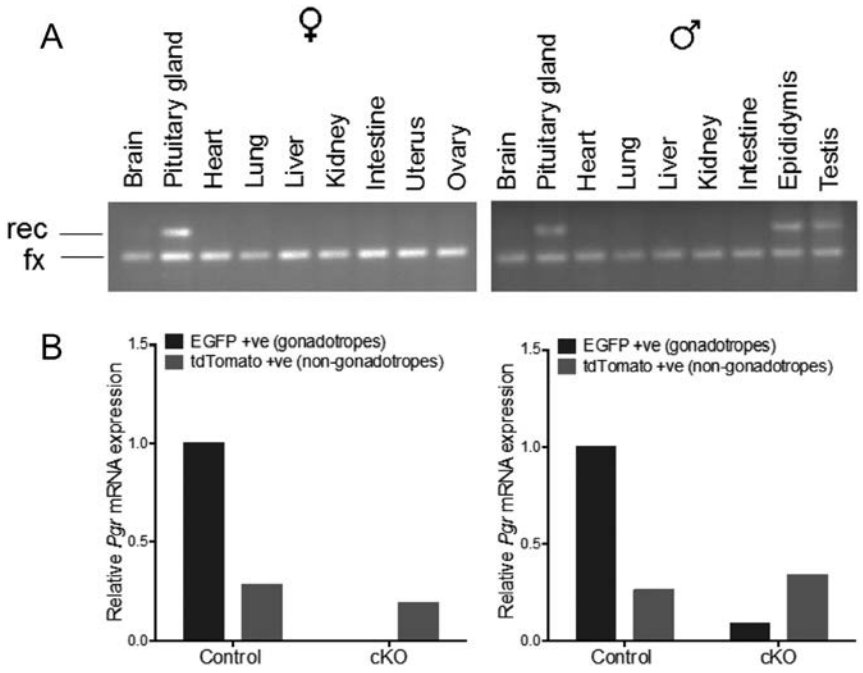

Figure 1
Pgr recombination efficiency and specificity in gonadotrope cells. (A) PCR of genomic DNA from different tissues shows the specificity of recombination in the pituitary glands of female (left) and male cKOs (right), as well as in the epididymis and testis in males (right). rec: recombined; fx: floxed. (B) Quantitative-PCR of cDNA from control ($Pgr^{+/+}$;$Rosa26^{mTmG/+}$;$Gnrhr^{GRIC/+}$) and cKO ($Pgr^{fx/fx}$;$Rosa26^{mTmG/+}$;$Gnrhr^{GRIC/+}$) mice, showing *Pgr* expression in purified gonadotrope (EGFP +ve, black) versus non-gonadotrope (tdTomato +ve, gray) cells, in females (left) and males (right).

populations in the pituitary (Cre-negative, tdTomato-positive). In both male and female cKOs, *Pgr* expression was markedly reduced in gonadotropes (Fig. 1B, green bars). *Pgr* expression in non-gonadotropes (lactotropes) was intact (Fig. 1B, red bars). Recent single-cell RNA-seq data confirm that *Pgr* expression is enriched in gonadotropes and lactotropes in murine pituitaries (Cheung *et al*. 2018).

Normal fertility and gonadal development in *Pgr* cKO mice

cKO females and their control littermates reached puberty at similar ages, as assessed by vaginal opening (Fig. 2A). We did not measure the day of first estrus, which is considered by some to be a more robust measure of puberty onset

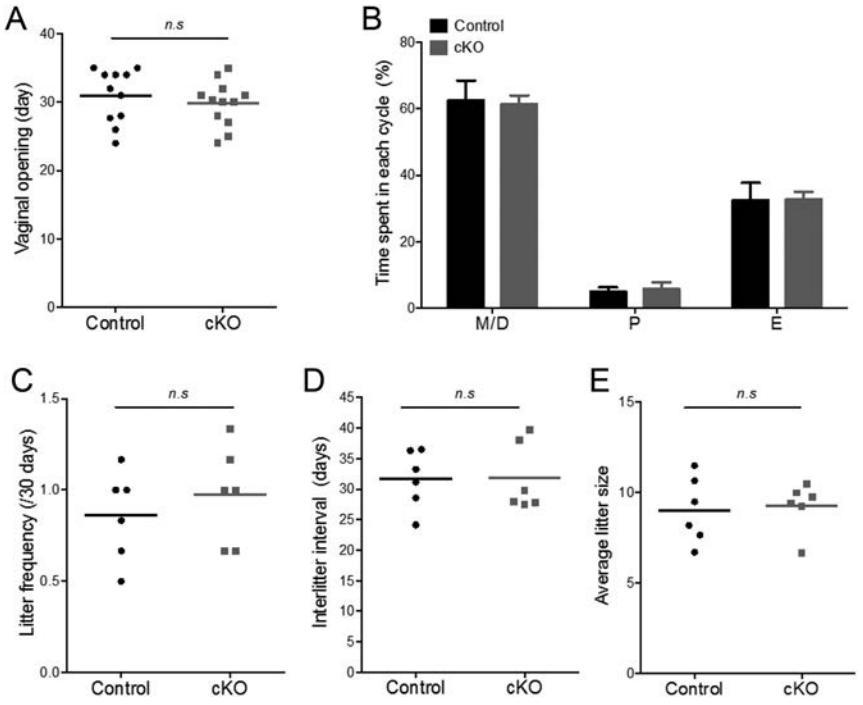

Figure 2
Pgr expression in gonadotropes is not essential for normal reproductive function in female mice. (A) Age of vaginal opening (days) in female control (black) and cKO mice (gray). (B) Percentage of time spent in each stage of the estrous cycle in control and cKO females. (C, D and E) Fertility in control and cKO females. (C) Frequency of delivery per 30 days, (D) inter-litter interval (days), and (E) average litter size for each mouse ($n = 6$ per genotype). Two samples Student *t*-test was performed for statistical analysis. n.s, non-significant; M/D, metestrus/diestrus; P, proestrus; and E, estrus.

https://joe.bioscientifica.com
https://doi.org/10.1530/JOE-19-0013

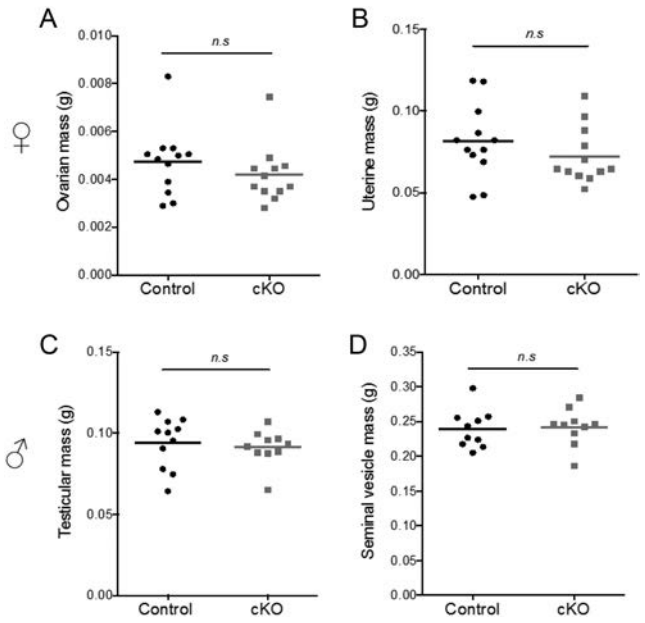

Figure 3
Normal reproductive organ weights in female and male *Pgr* cKO mice. (A) Ovarian and (B) uterine mass in 10-week-old control and cKO females ($n = 12$). (C) Testicular and (D) seminal vesicle mass in 10-week-old control and cKO males ($n = 10$). Student *t*-tests were performed for statistical analysis. n.s, non-significant.

than vaginal opening. However, the other phenotypes in these mice (or lack thereof) suggest that day of first estrus was unlikely to be affected. *Pgr* cKO females had normal estrous cyclicity, as assessed by vaginal cytology (Fig. 2B). In breeding trials, frequency of delivery, inter-litter interval, and average litter size were comparable between control and cKO females (Fig. 2C, D and E). Ovarian and uterine masses were also normal in cKO females (Fig. 3A and B). In males, testicular and seminal vesicle masses were equivalent between genotypes (Fig. 3C and D).

FSH and LH production is intact in *Pgr* cKO mice

Although fertility and gonadal development were apparently unaffected in the absence of gonadotrope PR function, we measured serum LH and FSH levels in both females and males. Blood samples were collected from control and cKO females on the morning of estrus, just after lights on. Serum FSH (Fig. 4A and B) and LH levels (Fig. 4C and D) were equivalent between genotypes. Similarly, pituitary expression of the gonadotropin subunit genes (*Fshb*, *Lhb*, and *Cga*) and the GnRH receptor (*Gnrhr*, Fig. 5) did not differ between control and cKO mice, with two exceptions (Fig. 5F and H). *Cga* mRNA levels were reduced and *Gnrhr* mRNA levels increased in cKO males relative to controls. The variation in serum FSH and pituitary *Fshb* mRNA levels is likely explained by the fact that some females were still in the midst of the secondary surge, while others were not at the time of sampling.

Pulsatile LH secretion is normal in *Pgr* cKO males

While there were no apparent effects of PR loss on LH production, we next examined LH pulse frequency. We focused on males, as LH pulsatility varies markedly across the estrous cycle in females (Czieselsky *et al.* 2016). There were no genotype-dependent differences in LH pulse amplitude or frequency (Fig. 6 and Table 2).

Female *Pgr* cKO mice have blunted preovulatory LH surges

We assessed the role of PR in gonadotropes on the LH surge. Profiles of the LH surge in controls (left) and cKOs (right) are shown in Fig. 7A and B, respectively. The number of surges detected across the 10-day sampling period appeared to be reduced in cKO females, but this was not statistically significant (Fig. 7C). Next, we compared the amplitude of the LH surge between controls and cKOs.

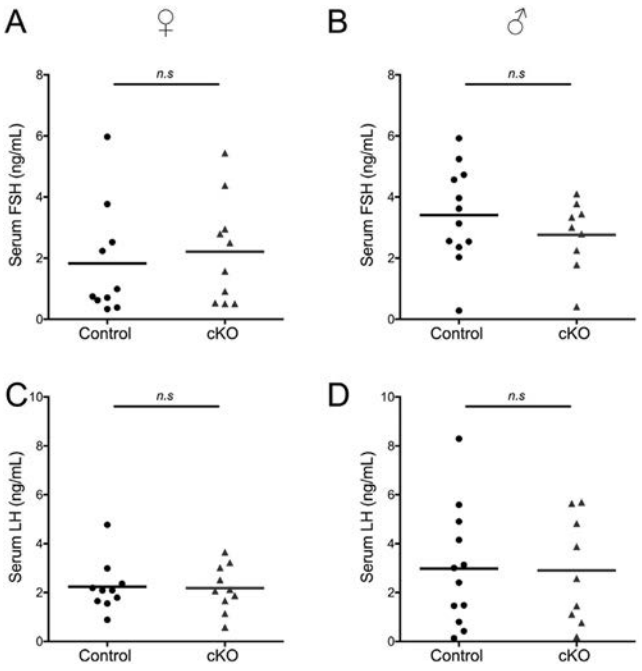

Figure 4
Intact serum gonadotropin levels in both female and male *Pgr* cKO mice. (A and B) Serum FSH and (C and D) LH levels in 10-week-old control and cKO females ($n = 10$ per genotype, left panels) and males ($n = 12$ controls and $n = 9$ cKO, right panels). Female samples were collected at 07:00 h on estrous morning. Student *t*-tests were performed for statistical analysis. n.s., non-significant.

https://joe.bioscientifica.com
https://doi.org/10.1530/JOE-19-0013

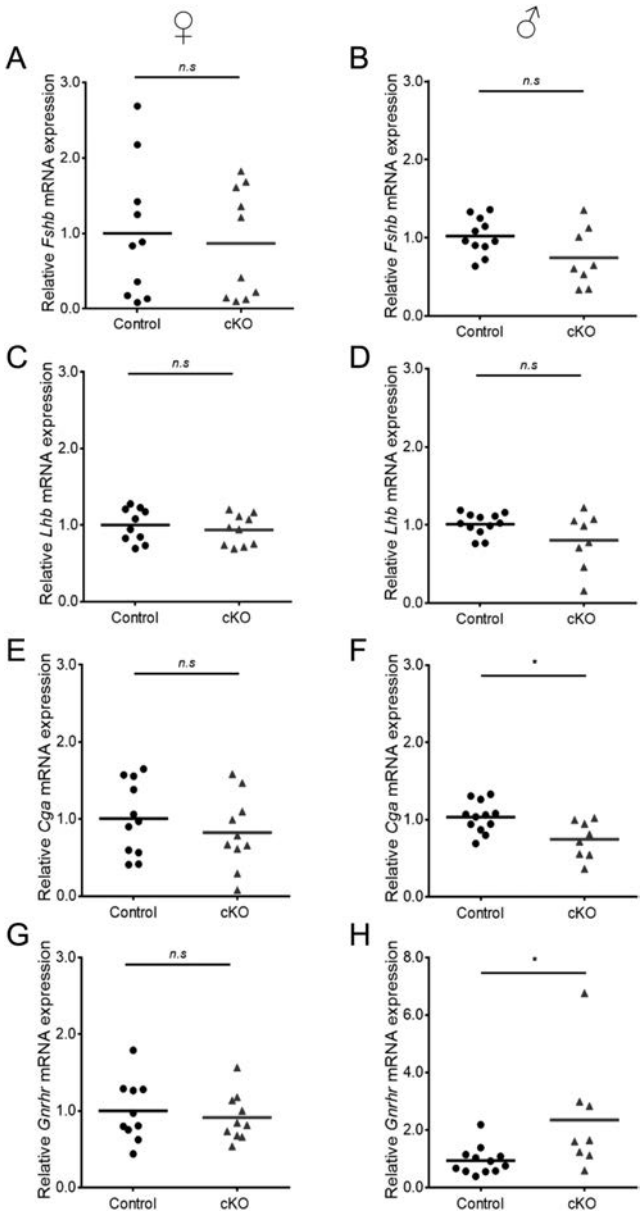

Figure 5
No differences in the expression of pituitary gonadotropin subunits in *Pgr* cKO mice. (A and B) FSHβ-subunit (*Fshb*), (C and D) LH β-subunit (*Lhb*), (E and F) common α-subunit (*Cga*), and (G and H) GnRH receptor (*Gnrhr*) mRNA levels in 10-week-old control and cKO females ($n = 10$ per genotype, left panels) and males ($n = 12$ controls and $n = 8$ cKO, right panels). Female samples were collected at 07:00 h on estrous morning. Student *t*-tests were performed for statistical analysis. $^*P < 0.05$, n.s, non-significant.

Consistent with data from the morning of estrus (Fig. 4C), there was no genotype difference in LH levels on the morning of proestrus. Although most of the mice surged during the 10-day period (Fig. 7A, B and C), the maximal LH levels measured during the surge were significantly lower in cKO relative to control females (Fig. 7D).

Female *Pgr* cKO mice do not display impaired GnRH self-priming

Finally, based on previous reports (Waring & Turgeon 1992, Turgeon & Waring 1994, 2001, Chappell *et al.* 1999, Aguilar *et al.* 2003, Attardi *et al.* 2007), we assessed the effects of gonadotrope-specific PR loss on GnRH self-priming as a potential mechanism underlying reduced LH surge amplitude in these animals. Mean serum LH levels before the first GnRH injection and 10 min after each injection (six injections in total) are shown in Fig. 8. The amplitude of GnRH-stimulated LH release increased following successive GnRH injections, indicating that self-priming occurred in both genotypes. Blood LH concentrations increased after GnRH administration (ANOVA: $P<0.0001$), but there was no difference between genotypes ($P=0.90$) and no interaction between time and genotype ($P=0.70$). There was a highly significant difference in LH increase between the first and subsequent GnRH injections, and the second and the fourth and following administrations (P values between 0.0001 and 0.012), but thereafter this effect leveled off.

Discussion

We generated conditional *Pgr*-knockout mice to assess PR function in pituitary gonadotrope cells. The data suggest that PR's primary role in this cell type is to regulate the amplitude of the LH surge in females. We did not observe any other alterations in reproductive physiology in either sex. As *Pgr* knockdown was highly efficient, the apparently normal gonadotropin synthesis and secretion in males and females (except on proestrus) is unlikely to derive from preservation of some PR function (i.e., incomplete recombination by Cre). Indeed, global *Pgr*-knockout mice similarly show normal LH and FSH production under most conditions (Chappell *et al.* 1997). Overall, our results confirm and extend some previous observations, while challenging other *in vivo* and *in vitro* findings.

Results from global *Pgr*-knockout mice suggest that the PR plays an important role in GnRH self-priming in gonadotropes (Chappell *et al.* 1999, Turgeon & Waring 2001). Therefore, the most parsimonious explanation of the blunted LH surge in *Pgr* cKO mice would be impaired GnRH self-priming. However, we did not observe any such impairment, at least under the conditions used here. We attempted to employ the protocol described in Chappell *et al.* (1999), but the GnRH dose used previously (~4 ng) was insufficient to stimulate LH release in our hands

https://joe.bioscientifica.com
https://doi.org/10.1530/JOE-19-0013

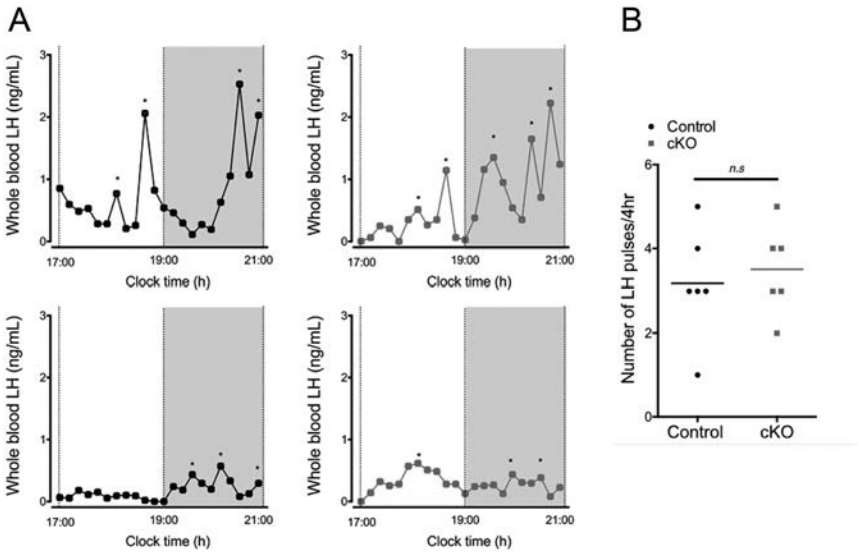

Figure 6
Normal LH pulses in cKO males. Blood samples were collected over 4 h at 10-min intervals from either control ($n = 7$) and cKO ($n = 6$) males. (A) Representative profiles of LH secretion from two control (black graphs, left) and two cKO (gray graphs, right) males. The gray area represents the period of lights-off on a 07:00/19:00 h (on/off) light/dark cycle. Each asterisk (*) indicates a pulse. (B) Quantification of the number of LH pulses in the 4-h sampling period. Student *t*-tests were performed for statistical analysis. n.s, non-significant.

(data not shown). We developed a new protocol based on a previous report in rats (Higuchi & Kawakami 1982). Here, we modified the estrogen priming (no 17β-estradiol implant added during the ovariectomy, and we increased the amount of EB to 2μg), GnRH dose (50 ng per injection), and frequency of GnRH treatment (once per hour, for a total of six injections) relative to Chappell *et al.* (1999). We observed enhanced LH release with successive GnRH injections (indicative of self-priming), but there was no difference between genotypes. The data suggest that PR is not required for GnRH self-priming in murine gonadotropes and that PR regulates LH surge amplitude via a distinct mechanism in these cells.

It is also possible that reduced LH surge amplitude might be explained by effects originating outside of the gonadotrope. For example, *Pgr* cKO females could have reduced circulating estradiol levels relative to control. We did not assess this parameter as, in our experience, measurements of serum estradiol levels in mice are unreliable (Haisenleder *et al.* 2011, Fortin *et al.* 2014, Li *et al.* 2017). However, as FSH and LH production, and ovary and litter sizes, are normal in *Pgr* cKO mice, there is no reason to suspect impairments in gonadotropin-stimulated estradiol production. Alternatively, as Cre activity has been observed in some neurons of GRIC mice (Wen *et al.* 2010, Schauer *et al.* 2015), it is possible that the reduced LH surge amplitude might derive from loss of PR in the brain in addition to the pituitary. Indeed, PR expression in the AVPV is necessary for LH surge induction (Chappell & Levine 2000). However, there is no Cre activity in either GnRH neurons (Wen *et al.* 2010) or kisspeptin neurons in the AVPV or arcuate nucleus (Fig. 9) of GRIC mice. In addition, female mice lacking PR in kisspeptin neurons show more dramatic reproductive deficits than what we observe here, including advanced onset of puberty, reduced fertility, and impaired ovulation (Stephens *et al.* 2015). We therefore conclude that it is unlikely that the phenotypes described in the *Pgr* cKO mice derive from loss of the PR in GnRH or kisspeptin neurons.

Table 2 Deconvolution analysis of circulating LH in six control and six KO mice sampled at 10-min intervals for 4 h.

	Control mice	**KO mice**	***P* value**	***P* value** (log-transformed data)
Burst number (#/4 h)	3.2 ± 0.5	3.5 ± 0.5	0.64	0.55
Fast half-life (min)	1.0	1.0		
Slow half-life (min)	5.5 ± 1.1	6.5 ± 0.7	0.44	0.36
Mode (min)	10.8 ± 2.0	11.3 ± 2.1	0.84	0.90
Basal secretion (IU/mL)	10.6 ± 2.7	7.7 ± 2.7	0.46	0.54
Pulsatile secretion (IU/mL)	8.8 ± 2.9	10.8 ± 4.1	0.70	0.79
Total secretion (IU/mL)	19.4 ± 3.9	18.5 ± 5.5	0.89	0.69
Mean pulse mass (IU/mL)	2.7 ± 1.0	3.1 ± 1.2	0.78	0.98

Data are mean ± S.E.M. Statistical comparisons were done with the Student's two-sided *t*-test for unpaired data.

https://joe.bioscientifica.com
https://doi.org/10.1530/JOE-19-0013

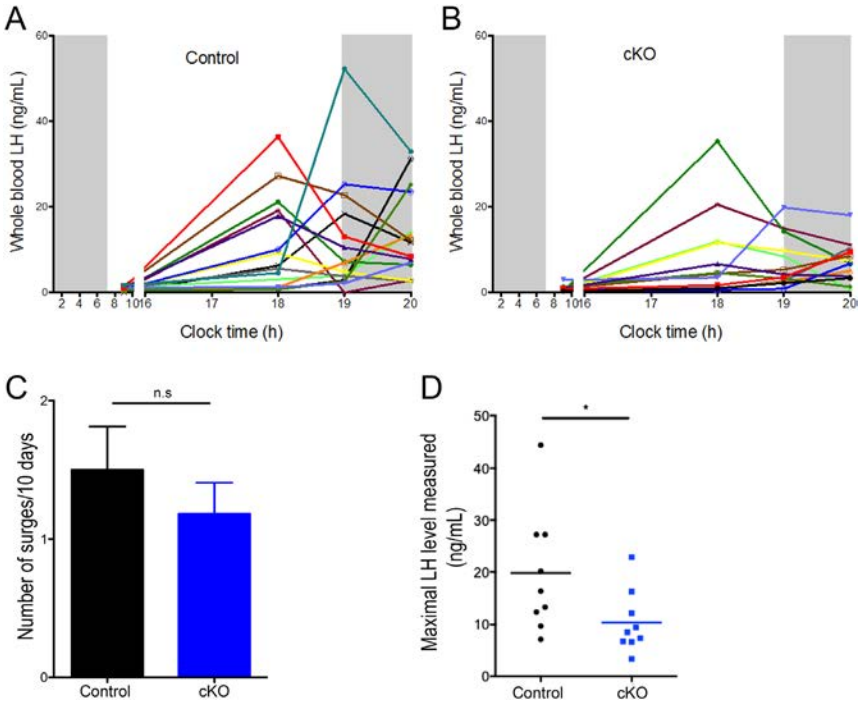

Figure 7
The LH surge is blunted in *Pgr*-knockout females. Blood samples were collected four times daily for 10 consecutive days. Representative profiles of the LH secretion obtained on proestrus from control (A) and cKO (B) female mice. Different colors indicate different mice. Gray areas represent the dark phase of the light/dark cycle. (C) Number of surges observed in each mouse during the 10 days of the experiment. (D) Maximal LH levels measured on proestrus from control ($n = 9$) and cKO ($n = 9$) females. Student *t*-tests were performed for statistical analysis. *$P < 0.05$. n.s, non-significant. Note: maximal values in panel D are lower than in panels A and B because averages were used in panel D in mice that surged more than once (see 'Methods' section). A full colour version of this figure is available at https://doi.org/10.1530/JOE-19-0013.

Based on previous reports, we would have expected effects of PR deletion on FSH. Estradiol-treated pre-menopausal women show increased FSH production in response to exogenous progesterone administration (Hutchens *et al.* 2016). Also, pre-menopausal women co-treated with estradiol benzoate and progesterone produce more FSH in response to exogenous GnRH compared to women treated with estradiol benzoate alone (Lasley *et al.* 1975). In rodents, PR and progesterone also appear to stimulate FSH production. For example, progesterone and its analogs (e.g., R5020), both alone or in synergy with activin A, strongly stimulate the activity of murine *Fshb* promoter-reporters in immortalized murine gonadotrope cells, LβT2 (Thackray *et al.* 2006, Thackray & Mellon 2008). There was some suggestion that GnRH might stimulate *Fshb* mRNA expression in a PR-dependent fashion in these cells (An *et al.* 2009). In rats, the PR antagonists, RU486 and Org31710, attenuate the primary LH and FSH surges on proestrus, while blocking the secondary FSH surge on the morning of estrus (Knox & Schwartz 1992, Knox *et al.* 1993, Roa *et al.* 2008*a*,*b*). Nevertheless, we did not detect the differences in serum FSH or pituitary *Fshb* mRNA levels between genotypes in either sex. One interpretation of these data is that we did not sample females at the appropriate cycle stage to observe effects of the gene deletion on FSH. Though we collected blood and pituitaries on the morning of estrus, it was a few hours after the peak of the secondary surge (Li *et al.* 2018*a*). Nonetheless, litter size is normal, arguing against an impairment in FSH production at any cycle stage. Although the data suggest that PR is dispensable for FSH production, it is important to consider that there may be functional redundancy in the system. Specifically, the related androgen and/or glucocorticoid receptors might compensate for the absence of PR in gonadotropes (Turgeon & Waring 1999, McGillivray *et al.* 2007, Wu *et al.* 2014).

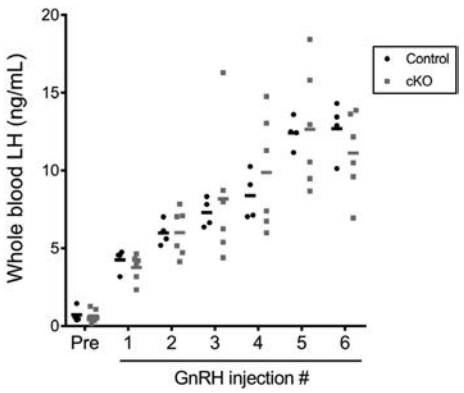

Figure 8
Control and cKO females show equivalent levels of GnRH self-priming. Blood samples were collected from ovariectomized, EB-injected females at 07:00 h. Females were then given six injections of GnRH (50 ng per injection) at 1-h intervals. Blood samples were collected 10 min after each injection. Mean whole blood LH levels in control ($n = 4$) and cKO ($n = 6$) females are shown. GLM procedure for repeated measurements was used for statistical analysis.

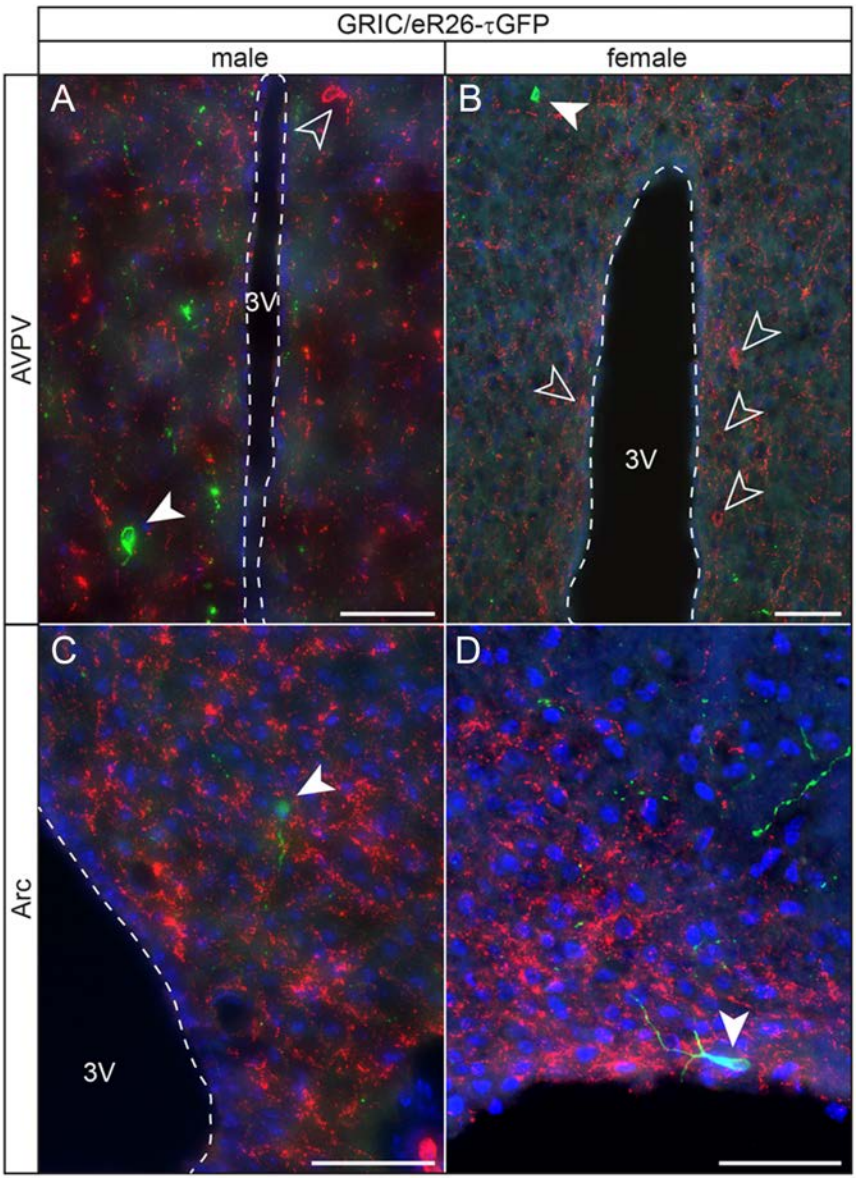

Figure 9
Kisspeptin neurons in the anteroventral periventricular nucleus (AVPV) and arcuate nucleus (Arc) do not express GnRHR. (A, B, C and D) Immunofluorescence staining for kisspeptin (red) in brain sections showing the AVPV (A and B) and the Arc (C and D) from adult male and female GRIC/eR26-τGFP mice. Note that GnRHR neurons (green, filled arrowheads) do not colocalize with kisspeptin neurons (empty arrowheads). Nuclei were stained with Hoechst 33258 (blue); Scalebars: 50 µm. 3V, third ventricle.

In summary, LH surge amplitude is reduced in gonadotrope-specific *Pgr*-knockout mice, but gonadotropin production and fertility are otherwise intact in these animals. The data suggest that progesterone-negative feedback at the level of the pituitary may be negligible, but that PR contributes to positive feedback effects of estrogens at this level of the HPG axis. Future studies should determine the mechanisms through which PR regulates LH surge amplitude as the receptor does not appear to play a necessary role in GnRH self-priming.

Declaration of interest
The authors declare that there is no conflict of interest that could be perceived as prejudicing the impartiality of the research reported.

Funding
This work was supported by the Canadian Institutes of Health Research (operating grants MOP-123447 and 133394 to D J B, and Doctoral Research Award 152308 to G S), the Natural Sciences and Engineering Research Council of Canada (2015-05178 to D J B), Fonds de Recherche du Québec – Santé (fellowship number 31338 to G S), a Samuel Solomon Fellowship in Reproductive Endocrinology (to G S), Réseau Québecois en Reproduction (to C T), and Centre for Research in Reproduction and Development (to C T).

References

Abdilnour G & Bourne GA 1995 Adenosine 3′,5′-cyclic monophosphate and the self-priming effect of gonadotrophin-releasing hormone. *Molecular and Cellular Endocrinology* **107** 1–7. (https://doi.org/10.1016/0303-7207(94)03418-s)

Aguilar R, Bellido C & Sanchez-Criado JE 2003 The role of estrogen-dependent progesterone receptor in protein kinase C-mediated LH

secretion and GnRH self-priming in rat anterior pituitary glands. *Journal of Endocrinological Investigation* **26** 527–532. (https://doi.org/10.1007/BF03345215)

An BS, Poon SL, So WK, Hammond GL & Leung PC 2009 Rapid effect of GNRH1 on follicle-stimulating hormone beta gene expression in LbetaT2 mouse pituitary cells requires the progesterone receptor. *Biology of Reproduction* **81** 243–249. (https://doi.org/10.1095/biolreprod.109.076216)

Attardi B, Scott R, Pfaff D & Fink G 2007 Facilitation or inhibition of the oestradiol-induced gonadotrophin surge in the immature female rat by progesterone: effects on pituitary responsiveness to gonadotrophin-releasing hormone (GnRH), GnRH self-priming and pituitary mRNAs for the progesterone receptor A and B isoforms. *Journal of Neuroendocrinology* **19** 988–1000. (https://doi.org/10.1111/j.1365-2826.2007.01613.x)

Caligioni CS 2009 Assessing reproductive status/stages in mice. *Current Protocols in Neuroscience* **48** A.4I.1–A.4I.8. (https://doi.org/10.1002/0471142301.nsa04is48)

Chappell PE & Levine JE 2000 Stimulation of gonadotropin-releasing hormone surges by estrogen. I. Role of hypothalamic progesterone receptors. *Endocrinology* **141** 1477–1485. (https://doi.org/10.1210/endo.141.4.7428)

Chappell PE, Lydon JP, Conneely OM, O'Malley BW & Levine JE 1997 Endocrine defects in mice carrying a null mutation for the progesterone receptor gene. *Endocrinology* **138** 4147–4152. (https://doi.org/10.1210/endo.138.10.5456)

Chappell PE, Schneider JS, Kim P, Xu M, Lydon JP, O'Malley BW & Levine JE 1999 Absence of gonadotropin surges and gonadotropin-releasing hormone self-priming in ovariectomized (OVX), estrogen (E2)-treated, progesterone receptor knockout (PRKO) mice. *Endocrinology* **140** 3653–3658. (https://doi.org/10.1210/endo.140.8.6895)

Cheung LYM, George AS, McGee SR, Daly AZ, Brinkmeier ML, Ellsworth BS & Camper SA 2018 Single-cell RNA sequencing reveals novel markers of male pituitary stem cells and hormone-producing cell types. *Endocrinology* **159** 3910–3924. (https://doi.org/10.1210/en.2018-00750)

Colin IM, Bauer-Dantoin AC, Sundaresan S, Kopp P & Jameson JL 1996 Sexually dimorphic transcriptional responses to gonadotropin-releasing hormone require chronic in vivo exposure to estradiol. *Endocrinology* **137** 2300–2307. (https://doi.org/10.1210/endo.137.6.8641179)

Czieselsky K, Prescott M, Porteous R, Campos P, Clarkson J, Steyn FJ, Campbell RE & Herbison AE 2016 Pulse and surge profiles of luteinizing hormone secretion in the mouse. *Endocrinology* **157** 4794–4802. (https://doi.org/10.1210/en.2016-1351)

Dafopoulos K, Kotsovassilis CG, Milingos S, Kallitsaris A, Galazios G, Zintzaras E, Sotiros P & Messinis IE 2004 Changes in pituitary sensitivity to GnRH in estrogen-treated post-menopausal women: evidence that gonadotrophin surge attenuating factor plays a physiological role. *Human Reproduction* **19** 1985–1992. (https://doi.org/10.1093/humrep/deh383)

d'Anglemont de Tassigny X, Fagg LA, Carlton MB & Colledge WH 2008 Kisspeptin can stimulate gonadotropin-releasing hormone (GnRH) release by a direct action at GnRH nerve terminals. *Endocrinology* **149** 3926–3932. (https://doi.org/10.1210/en.2007-1487)

Fernandez-Valdivia R, Jeong J, Mukherjee A, Soyal SM, Li J, Ying Y, Demayo FJ & Lydon JP 2010 A mouse model to dissect progesterone signaling in the female reproductive tract and mammary gland. *Genesis* **48** 106–113. (https://doi.org/10.1002/dvg.20586)

Fortin J, Boehm U, Deng CX, Treier M & Bernard DJ 2014 Follicle-stimulating hormone synthesis and fertility depend on SMAD4 and FOXL2. *FASEB Journal* **28** 3396–3410. (https://doi.org/10.1096/fj.14-249532)

Gal A, Lin PC, Cacioppo JA, Hannon PR, Mahoney MM, Wolfe A, Fernandez-Valdivia R, Lydon JP, Elias CF & Ko C 2016 Loss of fertility in the absence of progesterone receptor expression in kisspeptin neurons of female mice. *PLoS ONE* **11** e0159534. (https://doi.org/10.1371/journal.pone.0159534)

Haisenleder DJ, Schoenfelder AH, Marcinko ES, Geddis LM & Marshall JC 2011 Estimation of estradiol in mouse serum samples: evaluation of commercial estradiol immunoassays. *Endocrinology* **152** 4443–4447. (https://doi.org/10.1210/en.2011-1501)

Higuchi T & Kawakami M 1982 Luteinizing hormone responses to repeated injections of luteinizing hormone releasing hormone in the rat during the oestrous cycle and after ovariectomy with or without oestrogen treatment. *Journal of Endocrinology* **93** 161–168. (https://doi.org/10.1677/joe.0.0930161)

Ho CC, Zhou X, Mishina Y & Bernard DJ 2011 Mechanisms of bone morphogenetic protein 2 (BMP2) stimulated inhibitor of DNA binding 3 (Id3) transcription. *Molecular and Cellular Endocrinology* **332** 242–252. (https://doi.org/10.1016/j.mce.2010.10.019)

Hutchens EG, Ramsey KA, Howard LC, Abshire MY, Patrie JT & McCartney CR 2016 Progesterone has rapid positive feedback actions on LH release but fails to reduce LH pulse frequency within 12 h in estradiol-pretreated women. *Physiological Reports* **4** e12891. (https://doi.org/10.14814/phy2.12891)

Knox KL & Schwartz NB 1992 RU486 blocks the secondary surge of follicle-stimulating hormone in the rat without blocking the drop in serum inhibin. *Biology of Reproduction* **46** 220–225. (https://doi.org/10.1095/biolreprod46.2.220)

Knox KL, Ringstrom SJ & Schwartz NB 1993 RU486 blocks the effects of inhibin antiserum or luteinizing hormone on the secondary follicle-stimulating hormone surge. *Endocrinology* **133** 277–283. (https://doi.org/10.1210/endo.133.1.8319576)

Lasley BL, Wang CF & Yen SS 1975 The effects of estrogen and progesterone on the functional capacity of the gonadotrophs. *Journal of Clinical Endocrinology and Metabolism* **41** 820–826. (https://doi.org/10.1210/jcem-41-5-820)

Li Y, Schang G, Boehm U, Deng CX, Graff J & Bernard DJ 2017 SMAD3 regulates follicle-stimulating hormone synthesis by pituitary gonadotrope cells in vivo. *Journal of Biological Chemistry* **292** 2301–2314. (https://doi.org/10.1074/jbc.M116.759167)

Li Y, Fortin J, Ongaro L, Zhou X, Boehm U, Schneyer A, Bernard DJ & Lin HY 2018*a* Betaglycan (TGFBR3) functions as an inhibin A, but not inhibin B, coreceptor in pituitary gonadotrope cells in mice. *Endocrinology* **159** 4077–4091. (https://doi.org/10.1210/en.2018-00770)

Li Y, Schang G, Wang Y, Zhou X, Levasseur A, Boyer A, Deng CX, Treier M, Boehm U, Boerboom D, *et al*. 2018*b* Conditional deletion of FOXL2 and SMAD4 in gonadotropes of adult mice causes isolated FSH deficiency. *Endocrinology* **159** 2641–2655. (https://doi.org/10.1210/en.2018-00100)

Livak KJ & Schmittgen TD 2001 Analysis of relative gene expression data using real-time quantitative PCR and the 2(-Delta Delta C(T)) method. *Methods* **25** 402–408. (https://doi.org/10.1006/meth.2001.1262)

Lydon JP, DeMayo FJ, Funk CR, Mani SK, Hughes AR, Montgomery Jr CA, Shyamala G, Conneely OM & O'Malley BW 1995 Mice lacking progesterone receptor exhibit pleiotropic reproductive abnormalities. *Genes and Development* **9** 2266–2278. (https://doi.org/10.1101/gad.9.18.2266)

McGillivray SM, Thackray VG, Coss D & Mellon PL 2007 Activin and glucocorticoids synergistically activate follicle-stimulating hormone beta-subunit gene expression in the immortalized LbetaT2 gonadotrope cell line. *Endocrinology* **148** 762–773. (https://doi.org/10.1210/en.2006-0952)

Messager S, Chatzidaki EE, Ma D, Hendrick AG, Zahn D, Dixon J, Thresher RR, Malinge I, Lomet D, Carlton MB, *et al*. 2005 Kisspeptin directly stimulates gonadotropin-releasing hormone release via G protein-coupled receptor 54. *PNAS* **102** 1761–1766. (https://doi.org/10.1073/pnas.0409330102)

Pickering AJ & Fink G 1976 Priming effect of luteinizing hormone releasing factor: in-vitro and in-vivo evidence consistent with its

dependence upon protein and RNA synthesis. *Journal of Endocrinology* **69** 373–379. (https://doi.org/10.1677/joe.0.0690373)

Roa J, Vigo E, Castellano JM, Gaytan F, Garcia-Galiano D, Navarro VM, Aguilar E, Dijcks FA, Ederveen AG, Pinilla L, *et al*. 2008*a* Follicle-stimulating hormone responses to kisspeptin in the female rat at the preovulatory period: modulation by estrogen and progesterone receptors. *Endocrinology* **149** 5783–5790. (https://doi.org/10.1210/en.2008-0604)

Roa J, Vigo E, Castellano JM, Gaytan F, Navarro VM, Aguilar E, Dijcks FA, Ederveen AG, Pinilla L, van Noort PI, *et al*. 2008*b* Opposite roles of estrogen receptor (ER)-alpha and ERbeta in the modulation of luteinizing hormone responses to kisspeptin in the female rat: implications for the generation of the preovulatory surge. *Endocrinology* **149** 1627–1637. (https://doi.org/10.1210/en.2007-1540)

Schauer C, Tong T, Petitjean H, Blum T, Peron S, Mai O, Schmitz F, Boehm U & Leinders-Zufall T 2015 Hypothalamic gonadotropin-releasing hormone (GnRH) receptor neurons fire in synchrony with the female reproductive cycle. *Journal of Neurophysiology* **114** 1008–1021. (https://doi.org/10.1152/jn.00357.2015)

Stephens SB, Tolson KP, Rouse Jr ML, Poling MC, Hashimoto-Partyka MK, Mellon PL & Kauffman AS 2015 Absent progesterone signaling in kisspeptin neurons disrupts the LH surge and impairs fertility in female mice. *Endocrinology* **156** 3091–3097. (https://doi.org/10.1210/en.2015-1300)

Steyn FJ, Wan Y, Clarkson J, Veldhuis JD, Herbison AE & Chen C 2013 Development of a methodology for and assessment of pulsatile luteinizing hormone secretion in juvenile and adult male mice. *Endocrinology* **154** 4939–4945. (https://doi.org/10.1210/en.2013-1502)

Thackray VG & Mellon PL 2008 Synergistic induction of follicle-stimulating hormone beta-subunit gene expression by gonadal steroid hormone receptors and Smad proteins. *Endocrinology* **149** 1091–1102. (https://doi.org/10.1210/en.2007-1498)

Thackray VG, McGillivray SM & Mellon PL 2006 Androgens, progestins, and glucocorticoids induce follicle-stimulating hormone beta-subunit gene expression at the level of the gonadotrope. *Molecular Endocrinology* **20** 2062–2079. (https://doi.org/10.1210/me.2005-0316)

Turgeon JL & Waring DW 1994 Activation of the progesterone receptor by the gonadotropin-releasing hormone self-priming signaling pathway. *Molecular Endocrinology* **8** 860–869. (https://doi.org/10.1210/mend.8.7.7984148)

Turgeon JL & Waring DW 1999 Androgen modulation of luteinizing hormone secretion by female rat gonadotropes. *Endocrinology* **140** 1767–1774. (https://doi.org/10.1210/endo.140.4.6642)

Turgeon JL & Waring DW 2001 Luteinizing hormone secretion from wild-type and progesterone receptor knockout mouse anterior pituitary cells. *Endocrinology* **142** 3108–3115. (https://doi.org/10.1210/endo.142.7.8282)

Turgeon MO, Silander TL, Doycheva D, Liao XH, Rigden M, Ongaro L, Zhou X, Joustra SD, Wit JM, Wade MG, *et al*. 2017 TRH action is impaired in pituitaries of male IGSF1-deficient mice. *Endocrinology* **158** 815–830. (https://doi.org/10.1210/en.2016-1788)

Veldhuis J, Yang R, Roelfsema F & Takahashi P 2016 Proinflammatory cytokine infusion attenuates LH's feedforward on testosterone secretion: modulation by age. *Journal of Clinical Endocrinology and Metabolism* **101** 539–549. (https://doi.org/10.1210/jc.2015-3611)

Waring DW & Turgeon JL 1980 Luteinizing hormone-releasing hormone-induced luteinizing hormone secretion in vitro: cyclic changes in responsiveness and self-priming. *Endocrinology* **106** 1430–1436. (https://doi.org/10.1210/endo-106-5-1430)

Waring DW & Turgeon JL 1992 A pathway for luteinizing hormone releasing-hormone self-potentiation: cross-talk with the progesterone receptor. *Endocrinology* **130** 3275–3282. (https://doi.org/10.1210/endo.130.6.1317780)

Wen S, Schwarz JR, Niculescu D, Dinu C, Bauer CK, Hirdes W & Boehm U 2008 Functional characterization of genetically labeled gonadotropes. *Endocrinology* **149** 2701–2711. (https://doi.org/10.1210/en.2007-1502)

Wen S, Ai W, Alim Z & Boehm U 2010 Embryonic gonadotropin-releasing hormone signaling is necessary for maturation of the male reproductive axis. *PNAS* **107** 16372–16377. (https://doi.org/10.1073/pnas.1000423107)

Wen S, Gotze IN, Mai O, Schauer C, Leinders-Zufall T & Boehm U 2011 Genetic identification of GnRH receptor neurons: a new model for studying neural circuits underlying reproductive physiology in the mouse brain. *Endocrinology* **152** 1515–1526. (https://doi.org/10.1210/en.2010-1208)

Wu S, Chen Y, Fajobi T, DiVall SA, Chang C, Yeh S & Wolfe A 2014 Conditional knockout of the androgen receptor in gonadotropes reveals crucial roles for androgen in gonadotropin synthesis and surge in female mice. *Molecular Endocrinology* **28** 1670–1681. (https://doi.org/10.1210/me.2014-1154)

Zhou X, Wang Y, Ongaro L, Boehm U, Kaartinen V, Mishina Y & Bernard DJ 2016 Normal gonadotropin production and fertility in gonadotrope-specific Bmpr1a knockout mice. *Journal of Endocrinology* **229** 331–341. (https://doi.org/10.1530/JOE-16-0053)

Received in final form 17 September 2019
Accepted 4 October 2019
Accepted Manuscript published online 4 October 2019

nature genetics

Genome-wide analysis identifies 12 loci influencing human reproductive behavior

The genetic architecture of human reproductive behavior—age at first birth (AFB) and number of children ever born (NEB)—has a strong relationship with fitness, human development, infertility and risk of neuropsychiatric disorders. However, very few genetic loci have been identified, and the underlying mechanisms of AFB and NEB are poorly understood. We report a large genome-wide association study of both sexes including 251,151 individuals for AFB and 343,072 individuals for NEB. We identified 12 independent loci that are significantly associated with AFB and/or NEB in a SNP-based genome-wide association study and 4 additional loci associated in a gene-based effort. These loci harbor genes that are likely to have a role, either directly or by affecting non-local gene expression, in human reproduction and infertility, thereby increasing understanding of these complex traits.

Human reproductive behavior—AFB and NEB—has been associated with human development[1,2], infertility[3,4] and neuropsychiatric disorders[5]. Reproductive tempo (AFB) and quantum (NEB) are cross-cutting topics in the medical, biological, evolutionary and social sciences and are central in national and international policies[6]. Advanced societies have experienced a rapid postponement of AFB, with the mean AFB of women now being 28–29 years in many countries[7]. This increase in AFB has been linked to lower fertility rates, unprecedented rates of childlessness (~20%) and infertility, which affects 10 to 15% of couples[8]. An estimated 48.5 million couples worldwide are infertile, with a large part of subfertility, particularly in men, remaining unexplained[9]. Although infertility has been related to advanced AFB, ovulation defects, failure of spermatogenesis, and single-gene or polygenic defects, the causal effects for these factors remain unsubstantiated[10].

Recently, genetic and clinical research has focused on proximal infertility phenotypes[3,4,10,11]. AFB and NEB represent accurate measures of complex reproductive outcomes, are frequently recorded and consistently measured, and are key parameters for demographic population forecasting[12]. There is evidence of a genetic component underlying reproduction, with heritability estimates of up to 50% for AFB and NEB (**Supplementary Fig. 1**)[6]. A recent study attributed 15% of the variance in AFB and 10% of the variance in NEB to common genetic variants[13]. There are also sex-specific differences in human reproduction, related to the timing of fertility, fecundability and sex–genotype interactions (**Supplementary Note**). Researchers have given less attention to traits such as NEB because of an erroneous and frequently repeated misinterpretation of Fisher's fundamental theorem of natural selection[14] that the additive genetic variance in fitness should be close to zero. This misreading of the theorem had a naively intuitive appeal: genes that reduce fitness should be passed on less frequently. Fisher, however, actually argues that fitness is moderately heritable in human populations (for a discussion, see the **Supplementary Note**). As no established genes are currently available for clinical testing of infertility[10], isolating genetic loci and their causative effects has the potential to provide new insights into the etiology of reproductive diseases and novel diagnostic and clinical technologies for infertility treatment.

RESULTS

We report a large meta-analysis of genome-wide association studies (GWAS) of 251,151 individuals for AFB and 343,072 individuals for NEB from a total of 62 cohorts of European ancestry. We identify 12 independent loci (10 of which are new and 2 of which were previously identified in a study on age at first sexual intercourse[11]) that are significantly associated with AFB and/or NEB in men, women or both sexes combined (**Table 1**). Follow-up analyses identified a number of genetic variants and genes that likely drive the GWAS associations. We also quantified the genetic overlap with biologically adjacent reproductive, developmental, neuropsychiatric and behavioral phenotypes. A detailed description of all materials and methods is available in the **Supplementary Note**.

Meta-analysis of GWAS

Associations of AFB (mean ± s.d., 26.8 ± 4.78 years) and/or NEB (mean ± s.d., 2.3 ± 1.43 children) with SNPs imputed from NCBI Build 37 HapMap phase 2 data were examined in 62 cohorts using multiple linear regression under an additive model, in men and women separately (**Supplementary Note**). Associations were adjusted for principal components, to reduce confounding by population stratification[15], as well as for the birth year of the respondent and its square and cube to control for nonlinear birth cohort effects (**Supplementary Tables 1** and **2**, and **Supplementary Note**). NEB was assessed only for those who had completed their reproductive period (age ≥45 years for women and ≥55 years for men), while AFB was only assessed for those who were parous. Quality control was conducted in two independent centers using QCGWAS[16] and EasyQC[17] (**Supplementary Note**). Results were subsequently submitted to meta-analysis for the 2.4 million SNPs that passed quality control filters (**Supplementary Note**) and are reported for men and women combined and separately.

A full list of authors and affiliations appears at the end of the paper.

Received 12 June; accepted 22 September; published online 31 October 2016; doi:10.1038/ng.3698

Table 1 GWAS meta-analysis results for independent loci that are genome-wide significantly ($P < 5.0 \times 10^{-8}$) associated with AFB or NEB in either the combined or sex-specific meta-analysis

SNP	Chr.	Position (bp)	Nearest gene	Annotation	Effect allele/ other allele	EAF	β	*P* value	*n* (pooled)	β (men)	*P* value (men)	β (women)	*P* value (women)
Age at first birth													
rs10908557	1	153,927,052	*CRTC2*	N, R, ctQ, ctM	C/G	0.695	0.091	**5.59×10^{-10}**	249,025	0.185	2.98×10^{-7}	0.076	5.38×10^{-6}
rs1160544	2	100,832,218	*LINC01104*	R, cQ, cM	A/C	0.395	−0.082	**2.90×10^{-9}**	250,330	−0.042	2.12×10^{-1}	−0.092	**5.00×10^{-9}**
rs2777888	3	49,898,000	*CAMKV*	N, R, ctQ, ctM	A/G	0.507	0.106	**4.58×10^{-15}**	250,941	0.155	2.40×10^{-6}	0.095	**6.07×10^{-10}**
rs6885307	5	45,094,503	*MRPS30, HCN1*	R, ctQ, cM	A/C	0.799	−0.107	**2.32×10^{-10}**	248,999	−0.131	2.07×10^{-3}	−0.104	**3.90×10^{-8}**
rs10056247	5	133,898,136	*JADE2*	cQ, cM	T/C	0.289	0.082	**4.37×10^{-8}**	249,429	0.050	1.68×10^{-1}	0.089	1.28×10^{-7}
rs2347867	6	152,229,850	*ESR1*	cM	A/G	0.649	0.091	**1.38×10^{-10}**	248,039	0.098	4.69×10^{-3}	0.097	**1.80×10^{-9}**
rs10953766	7	114,313,218	*FOXP2*	cM	A/G	0.429	0.087	**1.82×10^{-10}**	248,039	0.106	1.31×10^{-3}	0.089	**8.41×10^{-9}**
rs2721195	8	145,677,011	*CYHR1*	R, cQ, ctM	T/C	0.469	−0.073	6.25×10^{-7}	250,493	−0.014	6.85×10^{-1}	−0.099	**6.13×10^{-9}**
rs293566	20	31,097,877	*NOL4L*	cQ, cM	T/C	0.650	0.081	**1.41×10^{-8}**	245,995	0.110	1.47×10^{-3}	0.079	1.31×10^{-6}
rs242997	22	34,503,059	*LARGE1, ISX*		A/G	0.613	−0.084	**3.38×10^{-9}**	238,002	−0.139	8.51×10^{-5}	−0.076	1.82×10^{-6}
Number of children ever born													
rs10908474	1	153,753,725	*SLC27A3, GATAD2B*		A/C	0.384	0.020	**2.08×10^{-8}**	342,340	0.021	8.10×10^{-4}	0.020	7.89×10^{-6}
rs13161115	5	107,050,002	*EFNA5, FBXL17*	cM	C/G	0.234	−0.041	1.34×10^{-2}	341,737	−0.041	**1.37×10^{-8}**	0.005	3.29×10^{-1}
rs2415984	14	46,873,776	*LINC00871*	cM	A/G	0.470	−0.020	**2.34×10^{-8}**	315,167	−0.029	2.41×10^{-6}	−0.016	3.71×10^{-4}

The rows in bold correspond to the independent signals reaching $P < 5 \times 10^{-8}$ in the meta-analysis. Annotation shows for each of the 12 independent lead SNPs (excluding rs10908474 on chromosome 1) whether it is (i) in strong LD ($r^2 > 0.8$) with a nonsynonymous variant (N) or one or more variants prioritized by RegulomeDB (R) with evidence of having functional consequences (defined by a score <4); (ii) associated with an eQTL in *cis* and/or *trans* (ctQ); and (iii) associated with an meQTL in *cis* and/or *trans* (ctM). EAF, effect allele frequency of the pooled meta-analysis; β, effect size in the AFB and NEB analyses. All *P* values are from the sample-size-weighted fixed-effects meta-analysis.

We applied a single genomic control at the cohort level and performed meta-analysis of results using a sample-size-weighted fixed-effect method in METAL (**Supplementary Note**). The PLINK clumping function isolated 'lead SNPs'—those with the lowest *P* value for association that are independently associated—using an r^2 threshold of 0.1 and a distance threshold of 500 kb. For AFB, we identified ten loci associated at genome-wide significance ($P < 5 \times 10^{-8}$ for combined results and $P < 1.67 \times 10^{-8}$ for sex-specific results adjusted for multiple testing), of which 9 were significantly associated in both sexes combined and 1 was associated in women only (n = 154,839) (**Fig. 1a** and **Table 1**). Three loci were significantly associated with NEB: two in both sexes combined and one in men only (n = 103,736) (**Fig. 1b**, **Table 1** and **Supplementary Note**). One locus on chromosome 1 reached significance for association with both AFB and NEB with $r^2 = 0.57$ between the two lead SNPs, suggesting a shared genetic basis for the two traits (**Table 2**). A statistical test of sex-specific effects confirmed that differences are mainly due to variation in sample size and not variation in effect size (**Supplementary Note**).

As for other complex traits[18], the quantile–quantile plots of the meta-analyses exhibited strong inflation of low *P* values (**Fig. 2**), suggesting that, although cohorts controlled for the top principal components and cohort-level genomic control was applied (**Supplementary Note**), residual population stratification may remain. However, the LD Score intercept method[19] as well as a series of individual and within-family regression analyses using polygenic scores as predictors[20,21] (**Supplementary Note**) indicated that the observed inflation was almost entirely attributable to a true polygenic signal, rather than population stratification.

Gene-based GWAS

To increase the power to find statistically significant associations and causal genes, we additionally performed a gene-based GWAS using VEGAS[22,23]. The results confirmed top hits from the single-SNP analyses. For AFB, seven loci from the SNP-based GWAS were also represented in the gene-based analysis (**Supplementary Table 3**), and three additional loci emerged, represented by *SLF2* (chromosome 10), *ENO4* (chromosome 10) and *TRAF3-AMN* (chromosome 14). For NEB, one locus from the SNP-based GWAS was represented in the gene-based analysis—*GATAD2B* (chromosome 1)—and one new locus on chromosome 17 was identified (**Supplementary Table 4**).

Causal variants

To identify functional and potentially causal variants, both coding and regulatory, within loci identified in the SNP-based GWAS (**Table 1**), we first performed an *in silico* sequencing annotation analysis using the post-GWAS pipeline reported by Vaez *et al.*[24]. This showed that rs10908557 on chromosome 1 is in high linkage disequilibrium (LD) with nonsynonymous SNPs in *CRTC2* (rs11264680; $r^2 = 0.98$) and *CREB3L4* (rs11264743; $r^2 = 0.94$) (**Supplementary Table 5**). Interestingly, rs11264743 is considered 'deleterious' and 'probably damaging' by SIFT and PolyPhen, respectively (Ensembl release 83). In addition, rs2777888 on chromosome 3 is in high LD with two nonsynonymous SNPs in *MST1R* (rs2230590, $r^2 = 0.95$ and rs1062633, $r^2 = 0.95$) (**Table 1** and **Supplementary Table 5**).

We subsequently performed a comprehensive analysis using results from the Encyclopedia of DNA Elements (ENCODE)[25] and Roadmap Epigenomics[26] projects, as integrated in RegulomeDB[27], to identify variants that likely influence downstream gene expression via regulatory pathways. Among all SNPs that reached $P < 5 \times 10^{-8}$ in the meta-analyses (n = 322), 50 SNPs in five loci showed the most evidence of having functional consequences (**Table 1** and **Supplementary Table 6**).

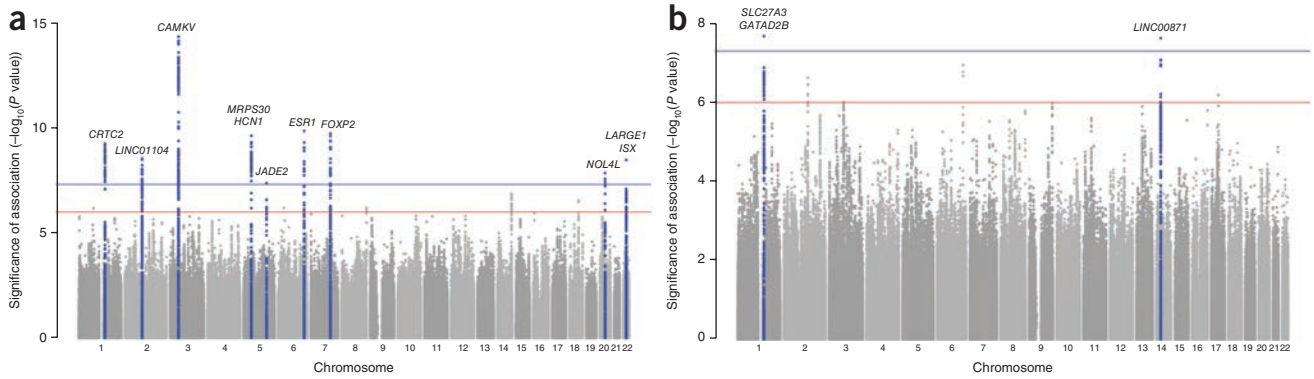

Figure 1 Manhattan plots of SNPs for age at first birth and number of children ever born in single-genomic-control meta-analysis. (**a**,**b**) SNPs are plotted on the *x* axis according to their position on each chromosome against association with AFB (**a**) and NEB (**b**). The solid blue line indicates the threshold for genome-wide significance ($P < 5 \times 10^{-8}$), and the red line represents the threshold for suggestive hits ($P < 5 \times 10^{-6}$). Blue points represent SNPs in a 100- kb region centered on genome-wide significant hits. Loci are annotated with the names of the genes closest to the significant SNPs.

Two sets of SNPs on chromosome 1 (18 SNPs) and chromosome 3 (25 SNPs) stand out in particular. The most promising SNP in the chromosome 1 locus (rs6680140) is located in a site of acetylation of histone H3 at lysine 27 (H3K27ac), often found near active regulatory elements, and lies in a DNase I hypersensitivity cluster where eight proteins are anticipated to bind. One of these proteins is cAMP responsive element binding (CREB)-binding protein, encoded by *CREBBP*. In the chromosome 3 locus, rs2526397 is located in a transcription factor binding site and is an expression quantitative trait locus (eQTL) for *HYAL3* in monocytes, while rs2247510 and rs1800688 are located in H3K27ac sites and DNase I hypersensitivity clusters where a large number of transcription factors are expected to bind (**Supplementary Table 6**). An analysis using Haploplotter showed that rs2247510 and rs7628058 in the chromosome 3 locus are among the 5% of signals showing the most evidence of positive selection in the population. The same applies to the lead SNP of the chromosome 14 locus for NEB (rs2415984).

Causal genes

Information on the function and anticipated relevance of genes in the 12 loci identified in the SNP-based GWAS that are most likely to be causal on the basis of all evidence discussed below is provided in **Table 2**.

Cis- and *trans*-eQTL and meQTL analyses

Identifying alterations in gene methylation status and/or expression levels in relation to GWAS-identified variants may help prioritize causal genes. We examined associations with gene expression and methylation status for the 12 independent lead SNPs in whole-blood BIOS eQTL ($n = 2{,}116$) and methylation quantitative trait locus (meQTL; $n = 3{,}841$) databases in *cis* and *trans*[28,29]. Seven SNPs were associated in *cis* with the expression of 54 unique genes (**Table 1** and **Supplementary Table 7**). Five of these seven SNPs were in high LD ($r^2 > 0.8$) with the strongest eQTL for at least one of the genes within the corresponding locus, indicating that the SNP associated with AFB or NEB and the SNP most significantly associated with expression tag the same functional site: rs10908557 (associated with the expression of *CRTC2* and *SLC39A1*), rs1160544 (*AFF3*), rs2777888 (*RBM6*, *RNF123* and *RBM5*), rs2721195 (*CYHR1*, *GPT*, *RECQL4* and *PPP1R16A*) and rs293566 (*NOL4L*). Three SNPs were associated with the expression of a total of eight genes in *trans* (**Table 1** and **Supplementary Table 8**). Of these SNPs, only rs2777888 was in high LD ($r^2 > 0.8$) with the strongest eQTL for three of its five associated genes: *LRFN1*, *LAMP2* and *FGD3*.

The meQTL analysis showed that 11 of the 12 independent lead SNPs were associated with DNA methylation of a total of 131 unique genes in *cis* (**Table 1** and **Supplementary Table 9**). Seven of the 11 SNPs were in high LD ($r^2 > 0.8$) with the strongest meQTL for one of the corresponding methylation sites: rs10908557 (associated with methylation of *CRTC2*, *SLC39A1*, *CREB3L4*, *DENND4B* and *RAB13*), rs1160544 (*AFF3*), rs2777888 (*CAMKV*), rs6885307 (*C5orf34*), rs10056247 (*JADE2*), rs2721195 (*CYHR1*) and rs13161115 (*EFNA5*). Three of the SNPs were associated with the same genes for both methylation and gene expression in *cis*: rs10908557 (*CRTC2*), rs1160544 (*AFF3*) and rs2721195 (*CYHR1*) (**Supplementary Tables 7** and **9**). Three SNPs were associated with methylation of a total of ten genes in *trans* (**Table 1** and **Supplementary Table 10**). Of these SNPs, only rs2777888 was in high LD ($r^2 > 0.8$) with the strongest meQTL for a corresponding methylation site (*ASAP3*). Of note, rs2777888 was also a *trans*-eQTL.

Gene prioritization

We used four publicly available bioinformatics tools to systematically identify genes that are more likely than neighboring genes to cause the associations identified by our GWAS. Of all genes that reached $P < 0.05$ in analyses using Endeavor[30], MetaRanker[31] and ToppGene[32], eight genes were prioritized for both AFB and NEB: *TPM3*, *GRM7*, *TKT*, *MAGI2*, *PTPRD*, *PTPRM*, *RORA* and *WT1*. DEPICT—a fourth comprehensive and unbiased recently described gene prioritization tool[33]—identified three genes in GWAS significant loci as likely being causal for AFB (*MON1A*, *RBM6* and *U73166.2*) (**Supplementary Tables 11** and **12**).

Gene-based results from RegulomeDB

An analysis using RegulomeDB identified 50 SNPs in five loci that most likely have regulatory consequences (**Supplementary Table 6**). Eighteen and 25 of these SNPs are within the chromosome 1 and chromosome 3 loci, respectively. Among the genes that, at a protein level, bind at the site of one or more of the 18 variants in the locus on chromosome 1 are *CREBBP*, *HNF4A*, *CDX2* and *ERG*. These genes may act upstream in the causal pathway and influence the expression of causal genes at this locus. Of the 25 SNPs on chromosome 3, 10 were eQTLs for *RBM6* in monocytes and 7 were eQTLs for *HYAL3* in monocytes. Among the genes that, at a protein level, bind at rs2247510 and rs1800688 in the chromosome 3 locus are *ARID3A*, *REST* and *TFAP2C*, as well as *HNF4A* and *CDX2*, which also bind at the chromosome 1 locus.

Table 2 Function and potential relevance for genes in GWAS-identified loci that are most likely causal on the basis of all available evidence

Lead SNP	Gene	Chr.	Evidence	Gene function and potential role in reproduction and (in)fertility	Ref.
rs10908557	*CRTC2*	1	G, V, ctQ, ctM, Q lymph. (R)	Functions as a Ca^{2+}- and cAMP-sensitive coincidence sensor; promotes CREB target gene expression; signal mediator in FSH and TGF-β1 steroidogenesis in ovarian granulosa cells	42
rs10908557	*CREB3L4*	1	N, V, cQ, cM	Has a role in protein maturation; involved in spermatid differentiation and male germ cell development; expressed in prostate, oocytes, fallopian tube and mammary gland	44,45
rs10908557	*GATAD2B*	1	V, Q monoc. (R)	Transcriptional repressor and a component of nucleosome remodeling complex Mi2/NuRD; increased expression in endometriosis; linked to a common gynecological disorder that causes pelvic pain and infertility	58,59
rs10908557	*SLC39A1*	1	V, cQ, cM	Zinc uptake transporter; major zinc regulator in prostate cells; involved in the regulation of zinc homeostasis by cumulus cells in the oocyte	60,61
rs10908557	*DENND4B*	1	cM	Paralog of *DENN1A*, which has been implicated in polycystic ovary syndrome; expressed at the protein level in the cervix	46,62
rs1160544	*AFF3*	2	cQ, cM	Lymphoid nuclear transcriptional activator implicated in tumorigenesis; same family as *AFF3* and *AFF4* (*FMR2* family member 4); transcriptional regulator in testicular somatic cells; essential for male germ cell differentiation and survival in mice	63,64
rs1160544	*LINC01104*	2	G, V	Unknown	
rs2777888	*HYAL3*	3	cM, Q monoc. (R)	Hyaluronidases, including HYAL3, are involved in degradation of hyaluronan, a major glycosaminoglycan of the extracellular matrix; acquired during sperm maturation in the epididymis and involved in sperm function and the acrosome reaction; required for *in vitro* cumulus penetration in mice, although its absence is not associated with infertility (perhaps compensated for by other hyaluronidases)	65
rs2777888	*RBM6*	3	V, cQ, cM, DEPICT, Q monoc. (R)	Involved in RNA splicing	66
rs2777888	*RNF123*	3	V, cQ, cM, Q liver (R)	Has a role in cellular transitioning from quiescence to a proliferative state through its E3 ubiquitin ligase activity toward cyclin-dependent kinase inhibitor 1B, which controls cell cycle progression in G1 phase	66–68
rs2777888	*RBM5*	3	V, cQ	Involved in cell cycle regulation; regulator of pre-mRNA splicing; involved in spermatogenesis and fertility in mice	47
rs2777888	*MON1A*	3	V, cM, DEPICT	Involved in the movement and trafficking of proteins (for example, ferroportin) through the secretory apparatus	69
rs2777888	*U73166.2*	3	DEPICT	Unknown	
rs2777888	*MST1R*	3	N, V, cM, MetaRanker, ToppGene and Endeavor	Cell surface receptor for MSP with tyrosine kinase activity, expressed on ciliated epithelia of the mucociliary transport apparatus of the lung; involved in host defense, expressed in sperm; may act in a regulatory system of ciliary motility, together with MSP, which sweeps eggs along the oviduct; expressed in mucous membrane and mammary gland	70
rs10056247	*JADE2*	5	G, V, cM	Involved in histone acetylation	
rs13161115	*EFNA5*	5	cM	Involved in development and differentiation of the nervous system and folliculogenesis regulation; required for normal fertility in female mice; expressed in embryonic stem cells and embryoid bodies	50
rs6885307	*HCN1*	5	G, cM	Hyperpolarization-activated cation channel that contributes to the native pacemaker current in, for example, neurons; HCN1 channels are present in kisspeptin (Kiss1) neurons in the rostral periventricular area of the third ventricle (RP3V), which provide an excitatory drive to gonadotropin-releasing hormone (GnRH)-expressing neurons that control fertility	71
rs2347867	*ESR1*	6	G, cM, binds at rs4851269 on chr. 2 (R)	Transcription factor involved in estrogen-responsive gene expression; essential for sexual development and reproductive function in women; genetic variants in *ESR1* may influence susceptibility to endometriosis or female fertility in patients with endometriosis; involved in male fertility by transferring estrogen effect; expressed in myometrium, endometrium, oocytes, uterus and fallopian tube	51,52, 72–74
rs10953766	*FOXP2*	7	G, cM, binds at rs6997 on chr. 3 (R)	Transcription factor expressed in fetal and adult brain that is involved in speech and language development; involved in regulation of neuronal development in the embryonic forebrain; expressed in mucous membrane and myometrium	75
rs2721195	*CYHR1*	8	cQ, cM	Histidine-cysteine-rich protein involved in spermatogenesis	53
rs2721195	*GPT*	8	V, cQ, cM, Q monoc. (R)	Involved in intermediary metabolism of glucose and amino acids; may have a role in spermatogenesis via testicular glucose metabolism, which is pivotal for the normal occurrence of spermatogenesis; levels in the normal range are positively associated with metabolic and endocrine abnormalities in women of reproductive age and negatively associated with FSH levels, independent of obesity	76,77
rs2721195	*RECQL4*	8	V, cQ, cM	Processing of aberrant DNA structures that arise during DNA replication and repair; predominantly expressed in testis	78
rs2721195	*PPP1R16A*	8	V, cQ, cM, Q monoc. (R)	Regulator of protein phosphatase PP1β; present in the sperm tail where it interacts with proteins that are important in sperm structure and motility; expressed in mammary gland and fallopian tube	79
rs293566	*NOL4L*	20	cQ, cM	Component of cytoplasm and nucleoplasm; expressed in umbilical vein	

Evidence categories include the nearest gene (G), nonsynonymous variants (N), gene-based GWAS performed in VEGAS (V), eQTLs in *cis* and/or *trans* (ctQ), meQTLs in *cis* and/or *trans* (ctM), eQTLs (Q) in lymphoblasts (lymph), monocytes (monoc) or liver based on RegulomeDB (R), gene prioritization using either DEPICT or MetaRanker, ToppGene and Endeavor, and protein binding at SNPs based on RegulomeDB (R). Chr., human chromosome on which the gene is located; FSH, follicle-stimulating hormone; CREB, cAMP response element–binding protein; TGF-β1, transforming growth factor β1; MSP, macrophage-stimulating protein. SNIPPER was used for the literature search, with the search terms "fertility," "sperm," "ovum" and "reproduction."
Gene Network was used to find the tissue or organ with high expression for a given gene (AUC > 0.8).

Five genes encode proteins that bind at the site of both SNPs on chromosome 2 that reach $P < 5 \times 10^{-8}$ in the meta-analysis of GWAS. One of these is *REST*; another one, *ESR1*, is the most likely causal gene in the chromosome 6 locus.

Functional network and enrichment analyses

Functional network analysis using five prioritized candidate gene sets as input (**Supplementary Note**) showed no significantly enriched biological function. No biological function was significantly enriched after correction for multiple testing using the Benjamini–Hochberg procedure. Similarly, no reconstituted gene sets and cell or tissue types were significantly enriched in the GWAS meta-analysis results based on results from the DEPICT analysis (**Supplementary Tables 13–20**). The lack of significantly enriched genes, tissue sets and biological functions reflects the need for a larger sample size but also the distal nature of the phenotypes, which are influenced by a mixture of biological, psychological and socioenvironmental factors.

Polygenic prediction

To assess the predictive power of our results, we produced polygenic scores for AFB and NEB with sets of SNPs whose nominal *P* values ranged from $P < 5 \times 10^{-8}$ (using only genome-wide significant SNPs) to 1 (using all SNPs that passed quality control) using PRSice[34] (**Supplementary Note**). We then performed a series of four different out-of-sample predictions in four independent cohorts: HRS, LifeLines, STR and TwinsUK. Across the four cohorts, the mean predictive power of a polygenic score constructed from all measured SNPs is 0.9% for AFB and 0.2% for NEB (**Supplementary Fig. 2**). Despite the low predictive power of the polygenic scores, the results showed that an increase of 1 s.d. in the NEB polygenic score is associated with a 9% (95% confidence interval (CI) = 5–13%) decrease in the probability of women remaining childless, with no significant association in men (**Supplementary Table 21**). When we controlled for right-censored data using a survival model for AFB, we found that an increase of 1 s.d. in the AFB polygenic score was associated with an 8% (95% CI = 7–10%) reduction in the hazard ratio of reproduction in women and a 3% (95% CI = 1–5%) reduction in men (**Supplementary Table 22**). As an additional test, we examined whether the aforementioned polygenic scores for AFB and NEB could predict related fertility traits such as age at menopause and age at menarche (**Supplementary Table 23**). Our estimates indicated that an increase of 1 s.d. in the AFB polygenic score was associated with a 3% decrease in the probability of natural menopause at any age (95% CI = 1–5%) and a 20-d increase in age at menarche (95% CI = 0.4–40 d).

Genetic association with related traits and diseases

Several loci for which the associations with AFB and NEB reached genome-wide significance are associated with behavioral and reproductive phenotypes. The lead SNPs in the chromosome 2 and chromosome 3 loci have been associated with educational attainment[35] and the locus on chromosome 5 has been associated with age at menarche[2], while the locus on chromosome 6 has recently been associated with age at first sexual intercourse[11] (**Supplementary Table 24**). Some of the 38 loci for age at first sexual intercourse that were recently identified[11] in 125,667 UK Biobank participants were also associated with AFB (in or near *RBM6–SEMA3F* and *ESR1*) and NEB (in or near *CADM2* and *ESR1*). The lead SNPs for *RBM6–SEMA3F* (rs2188151) and *ESR1* (rs67229052) are in LD with our lead SNPs for AFB on chromosome 3 ($r^2 = 0.44$) and chromosome 6 ($r^2 = 0.94$), respectively. An *in silico* pleiotropy analysis showed that our lead SNP in the chromosome 3 locus (rs2777888) is in LD ($r^2 = 0.59$) with rs6762477, which has been

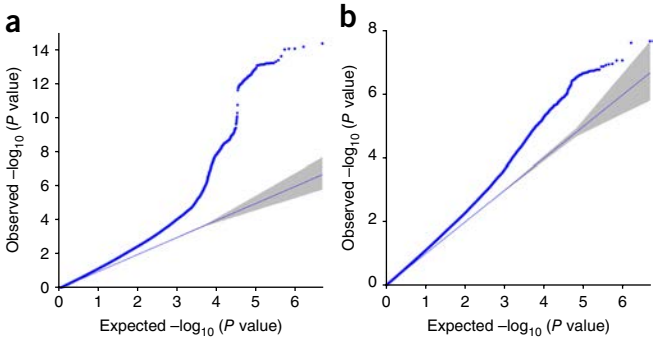

Figure 2 Quantile–quantile plots. (**a**,**b**) SNPs for AFB (**a**) and NEB (**b**) in single-genomic-control meta-analysis. The gray-shaded areas in the quantile–quantile plots represent the 95% confidence bands around the *P* values under the null hypothesis.

associated with age at menarche[2], while other SNPs in the same locus have been associated with HDL cholesterol[36] (rs2013208, $r^2 = 0.81$) and body mass index (BMI)[37] (rs7613875, $r^2 = 0.81$) (**Supplementary Table 5**). We next performed an exploratory analysis using the proxy phenotype method[38] to examine whether the SNPs strongly associated with AFB in women are empirically plausible candidate SNPs for related traits such as age at menarche and age at menopause (**Supplementary Note**). After controlling for multiple testing, we identified three AFB-associated SNPs near rs2777888 on chromosome 3 (rs9589, rs6803222 and rs9858889) that are also associated with age at menarche ($P < 4.10 \times 10^{-4}$). None of the AFB- or NEB-associated SNPs are associated with age at menopause.

We performed a bivariate LD score regression analysis[39] to estimate the pairwise genetic correlation with 27 publicly available GWAS results for traits associated with human reproductive behavior (**Supplementary Note**). AFB showed significant and positive genetic correlation with the human (reproductive) developmental traits of age at menarche, voice breaking, age at menopause, birth weight and age at first sexual intercourse, as well as with years of education. Conversely, having more AFB-increasing alleles was associated with a lower genetic risk of smoking (ever, number of cigarettes and later onset) and with lower insulin-resistance-related phenotypes, that is, BMI, waist–hip ratio adjusted for BMI, fasting insulin, triglyceride levels and risk of diabetes (**Fig. 3** and **Supplementary Table 25**). All genetic correlations remained significant after Bonferroni correction for multiple testing ($P < 2.6 \times 10^{-3}$). Years of education ($P = 6.6 \times 10^{-14}$) and age at first sexual intercourse ($P = 1.14 \times 10^{-15}$) are the only traits that showed significant and negative genetic correlation with NEB. We also observed significant genetic correlations of $r_g = 0.86$ (standard error (SE) = 0.052) for AFB and $r_g = 0.97$ (SE = 0.095) for NEB between men and women, implying that most genetic effects on reproductive behavior resulting from common SNPs are shared by both sexes.

DISCUSSION

This GWAS is a large-scale genetic epidemiological discovery effort for human reproduction, with implications for population fitness and physiological mechanisms linking hypothesized genes and observed phenotypes. Related studies previously focused on reproductive life span[40,41], age at first sexual intercourse[11] and more proximal infertility phenotypes[2–4], largely overlooking AFB and NEB. The rapid postponement of AFB and increased infertility and involuntary childlessness in many societies[7] make it important to uncover the genetic and biological architecture of reproduction. We identify ten

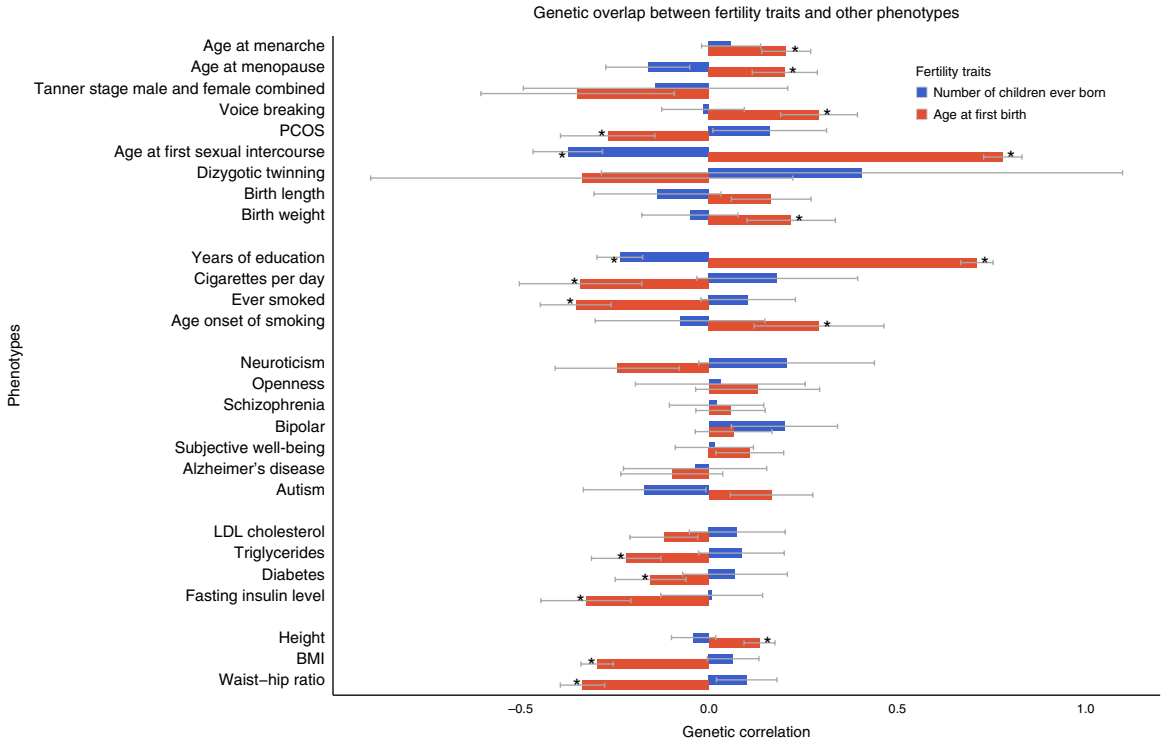

Figure 3 Genetic overlap between AFB or NEB and other related traits. Results from LD Score regressions show estimates of genetic correlation with developmental, reproductive, behavioral, neuropsychiatric and anthropometric phenotypes for which GWAS summary statistics were available in the public domain. The lengths of the bars correspond to estimates of genetic correlation. Gray error bars represent 95% confidence intervals. An asterisk indicates that the estimate of genetic correlation is statistically significant after controlling for multiple testing ($P < 0.05/27 = 1.85 \times 10^{-3}$).

new and confirm two recently identified genetic loci that are robustly associated with AFB and NEB, as well as variants and genes within these loci that potentially drive these associations. Four additional loci were identified in a gene-based GWAS.

Two loci that show interesting results in follow-up analyses are located on chromosomes 1 and 3. The lead SNPs of the chromosome 1 locus for AFB and NEB are in LD with likely functional nonsynonymous SNPs in genes encoding (i) CREB-regulated transcription co-activator 2 (*CRTC2*), which at the protein level acts as a critical signal mediator in follicle-stimulating hormone (FSH) and transforming growth factor (TGF)-β1–stimulated steroidogenesis in ovarian granulosa cells[42]; and (ii) CREB protein 3 like 4 (*CREB3L4*)[43], which in humans is highly expressed in the prostate, ovaries, uterus, placenta and testis and has a role in spermatid differentiation[44] and male germ cell development[45]. The lead SNP and/or functional variants in LD with it are also associated with the methylation status of these two genes and expression of *CRTC2* in whole blood and lymphocytes. Three promising functional variants in the chromosome 1 locus reside in binding sites of the transcriptional co-activator CREBBP. In addition to a direct effect of the above-mentioned nonsynonymous SNPs on protein function, the associations of AFB and NEB with variants in the locus on chromosome 1 may thus be mediated by alterations in cAMP responsive element binding in men and women. The locus on chromosome 1 also harbors *DENND4B*, a paralog of *DENND1A*, implicated in polycistic ovary syndrome (PCOS)[46]. Whereas *DENND1A* is expressed at the protein level in the ovary and testis, DENND4B is expressed in the cervix and its function and role are less well understood.

The lead SNP of the locus on chromosome 3 (rs2777888) is associated with methylation and expression of several genes, in *cis* and *trans*, that are known to have a role in cell cycle progression and/or sperm function. First, rs2777888 is associated with the expression of *RNF123* (or *KPC1*) in *cis*, which has a role in cellular transition from quiescence to a proliferative state. Second, rs2777888 or functional variants in LD with it may influence the cell cycle by altering the expression of *RBM5* and *RBM6* (RNA-binding motif proteins 5 and 6). The former has a role in cell cycle arrest and apoptosis induction and regulates haploid male germ cell pre-mRNA splicing and fertility in mice. *Rmb5*-mutant mice exhibit spermatid differentiation arrest, germ cell sloughing and apoptosis, leading to lack of sperm in ejaculation[47]. Third, rs2777888 affects expression of *LAMP2* in *trans*, which is located on the X chromosome and encodes a lysosomal membrane protein involved in the acrosome reaction, that is, the enzymatic drill allowing sperm to penetrate and fertilize ova[48]. *LAMP2* is expressed at the protein level in male and female reproductive organs with an effect size of rs2777888 for *LAMP2* mRNA expression that is almost twice as large in women than it is in men (**Supplementary Fig. 3**). This suggests an important role for the lysosome in both sperm and ova. Finally, functional variants in the chromosome 3 locus are associated with the mRNA expression of *HYAL3* (hyaluronoglucosaminidase 3) in monocytes. The encoded protein degrades hyaluronan, which also has an important role in sperm function and the acrosome reaction[47,49].

Functional follow-up experiments could disentangle the potential interplay between many candidate genes in the loci on chromosomes 1 and 3 in reproductive behavior and, given our *in silico* results, infertility. This can be extended to candidate genes in the remaining loci identified in the present study, some of which are relevant for fertility: mice lacking *Efna5* (chromosome 5 NEB locus) are subfertile[50], *ESR1* on chromosome 6 encodes an estrogen receptor[51,52] and *CYHR1* on chromosome 8 is involved in spermatogenesis[53]. Such experiments would help in understanding whether binding of estrogen receptor 1,

encoded by *ESR1* in the locus on chromosome 6, at the site of functional variants in the locus on chromosome 2 drives or mediates the association with AFB in the chromosome 2 locus, as well as to identify and characterize causal genes. Recent developments in high-throughput, multiplex mutagenesis using CRISPR/Cas9 allow such experiments to be performed using *in vivo* model systems[54].

AFB and NEB are not only driven by biological processes, but are also subject to individual choice and personal characteristics such as personality traits, as well as by the historical, cultural, economic and social environment (for example, effective contraception and childcare availability). Demographic research has shown a strong positive association between AFB and educational attainment[12]. We show that the associations between fecundity, reproductive behavior and educational attainment are partly driven by genetic factors and identified loci that are associated with AFB as well as with, for example, age at first sexual intercourse[11] and educational attainment[35].

Our findings could lead to insights into how postponing reproduction may be more detrimental for some, on the basis of their genetic make-up, than others, fuel experiments to determine 'how late can you wait' (ref. 55) and stimulate reproductive awareness. Causal genes in the loci we identified could potentially serve as novel drug targets, to prevent or delay age-related declines in fertility and sperm quality or to increase assisted reproductive technology efficiency, but further characterization is needed. Our study examines the genetics of reproductive behavior in both men and women, and, to our knowledge, it is the first that is adequately powered to identify loci in both women and men. We also provide support for Fisher's theorem that fitness is moderately heritable in human populations. Although the effect sizes of the identified common variants are small, there are examples of GWAS-identified loci of small effect that end up leading to important biological insights[56,57]. Many of our findings suggest a role for sperm quality, which is one lead for researchers to pursue. Because current sperm tests remain rudimentary, our findings could serve as a basis for 'good quality' sperm markers. We identified both coding and regulatory variants that are potentially causal, as well as a set of genes that could underlie the associations we identified. Follow-up experiments in animal models are required to confirm and characterize the causal genes in these loci.

URLs. Analysis plan predeposited at the Open Science Framework website, https://osf.io/53tea/; Gene Network, http://129.125.135.180:8080/GeneNetwork/; ReproGen, http://www.reprogen.org/data_download.html; Sociogenome, http://www.sociogenome.com/; Social Science Genetic Association Consortium, http://thessgac.org/.

METHODS

Methods and any associated references are available in the online version of the paper.

Note: Any Supplementary Information and Source Data files are available in the online version of the paper.

ACKNOWLEDGMENTS

For full acknowledgments, see the **Supplementary Note**. Funding to lead this consortium was provided by grants awarded to M.C.M.: ERC Consolidator Grant SOCIOGENOME (615603), a Dutch Science Foundation (NWO) grant (VIDI grant 452-10-012), a UK ESRC/NCRM SOCGEN grant (ES/N011856/1), the European Union's FP7 Families And Societies project (320116), and the Wellcome Trust ISSF and John Fell Fund. M.d.H. was supported by grants from the Swedish Research Council (2015-03657) and the Swedish Heart-Lung Foundation (20140543). Research was carried out in collaboration with the Social Science Genetic Association Consortium (SSGAC), with funding from the US National Science Foundation (EAGER: 'Workshop for the Formation of a Social Science Genetic Association Consortium'), a Supplementary grant from the National Institutes of Health Office of Behavioral and Social Science Research, the Ragnar Söderberg Foundation (E9/11), the Swedish Research Council (421-2013-1061), the Jan Wallander and Tom Hedelius Foundation, an ERC Consolidator Grant (647648 EdGe), the Pershing Square Fund of the Foundations of Human Behavior and the NIA/NIH through grants P01-AG005842, P01-AG005842-20S2, P30-AG012810 and T32-AG000186-23 to NBER and R01-AG042568-02 to the University of Southern California. X.S. was supported by a grant from the Swedish Research Council (537-2014-371). We thank X. Ding for research assistance, N. Pirastu, K. Coward and L. Layman for valuable comments, and the University of Oxford Advanced Research Computing (ARC) facility (http://dx.doi.org/10.5281/zenodo.22558). This research has been conducted using the UK Biobank Resource.

AUTHOR CONTRIBUTIONS

Senior investigators who led writing, analysis and study design: M.C.M., H. Snieder and M.d.H. Senior investigators who participated in study design: P.D.K., D.J.B. and D.C. Junior investigator who contributed to the study design and management: N. Barban. Population stratification: N. Barban and F.C.T. Genetic correlations and polygenic score prediction: N. Barban. Meta-analysis and quality control: N. Barban, R.d.V., J.J.M. and I.M.N. Biological annotation: R.J., M.d.H. and A.V. Sex-specific genetic effects: N. Barban and F.C.T. Bivariate and conditional analysis of the two fertility traits: X.S., J.F.W. and D.I.C. Gene-based analysis V.T. and S.W.v.d.L. Authors not listed contributed to recruitment, genotyping or data processing for the meta-analysis (**Supplementary Table 43**).

COMPETING FINANCIAL INTERESTS

The authors declare no competing financial interests.

1. Elks, C.E. *et al.* Thirty new loci for age at menarche identified by a meta-analysis of genome-wide association studies. *Nat. Genet.* **42**, 1077–1085 (2010).
2. Perry, J.R.B. *et al.* Parent-of-origin-specific allelic associations among 106 genomic loci for age at menarche. *Nature* **514**, 92–97 (2014).
3. Rahmioglu, N. *et al.* Genetic variants underlying risk of endometriosis: insights from meta-analysis of eight genome-wide association and replication datasets. *Hum. Reprod. Update* **20**, 702–716 (2014).
4. Day, F.R. *et al.* Causal mechanisms and balancing selection inferred from genetic associations with polycystic ovary syndrome. *Nat. Commun.* **6**, 8464 (2015).
5. Mehta, D. *et al.* Evidence for genetic overlap between schizophrenia and age at first birth in women. *JAMA Psychiatry* **73**, 497–505 (2016).
6. Mills, M.C. & Tropf, F.C. The biodemography of fertility: a review and future research frontiers. *Kolner Z. Soz. Sozpsychol.* **67** (Suppl. 1), 397–424 (2015).
7. Mills, M., Rindfuss, R.R., McDonald, P. & te Velde, E. Why do people postpone parenthood? Reasons and social policy incentives. *Hum. Reprod. Update* **17**, 848–860 (2011).
8. Boivin, J., Bunting, L., Collins, J.A. & Nygren, K.G. International estimates of infertility prevalence and treatment-seeking: potential need and demand for infertility medical care. *Hum. Reprod.* **22**, 1506–1512 (2007).
9. Mascarenhas, M.N., Flaxman, S.R., Boerma, T., Vanderpoel, S. & Stevens, G.A. National, regional, and global trends in infertility prevalence since 1990: a systematic analysis of 277 health surveys. *PLoS Med.* **9**, e1001356 (2012).
10. Venkatesh, T., Suresh, P.S. & Tsutsumi, R. New insights into the genetic basis of infertility. *Appl. Clin. Genet.* **7**, 235–243 (2014).
11. Day, F.R. *et al.* Physical and neurobehavioral determinants of reproductive onset and success. *Nat. Genet.* **48**, 617–623 (2016).
12. Balbo, N., Billari, F.C. & Mills, M.C. Fertility in advanced societies: a review of research. *Eur. J. Popul.* **29**, 1–38 (2012).
13. Tropf, F.C. *et al.* Human fertility, molecular genetics, and natural selection in modern societies. *PLoS One* **10**, e0126821 (2015).
14. Fisher, R.A. *The Genetical Theory of Natural Selection* (Oxford University Press, 1930).
15. Price, A.L. *et al.* Principal components analysis corrects for stratification in genome-wide association studies. *Nat. Genet.* **38**, 904–909 (2006).
16. van der Most, P.J. *et al.* QCGWAS: a flexible R package for automated quality control of genome-wide association results. *Bioinformatics* **30**, 1185–1186 (2014).
17. Winkler, T.W. *et al.* Quality control and conduct of genome-wide association meta-analyses. *Nat. Protoc.* **9**, 1192–1212 (2014).
18. Lango Allen, H. *et al.* Hundreds of variants clustered in genomic loci and biological pathways affect human height. *Nature* **467**, 832–838 (2010).
19. Bulik-Sullivan, B.K. *et al.* LD Score regression distinguishes confounding from polygenicity in genome-wide association studies. *Nat. Genet.* **47**, 291–295 (2015).
20. Wood, A.R. *et al.* Defining the role of common variation in the genomic and biological architecture of adult human height. *Nat. Genet.* **46**, 1173–1186 (2014).
21. Purcell, S.M. *et al.* Common polygenic variation contributes to risk of schizophrenia and bipolar disorder. *Nature* **460**, 748–752 (2009).
22. Liu, J.Z. *et al.* A versatile gene-based test for genome-wide association studies. *Am. J. Hum. Genet.* **87**, 139–145 (2010).

23. Mishra, A. & Macgregor, S. VEGAS2: software for more flexible gene-based testing. *Twin Res. Hum. Genet.* **18**, 86–91 (2015).
24. Vaez, A. *et al. In silico* post genome-wide association studies analysis of C-reactive protein loci suggests an important role for interferons. *Circ Cardiovasc Genet* **8**, 487–497 (2015).
25. ENCODE Project Consortium. ENCODE (ENCyclopedia Of DNA Elements) Project. *Science* **306**, 636–640 (2004).
26. Kundaje, A. *et al.* Integrative analysis of 111 reference human epigenomes. *Nature* **518**, 317–330 (2015).
27. Boyle, A.P. *et al.* Annotation of functional variation in personal genomes using RegulomeDB. *Genome Res.* **22**, 1790–1797 (2012).
28. Zhernakova, D. *et al.* Hypothesis-free identification of modulators of genetic risk factors. Preprint at *bioRxiv* http://dx.doi.org/10.1101/033217 (2015).
29. Bonder, M.J. *et al.* Disease variants alter transcription factor levels and methylation of their binding sites. Preprint at *bioRxiv* http://dx.doi.org/10.1101/033084 (2015).
30. Tranchevent, L.C. *et al.* ENDEAVOUR update: a web resource for gene prioritization in multiple species. *Nucleic Acids Res.* **36**, W377–W384 (2008).
31. Pers, T.H., Dworzyński, P., Thomas, C.E., Lage, K. & Brunak, S. MetaRanker 2.0: a web server for prioritization of genetic variation data. *Nucleic Acids Res.* **41**, W104–W108 (2013).
32. Chen, J., Bardes, E.E., Aronow, B.J. & Jegga, A.G. ToppGene Suite for gene list enrichment analysis and candidate gene prioritization. *Nucleic Acids Res.* **37**, W305–W311 (2009).
33. Pers, T.H. *et al.* Biological interpretation of genome-wide association studies using predicted gene functions. *Nat. Commun.* **6**, 5890 (2015).
34. Euesden, J., Lewis, C.M. & O'Reilly, P.F. PRSice: Polygenic Risk Score software. *Bioinformatics* **31**, 1466–1468 (2015).
35. Okbay, A. *et al.* Genome-wide association study identifies 74 loci associated with educational attainment. *Nature* **533**, 539–542 (2016).
36. Willer, C.J. *et al.* Discovery and refinement of loci associated with lipid levels. *Nat. Genet.* **45**, 1274–1283 (2013).
37. Locke, A.E. *et al.* Genetic studies of body mass index yield new insights for obesity biology. *Nature* **518**, 197–206 (2015).
38. Rietveld, C.A. *et al.* Common genetic variants associated with cognitive performance identified using the proxy-phenotype method. *Proc. Natl. Acad. Sci. USA* **111**, 13790–13794 (2014).
39. Bulik-Sullivan, B. *et al.* An atlas of genetic correlations across human diseases and traits. *Nat. Genet.* **47**, 1236–1241 (2015).
40. Day, F.R. *et al.* Large-scale genomic analyses link reproductive aging to hypothalamic signaling, breast cancer susceptibility and *BRCA1*-mediated DNA repair. *Nat. Genet.* **47**, 1294–1303 (2015).
41. Perry, J.R. *et al.* A genome-wide association study of early menopause and the combined impact of identified variants. *Hum. Mol. Genet.* **22**, 1465–1472 (2013).
42. Fang, W.-L. *et al.* CREB coactivator CRTC2/TORC2 and its regulator calcineurin crucially mediate follicle-stimulating hormone and transforming growth factor β1 upregulation of steroidogenesis. *J. Cell. Physiol.* **227**, 2430–2440 (2012).
43. Cao, G. *et al.* Molecular cloning and characterization of a novel human cAMP response element–binding (CREB) gene (*CREB4*). *J. Hum. Genet.* **47**, 373–376 (2002).
44. El-Alfy, M. *et al.* Stage-specific expression of the Atce1/Tisp40α isoform of CREB3L4 in mouse spermatids. *J. Androl.* **27**, 686–694 (2006).
45. Adham, I.M. *et al.* Reduction of spermatogenesis but not fertility in *Creb3l4*-deficient mice. *Mol. Cell. Biol.* **25**, 7657–7664 (2005).
46. McAllister, J.M. *et al.* Overexpression of a DENND1A isoform produces a polycystic ovary syndrome theca phenotype. *Proc. Natl. Acad. Sci. USA* **111**, E1519–E1527 (2014).
47. O'Bryan, M.K. *et al.* RBM5 is a male germ cell splicing factor and is required for spermatid differentiation and male fertility. *PLoS Genet.* **9**, e1003628 (2013).
48. Tsukamoto, S. *et al.* Functional analysis of lysosomes during mouse preimplantation embryo development. *J. Reprod. Dev.* **59**, 33–39 (2013).
49. Szucs, M., Osvath, P., Laczko, I. & Jakab, A. Adequacy of hyaluronan binding assay and a new fertility index derived from it for measuring of male fertility potential and the efficacy of supplement therapy. *Andrologia* **47**, 519–524 (2015).
50. Buensuceso, A.V. *et al.* Ephrin-A5 is required for optimal fertility and a complete ovulatory response to gonadotropins in the female mouse. *Endocrinology* **157**, 942–955 (2016).
51. Jisa, E. & Jungbauer, A. Kinetic analysis of estrogen receptor homo- and heterodimerization *in vitro*. *J. Steroid Biochem. Mol. Biol.* **84**, 141–148 (2003).
52. O'Donnell, L., Robertson, K.M., Jones, M.E. & Simpson, E.R. Estrogen and spermatogenesis. *Endocr. Rev.* **22**, 289–318 (2001).
53. Ly-Huynh, J.D. *et al.* Importin α2–interacting proteins with nuclear roles during mammalian spermatogenesis. *Biol. Reprod.* **85**, 1191–1202 (2011).
54. Varshney, G.K. *et al.* CRISPRz: a database of zebrafish validated sgRNAs. *Nucleic Acids Res.* **44**, D1, D822–D826 (2016).
55. Menken, J. Age and fertility: how late can you wait? *Demography* **22**, 469–483 (1985).
56. Manolio, T.A., Brooks, L.D. & Collins, F.S. A HapMap harvest of insights into the genetics of common disease. *J. Clin. Invest.* **118**, 1590–1605 (2008).
57. Hindorff, L.A. *et al.* Potential etiologic and functional implications of genome-wide association loci for human diseases and traits. *Proc. Natl. Acad. Sci. USA* **106**, 9362–9367 (2009).
58. Okkelman, I.A., Sukaeva, A.Z., Kirukhina, E.V., Korneenko, T.V. & Pestov, N.B. Nuclear translocation of lysyl oxidase is promoted by interaction with transcription repressor p66β. *Cell Tissue Res.* **358**, 481–489 (2014).
59. Joshi, N.R. *et al.* Altered expression of microRNA-451 in eutopic endometrium of baboons (*Papio anubis*) with endometriosis. *Hum. Reprod.* **30**, 2881–2891 (2015).
60. Franklin, R.B. *et al.* Human ZIP1 is a major zinc uptake transporter for the accumulation of zinc in prostate cells. *J. Inorg. Biochem.* **96**, 435–442 (2003).
61. Lisle, R.S., Anthony, K., Randall, M.A. & Diaz, F.J. Oocyte–cumulus cell interactions regulate free intracellular zinc in mouse oocytes. *Reproduction* **145**, 381–390 (2013).
62. Shan, B. *et al.* Association of *DENND1A* gene polymorphisms with polycystic ovary syndrome: a meta-analysis. *J. Clin. Res. Pediatr. Endocrinol.* **8**, 135–143 (2016).
63. Impera, L. *et al.* A novel fusion *5′AFF3/3′BCL2* originated from a t(2;18)(q11.2;q21.33) translocation in follicular lymphoma. *Oncogene* **27**, 6187–6190 (2008).
64. Urano, A. *et al.* Infertility with defective spermiogenesis in mice lacking AF5q31, the target of chromosomal translocation in human infant leukemia. *Mol. Cell. Biol.* **25**, 6834–6845 (2005).
65. Reese, K.L. *et al.* Acidic hyaluronidase activity is present in mouse sperm and is reduced in the absence of SPAM1: evidence for a role for hyaluronidase 3 in mouse and human sperm. *Mol. Reprod. Dev.* **77**, 759–772 (2010).
66. Heath, E., Sablitzky, F. & Morgan, G.T. Subnuclear targeting of the RNA-binding motif protein RBM6 to splicing speckles and nascent transcripts. *Chromosome Res.* **18**, 851–872 (2010).
67. Kamura, T. *et al.* Cytoplasmic ubiquitin ligase KPC regulates proteolysis of $p27^{Kip1}$ at G1 phase. *Nat. Cell Biol.* **6**, 1229–1235 (2004).
68. Kato, J.Y., Matsuoka, M., Polyak, K., Massagué, J. & Sherr, C.J. Cyclic AMP–induced G1 phase arrest mediated by an inhibitor ($p27^{Kip1}$) of cyclin-dependent kinase 4 activation. *Cell* **79**, 487–496 (1994).
69. Bagley, D.C., Paradkar, P.N., Kaplan, J. & Ward, D.M. Mon1a protein acts in trafficking through the secretory apparatus. *J. Biol. Chem.* **287**, 25577–25588 (2012).
70. Sakamoto, O. *et al.* Role of macrophage-stimulating protein and its receptor, RON tyrosine kinase, in ciliary motility. *J. Clin. Invest.* **99**, 701–709 (1997).
71. Zhang, C. *et al.* Molecular mechanisms that drive estradiol-dependent burst firing of Kiss1 neurons in the rostral periventricular preoptic area. *Am. J. Physiol. Endocrinol. Metab.* **305**, E1384–E1397 (2013).
72. Ponglikitmongkol, M., Green, S. & Chambon, P. Genomic organization of the human oestrogen receptor gene. *EMBO J.* **7**, 3385–3388 (1988).
73. de Mattos, C.S. *et al. ESR1* and *ESR2* gene polymorphisms are associated with human reproduction outcomes in Brazilian women. *J. Ovarian Res.* **7**, 114 (2014).
74. Lamp, M. *et al.* Polymorphisms in *ESR1*, *ESR2* and *HSD17B1* genes are associated with fertility status in endometriosis. *Gynecol. Endocrinol.* **27**, 425–433 (2011).
75. Chiu, Y.-C. *et al.* Foxp2 regulates neuronal differentiation and neuronal subtype specification. *Dev. Neurobiol.* **74**, 723–738 (2014).
76. Alves, M.G. *et al.* Metabolic fingerprints in testicular biopsies from type 1 diabetic patients. *Cell Tissue Res.* **362**, 431–440 (2015).
77. Mojiminiyi, O.A., Safar, F.H., Al Rumaih, H. & Diejomaoh, M. Variations in alanine aminotransferase levels within the normal range predict metabolic and androgenic phenotypes in women of reproductive age. *Scand. J. Clin. Lab. Invest.* **70**, 554–560 (2010).
78. Van Maldergem, L. *et al.* Revisiting the craniosynostosis-radial ray hypoplasia association: Baller–Gerold syndrome caused by mutations in the *RECQL4* gene. *J. Med. Genet.* **43**, 148–152 (2016).
79. Ruan, Y., Cheng, M., Ou, Y., Oko, R. & van der Hoorn, F.A. Ornithine decarboxylase antizyme Oaz3 modulates protein phosphatase activity. *J. Biol. Chem.* **286**, 29417–29427 (2011).

Nicola Barban[1,173], Rick Jansen[2], Ronald de Vlaming[3–5], Ahmad Vaez[6,7], Jornt J Mandemakers[8], Felix C Tropf[1], Xia Shen[9–11], James F Wilson[10,11], Daniel I Chasman[12], Ilja M Nolte[6], Vinicius Tragante[13], Sander W van der Laan[14], John R B Perry[15], Augustine Kong[16,17], BIOS Consortium[18], Tarunveer S Ahluwalia[19–21], Eva Albrecht[22], Laura Yerges-Armstrong[23], Gil Atzmon[24–26], Kirsi Auro[27,28], Kristin Ayers[29], Andrew Bakshi[30], Danny Ben-Avraham[25], Klaus Berger[31], Aviv Bergman[32], Lars Bertram[33,34], Lawrence F Bielak[35], Gyda Bjornsdottir[17], Marc Jan Bonder[36], Linda Broer[37], Minh Bui[38], Caterina Barbieri[39], Alana Cavadino[40,41], Jorge E Chavarro[42–44], Constance Turman[44], Maria Pina Concas[45], Heather J Cordell[29], Gail Davies[46,47], Peter Eibich[48], Nicholas Eriksson[49], Tõnu Esko[50,51],

Joel Eriksson[52], Fahimeh Falahi[6], Janine F Felix[4,53,54], Mark Alan Fontana[55], Lude Franke[36], Ilaria Gandin[56], Audrey J Gaskins[42], Christian Gieger[57,58], Erica P Gunderson[59], Xiuqing Guo[60], Caroline Hayward[10], Chunyan He[61], Edith Hofer[62,63], Hongyan Huang[44], Peter K Joshi[11], Stavroula Kanoni[64], Robert Karlsson[9], Stefan Kiechl[65], Annette Kifley[66], Alexander Kluttig[67], Peter Kraft[44,68], Vasiliki Lagou[69–71], Cecile Lecoeur[72], Jari Lahti[73–75], Ruifang Li-Gao[76], Penelope A Lind[77], Tian Liu[78], Enes Makalic[38], Crysovalanto Mamasoula[29], Lindsay Matteson[79], Hamdi Mbarek[80,81], Patrick F McArdle[23], George McMahon[82], S Fleur W Meddens[5,83], Evelin Mihailov[50], Mike Miller[84], Stacey A Missmer[44,85], Claire Monnereau[4,53,54], Peter J van der Most[6], Ronny Myhre[86], Mike A Nalls[87], Teresa Nutile[88], Ioanna Panagiota Kalafati[89], Eleonora Porcu[90,91], Inga Prokopenko[92–94], Kumar B Rajan[95], Janet Rich-Edwards[43,44,96], Cornelius A Rietveld[3–5], Antonietta Robino[97], Lynda M Rose[12], Rico Rueedi[98,99], Kathleen A Ryan[23], Yasaman Saba[100], Daniel Schmidt[38], Jennifer A Smith[35], Lisette Stolk[37], Elizabeth Streeten[23], Anke Tönjes[101], Gudmar Thorleifsson[17], Sheila Ulivi[97], Juho Wedenoja[102], Juergen Wellmann[31], Peter Willeit[65,103,104], Jie Yao[60], Loic Yengo[72,105], Jing Hua Zhao[15], Wei Zhao[35], Daria V Zhernakova[36], Najaf Amin[4], Howard Andrews[106], Beverley Balkau[72], Nir Barzilai[24], Sven Bergmann[98,99], Ginevra Biino[107], Hans Bisgaard[21], Klaus Bønnelykke[21], Dorret I Boomsma[80,81], Julie E Buring[12], Harry Campbell[11], Stefania Cappellani[97], Marina Ciullo[88,108], Simon R Cox[46,47], Francesco Cucca[90,91], Daniela Toniolo[39], George Davey-Smith[109], Ian J Deary[46,47], George Dedoussis[89], Panos Deloukas[64,110], Cornelia M van Duijn[4], Eco J C de Geus[80,81], Johan G Eriksson[75,111–114], Denis A Evans[95], Jessica D Faul[115], Cinzia Felicita Sala[39], Philippe Froguel[72], Paolo Gasparini[56,116], Giorgia Girotto[56,116], Hans-Jörgen Grabe[117], Karin Halina Greiser[118], Patrick J F Groenen[5,119], Hugoline G de Haan[76], Johannes Haerting[67], Tamara B Harris[120], Andrew C Heath[121], Kauko Heikkilä[28], Albert Hofman[4,5,44], Georg Homuth[122], Elizabeth G Holliday[123,124], John Hopper[38], Elina Hyppönen[40,125,126], Bo Jacobsson[86,127], Vincent W V Jaddoe[4,53,54], Magnus Johannesson[128], Astanand Jugessur[86], Mika Kähönen[129], Eero Kajantie[130–132], Sharon L R Kardia[35], Bernard Keavney[29,133], Ivana Kolcic[134], Päivikki Koponen[135], Peter Kovacs[136], Florian Kronenberg[137], Zoltan Kutalik[99,138], Martina La Bianca[97], Genevieve Lachance[139], William G Iacono[84], Sandra Lai[90], Terho Lehtimäki[140], David C Liewald[46], LifeLines Cohort Study[18], Cecilia M Lindgren[93,94,141,142], Yongmei Liu[143], Robert Luben[144], Michael Lucht[111], Riitta Luoto[145], Per Magnus[86], Patrik K E Magnusson[9], Nicholas G Martin[77], Matt McGue[84,146], Ruth McQuillan[11], Sarah E Medland[77], Christa Meisinger[58,147], Dan Mellström[52], Andres Metspalu[50,148], Michela Traglia[39], Lili Milani[50], Paul Mitchell[66], Grant W Montgomery[121,149], Dennis Mook-Kanamori[76,150,151], Renée de Mutsert[76], Ellen A Nohr[152], Claes Ohlsson[52], Jørn Olsen[153], Ken K Ong[15], Lavinia Paternoster[109], Alison Pattie[47], Brenda W J H Penninx[2,81], Markus Perola[27,28,50], Patricia A Peyser[35], Mario Pirastu[45], Ozren Polasek[134], Chris Power[40], Jaakko Kaprio[27,28,102], Leslie J Raffel[154], Katri Räikkönen[73], Olli Raitakari[155], Paul M Ridker[12], Susan M Ring[109], Kathryn Roll[60], Igor Rudan[11], Daniela Ruggiero[88], Dan Rujescu[156], Veikko Salomaa[27], David Schlessinger[157], Helena Schmidt[100], Reinhold Schmidt[62], Nicole Schupf[158], Johannes Smit[2,81], Rossella Sorice[88,108], Tim D Spector[139], John M Starr[46,159], Doris Stöckl[158], Konstantin Strauch[22,160], Michael Stumvoll[101,136], Morris A Swertz[36], Unnur Thorsteinsdottir[17,161], A Roy Thurik[3,5,162], Nicholas J Timpson[109], Joyce Y Tung[49], André G Uitterlinden[3,5,37], Simona Vaccargiu[45], Jorma Viikari[163], Veronique Vitart[10], Henry Völzke[164], Peter Vollenweider[165], Dragana Vuckovic[56,116], Johannes Waage[21], Gert G Wagner[166], Jie Jin Wang[66], Nicholas J Wareham[15], David R Weir[115], Gonneke Willemsen[80,81], Johann Willeit[65], Alan F Wright[10], Krina T Zondervan[167,168], Kari Stefansson[17,161], Robert F Krueger[84], James J Lee[84], Daniel J Benjamin[55,169], David Cesarini[170,171], Philipp D Koellinger[3,5,83], Marcel den Hoed[172,173], Harold Snieder[6,173] & Melinda C Mills[1,173]

[1]Department of Sociology and Nuffield College, University of Oxford, Oxford, UK. [2]Department of Psychiatry, VU University Medical Center, Amsterdam, the Netherlands. [3]Department of Applied Economics, Erasmus School of Economics, Rotterdam, the Netherlands. [4]Department of Epidemiology, Erasmus MC, University Medical Center Rotterdam, Rotterdam, the Netherlands. [5]Erasmus University Rotterdam Institute for Behavior and Biology, Rotterdam, the Netherlands. [6]Department of Epidemiology, University of Groningen, University Medical Center Groningen, Groningen, the Netherlands. [7]Research Institute for Primordial Prevention of Non-Communicable Disease, Isfahan University of Medical Sciences, Isfahan, Iran. [8]Sociology of Consumption and Households, Wageningen University Research, Wageningen, the Netherlands. [9]Department of Medical Epidemiology and Biostatistics, Karolinska Institutet, Stockholm, Sweden. [10]MRC Human Genetics Unit, MRC Institute of Genetics and Molecular Medicine, University of Edinburgh, Edinburgh, UK. [11]Centre for Global Health Research, Usher Institute of Population Health Sciences and Informatics, University of Edinburgh, Edinburgh, UK. [12]Brigham and Women's Hospital and Harvard Medical School, Boston, Massachusetts, USA. [13]Department of Cardiology, Division of Heart and Lungs, University Medical Center Utrecht, Utrecht, the Netherlands. [14]Laboratory of Experimental Cardiology, Division of Heart and Lungs, University Medical Center Utrecht, Utrecht, the Netherlands. [15]MRC Epidemiology Unit, Institute of Metabolic Science, University of Cambridge, Cambridge, UK. [16]School of Engineering and Natural Sciences, University of Iceland, Reykjavik, Iceland. [17]deCODE Genetics/Amgen, Inc., Reykjavik, Iceland. [18]A list of members and affiliations appears in the **Supplementary Note**. [19]Novo Nordisk Foundation Centre for Basic Metabolic Research, Section of Metabolic Genetics, Faculty of Health and Medical Sciences, University of Copenhagen, Copenhagen, Denmark. [20]Steno Diabetes Center, Gentofte, Denmark. [21]COPSAC, Copenhagen Prospective Studies on Asthma in Childhood, Herlev and Gentofte Hospital, University of Copenhagen, Copenhagen, Denmark.

[22]Institute of Genetic Epidemiology, Helmholtz Zentrum München–German Research Center for Environmental Health, Neuherberg, Germany. [23]Division of Endocrinology, Diabetes and Nutrition, University of Maryland School of Medicine, Baltimore, Maryland, USA. [24]Department of Medicine, Institute for Aging Research and the Diabetes Research Center, Albert Einstein College of Medicine, Bronx, New York, USA. [25]Department of Genetics, Institute for Aging Research and the Diabetes Research Center, Albert Einstein College of Medicine, Bronx, New York, USA. [26]Department of Natural Science, University of Haifa, Haifa, Israel. [27]Department of Health, National Institute for Health and Welfare, Helsinki, Finland. [28]Institute for Molecular Medicine (FIMM), University of Helsinki, Helsinki, Finland. [29]Institute of Genetic Medicine, Newcastle University, Newcastle-upon-Tyne, UK. [30]Queensland Brain Institute, University of Queensland, Brisbane, Queensland, Australia. [31]Institute of Epidemiology and Social Medicine, University of Münster, Münster, Germany. [32]Departments of Systems and Computational Biology, of Pathology and of Neuroscience, Albert Einstein College of Medicine, Bronx, New York, USA. [33]Lübeck Interdisciplinary Platform for Genome Analytics, Institutes of Neurogenetics and of Integrative and Experimental Genomics, University of Lübeck, Lübeck, Germany. [34]School of Public Health, Faculty of Medicine, Imperial College, London, UK. [35]Department of Epidemiology, University of Michigan, Ann Arbor, Michigan, USA. [36]Department of Genetics, Genomics Coordination Center, University of Groningen, University Medical Center Groningen, Groningen, the Netherlands. [37]Department of Internal Medicine, Erasmus Medical Center, Rotterdam, the Netherlands. [38]Centre for Epidemiology and Biostatistics, Melbourne School of Population and Global Health, University of Melbourne, Melbourne, Victoria, Australia. [39]Division of Genetics and Cell Biology, San Raffaele Research Institute, Milan, Italy. [40]Population, Policy and Practice, UCL Institute of Child Health, London, UK. [41]Centre for Environmental and Preventive Medicine, Wolfson Institute of Preventative Medicine, Queen Mary University of London, London, UK. [42]Department of Nutrition, Harvard T.H. Chan School of Public Health, Boston, Massachusetts, USA. [43]Department of Medicine, Brigham and Women's Hospital and Harvard Medical School, Boston, Massachusetts, USA. [44]Department of Epidemiology, Harvard T.H. Chan School of Public Health, Boston, Massachusetts, USA. [45]Institute of Genetic and Biomedical Research, National Research Council, UOS of Sassari, Sassari, Italy. [46]Centre for Cognitive Ageing and Cognitive Epidemiology, University of Edinburgh, Edinburgh, UK. [47]Department of Psychology, University of Edinburgh, Edinburgh, UK. [48]Health Economics Research Centre, University of Oxford, Oxford, UK. [49]23andMe, Inc., Mountain View, California, USA. [50]Estonian Genome Center, University of Tartu, Tartu, Estonia. [51]Broad Institute of MIT and Harvard, Cambridge, Massachusetts, USA. [52]Centre for Bone and Arthritis Research, Institute of Medicine, Sahlgrenska Academy, University of Gothenburg, Gothenburg, Sweden. [53]Generation R Study Group, Erasmus MC, University Medical Center Rotterdam, Rotterdam, the Netherlands. [54]Department of Pediatrics, Erasmus MC, University Medical Center Rotterdam, Rotterdam, the Netherlands. [55]Center for Economic and Social Research, University of Southern California, Los Angeles, California, USA. [56]Department of Medical, Surgical and Health Sciences, University of Trieste, Trieste, Italy. [57]Research Unit of Molecular Epidemiology, Helmholtz Zentrum München–German Research Center for Environmental Health, Neuherberg, Germany. [58]Institute of Epidemiology II, Helmholtz Zentrum München–German Research Center for Environmental Health, Neuherberg, Germany. [59]Cardiovascular and Metabolic Conditions Section, Division of Research, Kaiser Permanente Northern California, Oakland, California, USA. [60]Institute for Translational Genomics and Population Sciences, Los Angeles Biomedical Research Institute at Harbor-UCLA Medical Center, Torrance, California, USA. [61]Department of Epidemiology, Indiana University Richard M. Fairbanks School of Public Health, Indianapolis, Indiana, USA. [62]Clinical Division of Neurogeriatrics, Department of Neurology, Medical University of Graz, Graz, Austria. [63]Institute of Medical Informatics, Statistics and Documentation, Medical University of Graz, Graz, Austria. [64]William Harvey Research Institute, Barts and The London School of Medicine and Dentistry, Queen Mary University of London, London, UK. [65]Department of Neurology, Medical University of Innsbruck, Innsbruck, Austria. [66]Centre for Vision Research, Department of Ophthalmology and Westmead Institute for Medical Research, University of Sydney, Westmead, New South Wales, Australia. [67]Institute of Medical Epidemiology, Biostatistics and Informatics, Martin Luther University Halle-Wittenberg, Halle (Saale), Germany. [68]Department of Biostatistics, Harvard T.H. Chan School of Public Health, Boston, Massachusetts, USA. [69]Department of Neurosciences, KU Leuven, Leuven, Belgium. [70]Department of Microbiology and Immunology, KU Leuven, Leuven, Belgium. [71]Translational Immunology Laboratory, VIB, Leuven, Belgium. [72]University of Lille, CNRS, Institut Pasteur of Lille, Lille, France. [73]Institute of Behavioral Sciences, University of Helsinki, Helsinki, Finland. [74]Helsinki Collegium for Advanced Studies, University of Helsinki, Helsinki, Finland. [75]Folkhälsan Research Centre, Helsinki, Finland. [76]Department of Clinical Epidemiology, Leiden University Medical Center, Leiden, the Netherlands. [77]Psychiatric Genetics, QIMR Berghofer Medical Research Institute, Herston Brisbane, Queensland, Australia. [78]Center for Lifespan Psychology, Max Planck Institute for Human Development and Department of Vertebrate Genomics, Max Planck Institute for Molecular Genetics, Berlin, Germany. [79]Minnesota Center for Twin and Family Research, Department of Psychology, University of Minnesota, Minneapolis, Minnesota, USA. [80]Department of Biological Psychology, VU University, Amsterdam, the Netherlands. [81]EMGO+ Institute for Health and Care Research, Amsterdam, the Netherlands. [82]School of Social and Community Medicine, University of Bristol, Bristol, UK. [83]Complex Trait Genetics, VU University, Amsterdam, the Netherlands. [84]Department of Psychology, University of Minnesota, Minneapolis, Minnesota, USA. [85]Department of Obstetrics, Gynecology and Reproductive Biology, Brigham and Women's Hospital and Harvard Medical School, Boston, Massachusetts, USA. [86]Department of Genetics and Bioinformatics, Area of Health Data and Digitalization, Institute of Public Health, Oslo, Norway. [87]Laboratory of Neurogenetics, National Institute on Aging, US National Institutes of Health, Bethesda, Maryland, USA. [88]Institute of Genetics and Biophysics 'A. Buzzati-Traverso', CNR, Naples, Italy. [89]Department of Nutrition and Dietetics, School of Health Science and Education, Harokopio University, Athens, Greece. [90]Istituto di Ricerca Genetica e Biomedica, CMR, Cittadella Universitaria di Monserrato, Monserrato, Cagliari, Italy. [91]Dipartimento di Scienze Biomediche, Università di Sassari, Sassari, Italy. [92]Department of Genomics of Common Disease, School of Public Health, Imperial College London, London, UK. [93]Wellcome Trust Centre for Human Genetics, Nuffield Department of Medicine, University of Oxford, Oxford, UK. [94]Oxford Centre for Diabetes, Endocrinology and Metabolism, Radcliffe Department of Medicine, University of Oxford, Oxford, UK. [95]Rush University Medical Center, Chicago, Illinois, USA. [96]Connors Center for Women's Health and Gender Biology, Brigham and Women's Hospital and Harvard Medical School, Boston, Massachusetts, USA. [97]Institute for Maternal and Child Health, IRCCS 'Burlo Garofolo', Trieste, Italy. [98]Department of Computational Biology, University of Lausanne, Lausanne, Switzerland. [99]Swiss Institute of Bioinformatics, Lausanne, Switzerland. [100]Institute of Molecular Biology and Biochemistry, Centre for Molecular Medicine, Medical University of Graz, Graz, Austria. [101]Department of Medicine, University of Leipzig, Leipzig, Germany. [102]Department of Public Health, University of Helsinki, Helsinki, Finland. [103]King's British Heart Foundation Centre, King's College London, London, UK. [104]Department of Public Health and Primary Care, University of Cambridge, Cambridge, UK. [105]Centre for Neurogenetics and Statistical Genomics, University of Queensland, Brisbane, Queensland, Australia. [106]Data Coordinating Center, New York State Psychiatric Institute, New York, New York, USA. [107]Institute of Molecular Genetics, National Research Council of Italy, Pavia, Italy. [108]IRCCS Neuromed, Pozzilli, Isernia, Italy. [109]MRC Integrative Epidemiology Unit, University of Bristol, Bristol, UK. [110]Princess Al-Jawhara Al-Brahim Centre of Excellence in Research of Hereditary Disorders (PACER-HD), King Abdulaziz University, Jeddah, Saudi Arabia. [111]Department of Chronic Disease Prevention, National Institute for Health and Welfare, Helsinki, Finland. [112]Department of General Practice and Primary Health Care, University of Helsinki, Helsinki, Finland. [113]Unit of General Practice, Helsinki University Central Hospital, Helsinki, Finland. [114]Vasa Central Hospital, Vasa, Finland. [115]Survey Research Center, Institute for Social Research, University of Michigan, Ann Arbor, Michigan, USA. [116]Division of Experimental Genetics, Sidra, Doha, Qatar. [117]Department of Psychiatry, University Medicine Greifswald, Greifswald, Germany. [118]Division of Cancer Epidemiology, German Cancer Research Center, Heidelberg, Germany. [119]Econometric Institute, Erasmus School of Economics, Erasmus University Rotterdam, Rotterdam, the Netherlands. [120]Laboratory of Epidemiology and Population Sciences, National Institute on Aging, Bethesda, Maryland, USA. [121]Genetic Epidemiology, QIMR Berghofer Medical Research Institute, Brisbane, Queensland, Australia. [122]Interfaculty Institute for Genetics and Functional Genomics, University Medicine Greifswald, Greifswald, Germany. [123]School of Medicine and Public Health, University of Newcastle, Newcastle, New South Wales, Australia. [124]Hunter Medical Research Institute, Newcastle, New South Wales, Australia. [125]Centre for Population Health Research, Sansom Institute of Health Research and School of Health Sciences, University of South Australia, Adelaide, South Australia, Australia. [126]South Australian Health and Medical Research Institute, Adelaide, South Australia, Australia. [127]Department of Obstetrics and Gynecology, Institute of Clinical Sciences, Sahlgrenska Academy, Gothenburg University, Gothenburg, Sweden. [128]Department of Economics, Stockholm School of Economics, Stockholm, Sweden. [129]Department of Clinical Physiology, University of Tampere and Tampere University Hospital, Tampere, Finland. [130]Diabetes Prevention Unit, National Institute for Health and Welfare, Helsinki, Finland. [131]Children's Hospital, Helsinki University Central Hospital and University of Helsinki, Helsinki, Finland. [132]Department of Obstetrics and Gynecology, MRC Oulu, Oulu University Hospital and University of Oulu, Oulu, Finland. [133]Institute of Cardiovascular Sciences, University of Manchester, Manchester, UK. [134]Department of Public Health, Faculty of Medicine, University of Split, Split, Croatia. [135]Health Monitoring Unit, National Institute for Health and Welfare, Helsinki, Finland. [136]IFB Adiposity Diseases, University of Leipzig, Leipzig, Germany. [137]Division of Genetic Epidemiology, Medical University of Innsbruck, Innsbruck, Austria. [138]Institute of Social and Preventive Medicine, Lausanne University Hospital (CHUV), Lausanne, Switzerland. [139]Department of Twin Research and Genetic Epidemiology, King's College London, London, UK. [140]Department of Clinical Chemistry, Fimlab Laboratories and School of Medicine, University of Tampere, Tampere, Finland. [141]NIHR Oxford Biomedical Research Centre, Oxford, UK. [142]Li Ka Shing Centre for Health Information and Discovery, Big Data Institute, University of Oxford, Oxford, UK. [143]Division of Public Health Sciences, Wake Forest School of Medicine, Winston-Salem, North Carolina, USA. [144]Strangeways Research Laboratory, University of Cambridge, Cambridge, UK. [145]UKK Institute for

Health Promotion,Tampere, Finland. [146]Danish Aging Research Center and Danish Twin Registry, Institute of Public Health, University of Southern Denmark, Odense, Denmark. [147]MONICA/KORA Myocardial Infarction Registry, Central Hospital of Augsburg, Augsburg, Germany. [148]Institute of Molecular and Cell Biology, University of Tartu, Tartu, Estonia. [149]Molecular Bioscience, University of Queensland, Brisbane, Queensland, Australia. [150]Department of Public Health and Primary Care, Leiden University Medical Center, Leiden, the Netherlands. [151]Department of BESC, Epidemiology Section, King Faisal Specialist Hospital and Research Centre, Riyadh, Saudi Arabia. [152]Research Unit for Gynecology and Obstetrics, Department of Clinical Research, University of Southern Denmark, Odense, Denmark. [153]Department of Clinical Epidemiology, Aarhus University, Aarhus, Denmark. [154]Medical Genetics Institute, Cedars-Sinai Medical Center, Los Angeles, California, USA. [155]Research Centre of Applied and Preventive Cardiovascular Medicine, University of Turku and Department of Clinical Physiology and Nuclear Medicine, Turku University Hospital, Turku, Finland. [156]Department of Psychiatry, Martin Luther University Halle-Wittenberg, Halle (Saale), Germany. [157]Laboratory of Genetics, National Institute on Aging, Baltimore, Maryland, USA. [158]Departments of Epidemiology and Psychiatry, Columbia University Medical Center, New York, New York, USA. [159]Alzheimer Scotland Dementia Research Centre, University of Edinburgh, Edinburgh, UK. [160]Institute of Medical Informatics, Biometry and Epidemiology, Chair of Genetic Epidemiology, Ludwig Maximilians Universität, Munich, Germany. [161]Faculty of Medicine, University of Iceland, Reykjavik, Iceland. [162]Montpellier Business School, Montpellier, France. [163]Department of Medicine, University of Turku and Division of Medicine, Turku University Hospital, Turku, Finland. [164]Institute for Community Medicine, University Medicine Greifswald, Greifswald, Germany. [165]Department of Internal Medicine, Lausanne University Hospital (CHUV), Lausanne, Switzerland. [166]German Socio-Economic Panel Study (SOEP), Max Planck Institute for Human Development and Berlin University of Technology (TUB), Berlin, Germany. [167]Genetic and Genomic Epidemiology Unit, Wellcome Trust Centre for Human Genetics, University of Oxford, Oxford, UK. [168]Endometriosis CaRe Centre, Nuffield Department of Obstetrics and Gynaecology, University of Oxford, Oxford, UK. [169]National Bureau of Economic Research, Cambridge, Massachusetts, USA. [170]Department of Economics, New York University, New York, New York, USA. [171]Research Institute for Industrial Economics, Stockholm, Sweden. [172]Department of Medical Sciences, Molecular Epidemiology and Science for Life Laboratory, Uppsala University, Uppsala, Sweden. [173]These authors contributed equally to this work. Correspondence should be addressed to M.C.M. (melinda.mills@nuffield.ox.ac.uk), N.B. (nicola.barban@sociology.ox.ac.uk), H.S. (h.snieder@umcg.nl) or M.d.H. (marcel.den_hoed@medsci.uu.se).

ONLINE METHODS

GWAS of reproductive behavior study design in brief. Genome-wide association analyses of AFB and NEB were performed at the cohort level according to a prespecified analysis plan (**Supplementary Note**). Cohort-uploaded results were imputed using the HapMap 2 CEU (r22.b36) or 1000 Genomes Project reference sample. Cohorts were asked to only include participants of European ancestry, with no missing values for all relevant covariates (sex, birth year and cohort-specific covariates), who were successfully genotyped over the whole genome and passed cohort-specific quality control filters. We followed the quality control protocol of the GIANT Consortium's recent study of human height[20] and employed QCGWAS[16] and EasyQC[17] software, which allowed us to harmonize the files and identify possible sources of error in association results.

Cohort association results (after applying the quality control filters) were combined using sample-size-weighted meta-analysis with genomic control correction within each study, implemented in METAL[80]. SNPs were considered genome-wide significant at P values smaller than 5×10^{-8} ($\alpha = 5\%$, Bonferroni corrected for 1 million tests). The meta-analyses were carried out by two independent analysts. Detailed results for each genome-wide significant locus are shown in in **Supplementary Figures 4–29**.

The total sample size of the meta-analyses is $n = 251{,}151$ for AFB pooled and $n = 343{,}072$ for NEB pooled. The PLINK clumping function[81] was used to identify the most significant SNPs in associated regions (termed lead SNPs). Detailed cohort descriptions, information about cohort-level genotyping and imputation procedures, cohort-level measures and quality control filters are shown in **Supplementary Tables 26** and **27** and discussed in the **Supplementary Note**.

Dominant genetic variation in fertility. We applied a method recently developed by Zhu *et al.*[82] to estimate dominant genetic effects on the basis of the genetic relatedness of unrelated individuals. Our results, based on combined TwinsUK and LifeLines samples, showed no evidence of dominant genetic effects for either NEB (1.0×10^{-7}, SE = 0.07; $P = 0.45$) or AFB (0.02, SE = 0.08; $P = 0.43$). Results are shown in **Supplementary Table 28** and discussed in the **Supplementary Note**.

Bivariate and conditional analyses. As joint analysis of correlated traits may boost power for mapping functional loci, we applied a recently developed multiple-trait analysis method[83] to test the association between each variant and the two correlated traits AFB and NEB simultaneously using multivariate analysis of variance (MANOVA) (**Supplementary Table 29** and **Supplementary Note**). The analysis was performed on the basis of the genome-wide meta-analysis summary statistics for each single trait. Although this analysis did not identify additional genome-wide significant loci ($\lambda = 0.995$), it did account for the correlation between the two phenotypes, thus improving the strength of two signals on chromosomes 1 and 5, indicating possible pleiotropic architecture for AFB and NEB (**Supplementary Fig. 30**). The analysis also provided a conditional association test of the genetic effect of each variant on AFB including NEB as a covariate and the genetic effect on NEB including AFB as a covariate (**Supplementary Fig. 31**).

Population stratification. We used two methods to assess whether our GWAS results exhibited signs of population stratification (**Supplementary Note**). First, we used the LD Score intercept method described in Bulik-Sullivan *et al.*[19] to test whether inflation in χ^2 statistics was due to confounding biases such as cryptic relatedness and population stratification. In all six cases, the intercept estimates were not significantly different from 1, suggesting no appreciable inflation of the test statistics attributable to population stratification. Second, we conducted a series of individual and within-family regressions using polygenic scores as predictors[20,21,38] on a data set of dizygotic twins (STR and TwinsUK). The regression analyses showed that within-family regression coefficients for both AFB and NEB were statistically different from 0 when the P-value threshold was sufficiently high (**Supplementary Figs. 32** and **33**, and **Supplementary Tables 30** and **31**).

Sex-specific effects. In addition to the pooled GWAS for which results are presented in the main text, we also ran sex-specific GWAS meta-analyses for AFB and NEB (**Supplementary Note**). The sample sizes for sex-specific analysis were as follows: AFB in women, $n = 189{,}656$; AFB in men, $n = 48{,}408$; NEB in women, $n = 225{,}230$; NEB in men, $n = 103{,}909$. Our results identified six genome-wide significant ($P < 5 \times 10^{-8}$) independent SNPs for AFB in women and one genome-wide significant independent SNP for NEB in men (**Supplementary Figs. 34** and **35**, and **Supplementary Table 32**). We also used LD Score bivariate regression and GREML bivariate analysis to estimate the genetic correlation between men and women on the basis of the sex-specific summary statistics from the AFB and NEB meta-analyses. Our estimates based on LD bivariate regression indicated genetic correlations between the sexes of $r_g = 0.86$ (SE = 0.052) for AFB and $r_g = 0.97$ (SE = 0.095) for NEB. Results are shown in **Supplementary Tables 33** and **34** and discussed in the **Supplementary Note**.

Polygenic score prediction. We performed out-of-sample prediction and calculated polygenic scores for AFB and NEB, on the basis of genome-wide association meta-analysis results, and used regression models to predict the same phenotypes in four independent cohorts: HRS, LifeLines, STR and TwinsUK (**Supplementary Fig. 2** and **Supplementary Note**). We ran ordinary least-squares (OLS) regression models and report R^2 as a measure of goodness of fit for the model. In addition, we tested how well our polygenic scores for NEB could predict childlessness at the end of the reproductive period (using age 45 for women and 55 for men; **Supplementary Table 21**). Because AFB is observed only in parous women, we adopted an additional statistical model to account for censoring (Cox proportional hazard model; **Supplementary Table 22**) and selection (Heckman selection model; **Supplementary Table 35**). We additionally tested the predictive value of our polygenic scores for AFB on age at menarche (TwinsUK) and age at menopause (LifeLines) (**Supplementary Table 23**). Finally, we examined whether variants associated with menopause are associated with AFB. We calculated a polygenic score for age at menopause based on recent GWAS results from Day *et al.*[40] and applied the predictor to the LifeLines and TwinsUK cohorts (**Supplementary Table 36**).

Genetic correlations. We used information from 27 publicly available GWAS data sets to estimate the number of genetic correlations between AFB or NEB and related traits (**Fig. 3** and **Supplementary Table 25**) via LD Score bivariate regression. Details on these phenotypes are provided in the **Supplementary Note**. A conservative Bonferroni-corrected P-value threshold of $P < 1.85 \times 10^{-3}$ (= 0.05/27) was used to define significant associations. We also tested the correlation between NEB and AFB using bivariate GREML analysis on the Women's General Health Study (WGHS; $n = 40{,}621$).

Lookups and proxy phenotypes. Following up on the results of genetic overlap with other phenotypes, we tested in a quasi-phenotype replication setting whether the SNPs strongly associated with AFB in women were empirically plausible candidate SNPs for age at menarche and age at menopause (**Supplementary Note**). We used a two-stage approach applied in other contexts[38,84]. In the first stage, we conducted a meta-analysis of AFB excluding cohorts that were part of the meta-analysis for the phenotype we intended to replicate. We merged the SNPs from this meta-analysis with the publically available association results for the most recent GWAS on age at menarche[2] and age at menopause[40] from the ReproGen consortium website[1]. SNPs that were not present in both studies considered were dropped from the analysis. We aligned alleles and directions of effect using EasyStrata software[85]. We then selected independent SNPs with $P < 1 \times 10^{-5}$, using the clump procedure in PLINK[81] (window size of 1,000 kb and LD threshold of $r^2 > 0.1$) to identify the most significant SNPs in the associated regions included in both files. We defined 'prioritized SNP associations' as those that passed the Bonferroni correction for the number of SNPs tested ($0.05/122 = 4.10 \times 10^{-4}$, for both age at menarche and age at menopause). Our results identified three SNPs after Bonferroni correction that could be used as good candidates for age at menarche. We did not find any clear 'candidate SNP' for age at menopause (**Supplementary Fig. 36**).

Gene-based GWAS analysis. We performed gene-based testing with the full GWAS set (~2.5 million HapMap-imputed SNPs) for both phenotypes using VEGAS (**Supplementary Tables 3** and **4**, and **Supplementary Note**)[22,23].

This software has the advantage of accounting for LD structure and allowing a gene to be defined as a range with boundaries beyond the edges of the gene to include intergenic regions in the analysis. We defined genes including an additional 50-kb window around each gene. We considered every SNP for the gene-based analysis, ran the analyses for each chromosome with up to 10^6 permutations and considered $P < 2.5 \times 10^{-6}$ as the threshold for significance (0.05/~20.000 genes).

eQTL and meQTL analyses. For each of the 12 SNPs identified in the GWAS, local (*cis*; exons or methylation sites <1 Mb from the SNP) and genome-wide (*trans*; exons or methylation sites >5 Mb from the SNP) effects were identified by computing Spearman rank correlations between SNPs and local or global exons and methylation sites (**Supplementary Note**). Bonferroni correction for multiple testing was performed for the 12 SNPs tested ($P < 2.5 \times 10^{-6}$ for *cis*-meQTL analysis, $P < 1 \times 10^{-8}$ for *trans*-meQTL analysis, $P < 1.2 \times 10^{-6}$ for *cis*-eQTL analysis, $P < 1.3 \times 10^{-8}$ for *trans*-eQTL analysis). For each of the significant associations, the corresponding exons or methylation sites were selected, the strongest eQTLs were identified for these elements and the LD between the strongest eQTLs and the corresponding SNP identified in the GWAS was computed. LD was computed using BIOS genotypes (genotypes used for eQTL and meQTL mapping).

Functional variant analysis using RegulomeDB. We used RegulomeDB[27] to identify variants among the 322 SNPs that reached $P < 5 \times 10^{-8}$ for association with AFB and/or NEB in the meta-analysis of GWAS results that likely influence regulation of gene expression (**Supplementary Note**). RegulomeDB integrates results from the Roadmap Epigenomics[26] and ENCODE[86] projects. SNPs showing the most evidence of being functional—defined by having a RegulomeDB score <4—were subsequently examined in more detail in terms of effects on gene expression (eQTLs) and their protein-binding capacity (**Supplementary Table 6**).

Gene prioritization. Potentially causal genes for the associations identified by GWAS were identified using four previously described bioinformatics tools: ToppGene[4], Endeavor[5], MetaRanker[6] and DEPICT[7]. To this end, we first retrieved positional coordinates for all lead SNPs according to GRCh37/hg19 using Ensembl BioMart. These coordinates were used to extract all genes located within 40 kb of lead SNPs from the UCSC table browser. The identified genes then served as input for ToppGene and Endeavor. Genes with established roles in fertility served as training genes in this procedure, that is, *BRCA1*, *EGFR*, *ERBB2*, *ERBB3*, *ERBB4*, *HSD17B1*, *RBM5*, *ESR1*, *ESR2* and *FSHB*. For MetaRanker, we provided SNPs that reached $P < 5 \times 10^{-4}$ and their chromosomal positions as input, together with the above set of training genes. Because ToppGene, Endeavor and MetaRanker are biased toward larger and well-described genes, we also performed a gene prioritization procedure using DEPICT[7]. All SNPs that reached $P < 5 \times 10^{-4}$ in the meta-analysis served as input, and information on prioritized genes, gene set enrichment, and tissue and cell type enrichment was extracted. Genes were subsequently prioritized if they (i) reached $P < 0.05$ in DEPICT or (ii) reached $P < 0.05$ in ToppGene, Endeavor and MetaRanker (**Supplementary Table 37**).

Functional network and enrichment analyses. DEPICT was used to identify gene set, cell type and tissue enrichment, using the GWAS-identified SNPs with $P < 5 \times 10^{-4}$ as input (**Supplementary Note**). Because of the relatively small number of identified loci, DEPICT was only able to perform these analyses for AFB and NEB pooled and for AFB in women. To construct a functional association network, we combined five prioritized candidate gene sets into a single query gene set that was then used as input for functional network analysis[24]. We applied the GeneMANIA algorithm together with its large set of accompanying functional association data[87]. We used the Cytoscape software platform[88], extended by the GeneMANIA plugin (data version 8/12/2014, accessed 24 April 2016)[89]. All the genes in the composite network, from either the query or resulting gene sets, were then used for functional enrichment analysis against Gene Ontology (GO) terms[90] to identify the most relevant terms, using the same plugin[89].

Gene–environment interactions. Previous research based on twin studies shows differential heritability of fertility behavior across birth cohorts[91,92]. We used the Swedish Twin Register (STR) to examine whether the effect of a polygenic score for AFB or NEB varied across birth cohort. We followed the analysis presented in the recent GWAS of education[35] and divided the sample into six groups on the basis of year of birth. Each group spanned five birth years, with the oldest ranging from 1929–1933 and the youngest born from 1954–1958. **Supplementary Table 38** reports the estimated coefficients from these regressions. The results indicate a U-shaped trend in AFB and a linear decline in NEB, but they do not provide any clear evidence of interaction effects between the polygenic scores and birth cohort. We additionally tested the interaction effects for educational level and the polygenic scores for AFB and NEB in three different samples (LifeLines, STR and HRS). **Supplementary Table 39** reports the estimated coefficients from these regressions. The results indicate that years of education are positively associated with AFB in both the LifeLines and STR cohorts and negatively associated with NEB in the HRS cohort. With the exception of NEB in the HRS cohort, we found no evidence of gene–environment effects with education.

Robustness checks. To estimate the robustness of our results for AFB, we conducted two additional analyses. First, we estimated how the coefficients changed if we controlled for educational attainment. Using data from deCODE, we ran an additional association analysis using the ten loci that were genome-wide significant in the meta-analysis ($P < 5 \times 10^{-8}$). The analysis was restricted to individuals born between 1910 and 1975 who also had data available on completed education. The total sample size was 42,187 (17,996 males and 24,191 females). The analysis was adjusted for sex, year of birth (linear, squared and cubed), interaction between sex and year of birth, and the first ten principal components. Education is measured by years of education, ranging between 10 and 20 years. **Supplementary Table 40** reports the association results before and after adjusting for educational attainment. Our analysis shows that effect sizes shrink after including educational attainment as a covariate, with an average reduction of around 15%. We also estimated the effect of a polygenic risk score for AFB calculated from meta-analysis data excluding the deCODE cohort. The polygenic risk score remained highly significant. The effect of 1 s.d. for the AFB score decreased from 0.19 years (69 d) without controlling for education to 0.16 years (59 d) when we controlled for years of education. Second, we estimated how the coefficients changed after controlling for educational attainment and age at first sexual intercourse using the UK Biobank cohort ($n = 50{,}954$). We ran two association models: the first followed the GWAS analysis plan with no additional covariates, and the second added years of education and age at first sexual intercourse as covariates. The results are presented in **Supplementary Figure 37** and **Supplementary Table 41**. Our analysis shows that the effect sizes of our top hits are highly concordant ($R^2 = 0.94$). The inclusion of educational attainment and age at first sexual intercourse as covariates weakened the effect sizes on average by 40% and increased the *P* values of the estimated coefficients. Overall, we interpret this additional analysis as a robustness test that confirms that the top hits from our meta-analysis are robust to the inclusion of the confounding factors of educational attainment and age at first sexual intercourse.

Positive selection. We performed Haploplotter analysis[93] to examine whether lead SNPs and/or functional variants identified using RegulomeDB showed evidence of positive selection. Three variants showed standardized integrated haplotype scores <−2 or >2, indicating that these variants represent the top 5% of signals in the population. These SNPs are (i) rs7628058 on chromosome 3 for AFB, an eQTL for *RBM6* in monocytes; (ii) rs2247510 on chromosome 3 for AFB, an eQTL for *RBM6* and *HYAL3* in monocytes and a binding site for a range of transcription factors; and (iii) rs2415984, the lead SNP in the chromosome 14 locus for NEB. Results are presented in **Supplementary Table 42**.

Data availability. Results can be downloaded from the SOCIOGENOME and SSGAC website. Data come from multiple studies, most of which are subject to a MTA, and are listed in the **Supplementary Note**. Correspondence and requests for materials should be addressed to the corresponding authors or info@sociogenome.com.

doi:10.1038/ng.3698

80. Willer, C.J., Li, Y. & Abecasis, G.R. METAL: fast and efficient meta-analysis of genomewide association scans. *Bioinformatics* **26**, 2190–2191 (2010).
81. Purcell, S. *et al.* PLINK: a tool set for whole-genome association and population-based linkage analyses. *Am. J. Hum. Genet.* **81**, 559–575 (2007).
82. Zhu, Z. *et al*. Dominance genetic variation contributes little to the missing heritability for human complex traits. *Am. J. Hum. Genet.* **96**, 377–385 (2015).
83. Shen, X. *et al*. Simple multi-trait analysis identifies novel loci associated with growth and obesity measures. Preprint at *bioRxiv* http://dx.doi.org/10.1101/022269 (2015).
84. Okbay, A. *et al*. Genetic variants associated with subjective well-being, depressive symptoms, and neuroticism identified through genome-wide analyses. *Nat. Genet.* **48**, 624–633 (2016).
85. Winkler, T.W. *et al*. EasyStrata: evaluation and visualization of stratified genome-wide association meta-analysis data. *Bioinformatics* **31**, 259–261 (2015).
86. ENCODE Project Consortium. An integrated encyclopedia of DNA elements in the human genome. *Nature* **489**, 57–74 (2012).
87. Mostafavi, S., Ray, D., Warde-Farley, D., Grouios, C. & Morris, Q. GeneMANIA: a real-time multiple association network integration algorithm for predicting gene function. *Genome Biol.* **9** (Suppl. 1), S4 (2008).
88. Saito, R. *et al.* A travel guide to Cytoscape plugins. *Nat. Methods* **9**, 1069–1076 (2012).
89. Montojo, J. *et al*. GeneMANIA Cytoscape plugin: fast gene function predictions on the desktop. *Bioinformatics* **26**, 2927–2928 (2010).
90. Ashburner, M. *et al.* Gene ontology: tool for the unification of biology. *Nat. Genet.* **25**, 25–29 (2000).
91. Kohler, H.-P., Rodgers, J.L. & Christensen, K. Is fertility behavior in our genes? Findings from a Danish twin study. *Popul. Dev. Rev.* **25**, 253–288 (1999).
92. Tropf, F.C., Barban, N., Mills, M.C., Snieder, H. & Mandemakers, J.J. Genetic influence on age at first birth of female twins born in the UK, 1919–68. *Popul. Stud. (Camb.)* **69**, 129–145 (2015).
93. Voight, B.F., Kudaravalli, S., Wen, X. & Pritchard, J.K. A map of recent positive selection in the human genome. *PLoS Biol.* **4**, e72 (2006).